Combined presentation and immunogenicity analysis reveals a recurrent RAS.Q61K neoantigen in melanoma

Aviyah Peri, Erez Greenstein, Michal Alon, Joy A. Pai, Tamir Dingjan, Shlomit Reich-Zeliger, Eilon Barnea, Chaya Barbolin, Ronen Levy, Claudia Arnedo-Pac, Shelly Kalaora, Bareket Dassa, Ester Feldmesser, Ping Shang, Polina Greenberg, Yishai Levin, Gil Benedek, Mitchell P. Levesque, David J. Adams, Michal Lotem, James S. Wilmott, Richard A. Scolyer, Goran B. Jonsson, Arie Admon, Steven A. Rosenberg, Cyrille J. Cohen, Masha Y. Niv, Nuria Lopez-Bigas, Ansuman T. Satpathy, Nir Friedman, Yardena Samuels

Supplementary Information

Table of Contents

Supplementary Methods 3
Structural modeling of HLA-A*01:01 in complex ILDTAGKEEY 3
RAS.Q61 mutation status and HLA-typing of tumor tissue 4
cDNA sequencing 5
Establishment of double-transfectant 721.221 6
HLA-peptidomics 7
Fluorescence-based in vitro killing assay 10
Peptide pulsing on B-LCLs 11
Analysis of T-cell reactivity by IFNγ release assay 11
Flow cytometry analysis and fluorescence-activated cell sorting 11
IFNγ secretion assay 12
Antigen induced TIL expansion assay 13
Bulk TCR sequencing 13
Single-cell RNA and TCR sequencing of CD8+ TIL 14
TIL:melanoma co-incubation and tetramer sorting 14
10x library preparation and sequencing 15
Data processing of scRNA and TCR-seq libraries 15
Identification of neoantigen-reactive clones 16
Single cell data integration and clustering 16
TCR similarity analysis 17
TCR overexpression in PBMC 18
Peptide titration assay 18
Caspase-3 cleavage assay 19
Statistical analysis 19
References 20
Supplementary Figures 23

Supplementary Methods

Structural modeling of HLA-A*01:01 in complex ILDTAG<u>K</u>EEY

Structures of HLA-A*01:01 complexed with RAS.61-derived peptides were modelled using a crystal structure of HLA-A*01:01 in complex with an ALK tyrosine kinase receptor decapeptide (PDB: 6at9)(1). The crystallographic bound peptide was manually mutated to yield the *ILDTAG<u>K</u>EEY* and *ILDTAG<u>Q</u>EEY* peptides in complex with the HLA receptor. The HLA structure was truncated to the peptide-binding domain (chain A, residues 1 to 180). The resulting peptide-HLA structures were used as starting conformations for peptide docking and for molecule dynamics simulation.

Peptide docking was performed using the freely accessible web server interfaces FlexPepDock(2), ClusPro(3) and DINC(4). In addition, molecular dynamics simulations were performed using GROMACS version 2018.3.(5) with a GROMOS 54a7 united atom force field(6). The complex was placed in a rhombic dodecahedral box with a minimum distance of 10 Å between the solute and box wall, and solvated by SPC water. The system's charge was neutralized by the addition of 5 Na^+ counter ions. Steric clashes were removed by minimization, conducted using the steepest descent algorithm for a maximum of 5,000 steps. The system was equilibrated at constant volume and temperature (NVT ensemble) with all protein and peptide heavy atoms restrained for 100 ps at 10 K, followed by further equilibration without restraints for another 100 ps at 300 K. The system's pressure was equilibrated by simulation under constant atmospheric pressure (NPT ensemble) for 300 ps at 300 K. Positional restraints were applied to protein residues during all equilibration steps using the LINCS algorithm(7). The final coordinates resulting from equilibration were used to commence five independent production runs for both (*ILDTAG<u>K</u>EEY* and *ILDTAG<u>Q</u>EEY*) systems, each conducted for 500 ns in the NPT ensemble. The temperature was held constant at 300 K using the velocity rescaling thermostat(8) coupled with a time constant of 0.1 ps,

and the system's pressure was kept constant at 1 bar using the Parrinello-Rahman barostat(9) coupled with a time constant of 2 ps. A timestep of 2 fs was used to integrate the motions of the system. Long-range electrostatics were calculated using the Particle Mesh Ewald(10) method, while short-range cutoffs were set to 1.0 nm for both the vdW and Coulomb interactions. To focus on bound conformations, only conformations in which the RAS peptide's N- and C-termini were within 7 Å of the HLA B- and F-pockets, respectively, were analyzed. Distances were measured between the following atoms: HLA Tyr171 sidechain hydroxyl oxygen (OH) and peptide Ile1 backbone amide nitrogen (N), and between HLA Tyr123 sidechain phenolic carbon (CZ) and peptide Tyr10 sidechain gamma carbon (CG). Molecular structures were visualized using PyMOL version 1.3(11). The conformations from docking and from bound simulation frames were clustered by HLA-peptide hydrogen-bonding interactions. Hydrogen bonds were detected using the Wernet-Nilsson criteria(12) as implemented in MDTraj(13) version 1.9.2. Cluster centroids were identified as simulation frames for which the corresponding hydrogen bonding fingerprint possessed the lowest Manhattan/Cityblock distance to all cluster members.

RAS.Q61 mutation status and HLA-typing of tumor tissue

For 17T and 108T, both RAS.Q61 status and HLA-typing were extracted from whole-exome sequencing; HLA-typing was determined using the *PolySolver* software(14). For MM121224 and MM150414 HLA and mutation data were provided by its contributor. For 135T and snap-frozen tumors, RAS.Q61 status was informed by their contributors, while genomic DNA, extracted using QIAGEN's DNeasy Blood and Tissue kit (#69504), was utilized for HLA-typing (GenDx SBTexcellerator HLA-A kit #4100234 or the MX6-1 NGS typing kit, #7371464). Mutation and HLA data regarding cell-lines SK-MEL-30, MZ2-mel, HuT78,

Hs940T and Calu6 were extracted from the "TRON cell line portal"(14, 15). HLA-typing of EBV-transformed B-cells was provided by the IHWG Cell and DNA Bank(16).

cDNA sequencing

Total RNA was extracted from melanoma cell lines 17T, 135T, SK-MEL-30, MM121224, MZ2-mel, HuT78, Calu6 and Hs940T following the manufacturer's protocol using the RNeasy Mini Kit (#74104, QIAGEN), and eluted in 30µl diethylpyrocarbonate (DEPC)-treated distilled H_2O. A total of 500ng RNA was used for single-strand complementary DNA (cDNA) synthesis using the iScript Reverse Transcription Super mix for RT-qPCR kit (#1708841, Biorad) as per the manufacturer's protocol. NRAS and KRAS regions containing position 61 were amplified by PCR using the following primers: NRAS forward: 5'-TTGGAGCAGGTGGTGTTGGG -3', NRAS reverse: 5'-GTATCAACTGTCCTTGTTGGC 3', KRAS forward: 5'-TAAACTTGTGGTAGTTGGAGCTGGT-3', KRAS reverse: 5'-TTCTTTGCTGATTTTTTTCAA-3'.

2 µl of cDNA were taken for the PCR reaction, mixed with 2× KAPA HIFI (#KM2605, KAPA Biosystems) to a final volume of 25 µl, using a standard PCR program with the following parameters: one cycle at 95 °C for 3 min; 35 cycles of 98 °C for 20 sec; annealing temperature of 58 °C for 30 sec; and 72 °C for 1 min. The PCR products were separated on a 1% agarose gel and then purified by Wizard SV Gel and PCR Clean-Up System (#A9281, Promega), followed by Sanger sequencing using a 3730 DNA Analyzer (ABI). The sequencing primers were the same as the PCR primers. The sequencing results were analyzed using the SnapGene software (Version 4.3.2).

Establishment of double-transfectant 721.221

DNA sequences coding for HLA-A*01:01 and 25-mer minigenes (RAS.Q61K and RAS.Q61R) were designed with flanking *XbaI* and *NotI* restriction sites at the 5' and 3' ends, respectively. The designs were purchased as synthetic dsDNA from either Twist bioscience or IDT (gBlock) following optimization for human expression via the respective companies' platforms. PCR amplified templates were restriction cloned using *XbaI/NotI* (NEB, #R0145L and # R0189L) into lentiviral vectors pCDH-CMV-MCS-EF1α-Neo (SBI, #CD514B-1) and pCDH-CMV-MCS-EF1α-GreenPuro (SBI, #CD513B-1). HLA and minigene inserts were ligated into the Neomycin and Puromycin vectors, respectively, using T4 DNA ligase (NEB, #M0202L) yielding pCDH-Neo-A*01:01, pCDH-Puro-GFP-mRAS.Q61K and pCDH-Puro-GFP-mRAS.Q61R. Sequence verified cloned plasmids were used to produce lentiviral particles via co-transfection with envelope and packaging plasmids PMD2.G and psPAX2 into HEK293T cells using Lipofectamine 2000 (Invitrogen, #11668027), per manufacturer's instructions. Harvested virus containing supernatant was filtered, aliquoted and stored at -80^{o}C. Cells of the HLA-I deficient human B-LCL 721.221 were stepwise infected, first to express HLA-A*01:01 and then with the minigene virus (RAS.Q61K or RAS.Q61R). 48-72 hours post infection selection was started either with 800 μg/ml neomycin (G418) or 1 μg/ml Puromycin. Infected cells were continuously propagated under selection. Productive over-expression of HLA-A*01:01 was validated approximately two weeks post infection via flow cytometry, using the monoclonal antibody W6/32. After validation of HLA expression, 721.221$^{A*01:01}$ cells were infected and selected to induce minigene over-expression, as described above. 721.221$^{A*01:01;RAS.Q61K}$ and 721.221$^{A*01:01;RAS.Q61R}$ cells were grown in media containing both selection agents for approximately two weeks, and then propagated in antibiotics-devoid medium for additional two weeks before expansion for HLA-peptidomics.

HLA-peptidomics

Production and purification of membrane HLA molecules

Cell pellets consisting of $2x10^8$ cells each were collected and lysed on ice using a lysis buffer containing 0.25% sodium deoxycholate, 0.2 mM iodoacetamide, 1mM EDTA, 1:200 Protease Inhibitors Cocktail (Sigma-Aldrich, P8340), 1 mM PMSF and 1% octyl-β-D glucopyranoside in PBS. Samples were then incubated at 4 ˚C for 1 h. The lysates were cleared by centrifugation at 48,000 g for 60 min at 4 ˚C and then passed through a pre-clearing column containing Protein-A Sepharose beads.

HLA-I molecules were immunoaffinity purified from cleared lysate with the pan-HLA-I antibody (W6/32 antibody purified from HB95 hybridoma cells) covalently bound to Protein-A Sepharose beads (Thermo-Fisher Scientific, as reported previously)(17, 18). Affinity columns were washed first with 400 mM NaCl, 20 mM Tris–HCl pH 8.0 and then with 20 mM Tris–HCl, pH 8.0. The HLA peptides and HLA molecules were then eluted with 1% trifluoracetic acid, followed by separation of the peptides from the proteins by binding the eluted fraction to Sep-Pak (Waters). Elution of the peptides was done with 28% acetonitrile in 0.1% trifluoracetic acid(17).

Identification of eluted HLA peptides

Liquid chromatography:

Cell lines 17T, SK-MEL-30 and MM121224: The HLA peptides were dried by vacuum centrifugation, solubilized with 0.1% formic acid, and resolved with a 7-40% acetonitrile gradient with 0.1% formic acid for 180 min and 0.15 µL/min on a capillary column pressure-packed with Reprosil C18-Aqua (Dr. Maisch, GmbH, Ammerbuch-Entringen, Germany) as previously described(19). For cell lines 17T, SK-MEL-30 and MM121224, chromatography was performed with the UltiMate 3000 RSLCnano-capillary UHPLC system (Thermo Fisher

Scientific), which was coupled by electrospray to tandem mass spectrometry on Q-Exactive-Plus (Thermo Fisher Scientific). HLA peptides were eluted over 2 h with a linear gradient from 5% to 28% acetonitrile with 0.1% formic acid at a flow rate of 0.15 µl/min.

Cell lines 721.221$^{A*01:01;\ mRAS.Q61K}$,721.221$^{A*01:01;\ mRAS.Q61R}$,135T, MZ2-MEL, HuT78, Hs940T and 4 tumor samples (Mela-183,Mela-49, MM-1369 and MM-1319): The HLA peptides were dried by vacuum centrifugation, solubilized with 97:3 water: acetonitrile 0.1% formic acid. Desalting of the samples was performed online using a reversed-phase Symmetry C18 trapping column (180 µm internal diameter, 20 mm length, 5 µm particle size; Waters). Peptides were resolved with a 5-28% acetonitrile gradient with 0.1% formic acid for 120 min using a T3 HSS nano-column (75 µm internal diameter, 250 mm length, 1.8 µm particle size; Waters) at 0.35 µL/min. Chromatography was performed with the nanoAcquity (Waters), which was coupled by electrospray to tandem mass spectrometry on Q-Exactive-Plus (Thermo Fisher Scientific).

Mass Spectrometry:

Cell lines 721.221$^{A*01:01;\ mRAS.Q61K}$, 721.221$^{A*01:01;\ mRAS.Q61R}$ and 17T were run in discovery mode. Cell-lines: SK-MEL-30, MM121224 and 135T, as well as aliquots of the 721.221$^{A*01:01;\ mRAS.Q61K}$,721.221$^{A*01:01;\ mNRAS.Q61R}$,17T, MZ2-MEL, HuT78, Hs940T samples and 4 tumor samples (Mela-183,Mela-49, MM-1369 and MM-1319) were analyzed in an absolute targeted mass spectrometry, looking for *ILDTAGKEEY* or *ILDTAGREEY* specifically, and utilizing heavy-peptide spike-in, enabling also for peptide quantification. Synthetic heavy-isotope-labeled *ILDTAGKEEY*, with heavy lysine (13C6;15N2) or *ILDTAGREEY* with heavy arginine (13C6;15N4) incorporated, were purchased in >95% purity from *JPT*.

Discovery mode: Data was acquired using a data-dependent "top-10" method, fragmenting the peptides by higher-energy collisional dissociation. The full-scan MS spectra were acquired at a resolution of 70,000 at 200 m/z with a target value of $3x10^6$ ions. Ions were accumulated to

an automatic gain control (AGC) target value of 10^5 with a maximum injection time of generally 100 msec. The peptide match option was set to *Preferred*. The normalized collision energy was set to 25% and the MS/MS resolution was 17,500 at 200 m/z. Fragmented m/z values were dynamically excluded from further selection for 20 sec. MS data were analyzed using MaxQuant (version 1.5.8.3)(20) with FDR 0.05. The peptide identifications were based on the human section of the UniProt database(21) (April 2017) and a customized reference database that contained the mutated sequences identified for 17T by WES.

SK-MEL-30, MM121224 absolute targeted mode: 0.1pmol heavy peptide was added to the peptidome sample injected into the mass-spectrometer. Analysis was then performed using the PRM method. An inclusion list was imported into the method for MS/MS acquisitions. The instrument switched between full MS and MS/MS acquisitions to fragment the ions in the inclusion list. Full-scan MS spectra were acquired at a resolution of 70,000, with a mass-to-charge ratio (m/z) of 350-1,400 AMU. Fragmented masses were accumulated to an AGC target value of 10^5 with a maximum injection time of 400 msec and 1.8 m/z window. Analysis again utilized the MaxQuant software (version 1.5.8.3)(20) with the Andromeda search engine(22). Peptide identifications were based on the human section of the UniProt database(21) (April 2017) and a customized reference database containing the *ILDTAGKEEY* neo-antigen. The following parameters were used: precursor ion mass and fragment mass tolerance of 20 ppm, false discovery rate (FDR) of 0.05 for SK-MEL-30 and 0.3 for MM121224, and variable modification of oxidation (Met), acetylation (protein N-terminus) and heavy Lysine (13C6;15N2).

$721.221^{A*01:01;\,mRAS.Q61K}$,$721.221^{A*01:01;\,mRAS.Q61R}$, 17T, 135T, MZ2-MEL, HuT78, Hs940T and 4 tumor samples (Mela-183,Mela-49, MM-1369 and MM-1319): absolute targeted mode:

The nanoUPLC was coupled online through a nanoESI emitter (10 μm tip; New Objective; Woburn, MA, USA) to a quadrupole orbitrap mass spectrometer (Q Exactive Plus, Thermo

Scientific) using a FlexIon nanospray apparatus (Proxeon). Data was acquired in Parallel Reaction Monitoring (PRM) with one MS1 scan for every 10 PRM scans. MS1 scan range was set to 300-1800m/z, resolution of 70,000, AGC of 3e6 and maximum injection time was set to 120msec. The PRM channels were acquired at 35,000 resolution, maximum injection time of 200msec, AGC of 2e5, NCE of 27 and isolation of 1.7m/z.

Peptide quantification:

Raw PRM data was imported into Skyline(23). Absolute quantification was obtained by summing extracted ion chromatograms of all fragment ions per peptide and exporting the ratio of total signal of the native peptide versus the heavy labeled internal standard that was spiked into the sample, multiplied by the amount of internal standard.

Fluorescence-based in vitro killing assay

In this assay, loss of fluorescent content is used to quantify target cell death(24). GFP+ cells were established via lentiviral infection and antibiotic selection. Fluorescent target-cells were seeded at 70% confluence onto 48-well plates ($1x10^5$ and $5x10^4$ cells/well for 17T and 135T, respectively) a day prior to the experiment and let adhere. Cognate TIL were added at effector to target ratios ranging from 0:1 to 4:1 and were co-incubated with the melanoma for 16 hours. A triplicate was included for each condition. After incubation, non-adherent TIL and dead target-cells were washed away with PBS. The fluorescence of remaining live target cells was quantified using Tecan-M200 plate reader. Fluorescence reading was focused 3 mm above the plate surface. The percentage of specific lysis was calculated as $100\times(C-X)/C$, where C is fluorescence in the TIL-free condition and X is fluorescence in the presence of TILs.

Peptide pulsing on B-LCLs

Synthetic >95% pure peptides (*ILDTAGKEEY*, *ILDTAGREEY*, *ILDTAGQEEY*) were purchased from GenScript and dissolved in DMSO. B-LCLs bearing HLA-A*01:01 were suspended in complete medium at $1x10^6$ cells/ml, and incubated with the peptide of choice, at the desired concentration (10^{-11}-10^{-5} □), for 2-4 h in a 37 ˚C, 5% CO2, humidified incubator, in upright 15 ml conical tubes. DMSO volume was kept at 1% in all samples. For the no-peptide control, DMSO devoid of peptides was added. B-cells were washed in PBS three times before proceeding to the co-incubation with TILs.

Analysis of T-cell reactivity by IFNγ release assay

IFNγ's release from TIL, as measured in an enzyme-linked immunosorbent assay (ELISA), was used to measure reactivity. TILs were co-cultured with either cognate melanoma or B-LCLs at a 1:1 ratio (10^5-$2x10^6$ cells) in U-bottom 96-well plates and incubated overnight in a 37 ˚C, 5% CO_2, humidified incubator. The soluble IFNγ secreted from TIL was quantified from the co-culture supernatant using Biolegend Human IFNγ ELISA MAX Deluxe (#430106), using Tecan-M200 plate reader. All experiments were conducted in biological triplicates.

Flow cytometry analysis and fluorescence-activated cell sorting

PBS 1% BSA 2 mM EDTA was utilized as staining and analysis buffer for flow cytometry experiments unless otherwise specified. Cells were passed through a 40 μm cell strainer (Corning, #431750) prior to sorting. Single-cell suspensions were analyzed in BD LSR II (BD Biosciences) or CytoFlex (Beckman Coulter) for flow cytometry. BD FACSAria III or BD FACSAria II Cell Sorters (BD Biosciences) were used for fluorescence-activated cell sorting. Cells were incubated with antibodies/tetramers for 30 minutes, at 4ºC in the dark and then

washed. Tetramer and TCRβ or anti-CD8 staining were executed sequentially to avoid possible interference.

Tetramers were obtained from the NIH tetramer core facility, and were calibrated to minimize background staining: HLA-A*01:01/*ILDTAGKEEY* (BV421-conjugated) was used at 1:8000-10000, A*01:01/*ILDTAGREEY* (FITC-conjugated) was used at 1:4000. The following antibodies were purchased from Biolegend and utilized at 1:100 dilution: CD3 (PE/Cy7, #300316), CD4 (FITC, #317407), CD8 (APC #300911 or FITC #301006), 4-1BB (APC #309809), mouse TCRβ constant region (APC, #109211, Biolegend), CD19 (BV421, #302234). Staining with CellTrace far-red, anti-caspase3 and IFNγ capture antibodies was executed as described for the cleaved caspase3 killing and IFNγ secretion assays.

Size and granularity measures served to gate on viable singlets. Propidium iodine (Invitrogen #P3566) was used for live/dead staining, where specified. Sorting experiments gated on positive and negative sub-populations without overlap.

IFNγ secretion assay

To assess the percentage of A*01:01/*ILDTAGKEEY* reactive TIL, we employed an IFNγ secretion assay (Miltenyi Biotec, #130-090-762), as per the manufacturer's instructions. In this assay, IFNγ specific antibody is attached to the cell surface and captures the secreted cytokine upon cellular release. IFNγ molecules bound to the cell surface are subsequently stained as artificial surface molecules and the cells analyzed by flow-cytometry. This approach is complementary to tetramer-staining, as neoantigen-specific cells are identified based induced reactivity rather than TCR recognition. IHW01161 cells, serving as APCs in these experiments, were pulsed with either no-peptide (DMSO) or 10 μg/ml mutant (*ILDTAGKEEY*) or wild-type (*ILDTAGQEEY*) peptide. TIL were co-incubated with APC for the duration of four hours. The

no-peptide and wild-type conditions served as control scenarios and allowed to distinguish background from neoantigen-specific reactivity.

Antigen induced TIL expansion assay

IHW01161 cells, serving as APCs, were irradiated with 70 Gray, washed once with PBS, and then pulsed with 10 μg/ml of either mutant (*ILDTAGKEEY*) or wild-type (*ILDTAGQEEY*) peptide, as described above. 17TIL suspension of $2.5x10^6$ cell/ml was prepared in T-cell medium and dispensed in 100 μl aliquots into wells of a 96-well round-bottom tissue culture plate. The mutant and wild-type pulsed APCs were resuspended each in T-cell medium at $2.5x10^6$ cell/ml. Each well was added an additional 100 μl of either T-cell medium or pulsed APC suspension. Additional 1 μg/ml of mutant or wild-type peptide was added to the mutant/wild-type wells, respectively. Subsequently, cells were cultured for a total of ten days in 37ºC, 5% CO2, humidified incubator. At day three of the incubation, half the medium was replaced with fresh T-cell medium containing 100 IU/ml IL-2, 50 ng/ml IL-7 (Peprotech, #200-07) and 50 ng/ml IL-15 (Peprotech, #200-15). At day seven of the incubation, half the medium was again replaced with fresh T-cell medium containing 200 IU/ml IL-2, 50 ng/ml IL-7 and 50 ng/ml IL-15. At day ten of incubation, cells were harvested, co-stained with anti-CD4 antibody and the A*01:01/ILDTAGKEEY tetramer, and analyzed by flow cytometry.

Bulk TCR sequencing

We performed TCR library preparation on sorted TILs, as was previously described(25). In short, RNA was extracted from TIL pools and treated with DNase (RNeasy Micro kit (QIAGEN), RQ1 RNase free DNase (Promega)). Reverse transcription was then performed using primers directed at the constant regions of the TCR α/β chains (SuperScript III, #18080044, Invitrogen). Single stranded oligonucleotides consisting of both a universal primer

region and a unique molecular identifier (UMI) were ligated onto the 3' end of the TCR cDNA transcripts (T4 RNA ligase, #0204S, NEB). Over three consecutive PCR steps, the library was then adequately amplified and split into □ and □ chain pools. Libraries were sequenced with 300 cycles on the NextSeq Illumina platform and were processed using an in-house pipeline. Mainly, reads were: (1) clustered according to UMI, for accurate frequency evaluation; (2) annotated for V and J germline gene segments according to the IMGT predetermined library with TRDV genes manually added(26); and (3) determined for their CDR3 sequence at both the nucleotide and amino-acid level. The annotated output consisted of separate collections of □ and □ chains, and was further filtered to exclude non-productive and singleton sequences. $0.5x10^6$ cells were collected for each experimental condition.

For the tetramer sorted experiment TIL were stained with HLA-A*01:01/*ILDTAGKEEY* tetramer and anti-CD4 antibody and were sorted into: bulk CD4- and its tetramer+ and tetramer- subpopulations. All three populations were sequenced; the experiment was conducted in biological triplicates.

Single-cell RNA and TCR sequencing of CD8+ TIL

TIL:melanoma co-incubation and tetramer sorting

17TIL/17T and 135TIL/135T were plated in 1:1 ratio at $4x10^6$ cells per well in a 24-well tissue culture plate. After co-incubation overnight, the cells were resuspended by pipetting, washed in PBS and then frozen in CryoStor CS10 (#07930, STEMCELL Technologies) at 7-$10x10^6$ cell/ml. Cells were thawed on the day of 10x library preparation, into Benzonase (#E8263, Millipore Sigma) supplemented complete medium, washed and then stained in complete medium. Cells were stained with the HLA-A*01:01/ILDTAGKEEY tetramer, followed by staining for CD4 and CD8. Propidium iodine was used for live/dead staining. The samples were sorted into complete medium, separating CD8+tetramer+ (CD8+CD4-

tetramer+) from CD8+tetramer- (CD8+CD4-tetramer-) populations. Bulk CD8+ samples were also obtained by staining for CD4 and CD8 without tetramer staining and sorting for CD8+CD4- populations. Cells were forwarded to 10x library preparation immediately after sorting.

10x library preparation and sequencing

Samples were processed immediately after sorting, as described above, for single-cell library construction. Briefly, sorted cells were washed and resuspended with PBS containing 0.04% bovine serum albumin (BSA) and counted using trypan blue staining. Single cells were captured in droplets by loading onto the Chromium Controller with a targeted cell recovery of 10,000 cells per sample. Single-cell gene expression and TCR-enriched libraries were prepared using the Chromium Single Cell 5' V(D)J v1.1 Kit (10x Genomics) according to the manufacturer's protocol. Samples were sequenced on an Illumina NovaSeq with 26-bp read 1, 8-bp i7 index and 58-bp read 2 for gene expression libraries, and 150-bp paired end reads for TCR libraries.

Data processing of scRNA and TCR-seq libraries

Reads from 10x scRNA expression libraries were aligned to human genome assembly GRCh38 (hg38) and quantified using cellranger count (10x Genomics, version 3.1.0). The filtered feature-barcode matrices containing only cellular barcodes were used for further analysis. Single cell gene expression matrices were imported into R (version 3.6.1) and analyzed using Seurat (version 3.1.1). Cells with less than 4,000 or greater than 20,000 UMIs detected were filtered out. Additionally, cells with greater than 10% mitochondrial RNA reads were excluded from subsequent analyses.

Single cell TCR reads were aligned to human genome assembly GRCh38 (hg38) and assembled into reconstructed TCR consensus sequences using cellranger vdj (10x Genomics, version 3.1.0). Only productive TCRα and TCRβ sequences were considered for further analysis. Overall, TCR sequences were annotated for 95.2% of cells, with paired TCRαβ sequences detected for 37,934 out of 41,542 cells (91.3%). Only cells with conventional paired TCR chain combinations αβ or ααβ were kept for downstream analyses (34,966 cells; 84.1%). Cells sharing the same CDR3αβ amino acid sequences were defined as belonging to the same TCR clone.

Identification of neoantigen-reactive clones

TCR clonal frequencies were compared between the sorted tetramer+ and tetramer- populations for each patient. Clones were considered as tetramer-specific if: (1) ≥100-fold higher clone frequency in the tetramer+ than in tetramer- populations, and (2) each TCR-chain is ≥100-fold enriched in the tetramer+ than in the tetramer- populations in at least one replicate of the bulk TCR sequencing experiments. 12 and 1 neoantigen-reactive clones were defined as tetramer-specific for 17TIL and 135TIL respectively, based on the above criteria. Tetramer-specific clones consisting of at least five cells were retained for downstream neoantigen-specific single-cell analyses. N17.5 (7 cells), N17.6 (2 cells) and N17.7 (one cell) were included based on TCR similarity criteria.

Single cell data integration and clustering

In order to analyze the gene expression programs of neoantigen-reactive clones, the tetramer+ population (filtered for neoantigen-reactive clones) and bulk samples for both patients were integrated. Specifically, log normalization and variable feature selection based on variance stabilizing transformation was first performed on each sample individually. Then, anchors

between datasets were identified using FindIntegrationAnchors(), with the bulk samples as a reference and reciprocal PCA with 30 dimensions. The samples were then integrated using IntegrateData() with 30 dimensions. The integrated expression matrix was then scaled and centered for each feature. Next, linear dimensional reduction was performed on the integrated scaled data using PCA, excluding TCR and cell cycle genes. For visualization, UMAP projections were calculated using the first 30 principal components. To identify clusters based on gene expression profiles, we performed shared nearest neighbor (SNN) modularity optimization clustering using a k parameter of 20 and a resolution of 0.5.

TCR similarity analysis

For each of the three replicates of the bulk 17TIL TCR-sequencing experiment, we compared the tetramer+ repertoire to the bulk repertoire. We computed for each amino acid clonotype the ratio between the frequency in the tetramer+ repertoire to the frequency in the tetramer- repertoire. If the sequence was missing from the bulk repertoire, we estimated its frequency as $3 \cdot 10^{-5}$, which is slightly below the minimal frequency in the repertoires. We selected the sequences for which this ratio is above one (i.e., with higher frequency in the tetramer+ population). We concentrated on sequences that appear in this population for all three replicates of the experience. This procedure yielded ten α and eleven β chains. Within this population, we looked for sequences of low Hamming distance from N135.1. We calculated for each β sequence its sharing level in the Emerson data set(27), and for each α or β sequence its probability of generation according to the standard human models delivered with OLGA (28), a model for estimating the probability of generation of a given CDR3 (α or β). Studying the prevalence of HLA-A*01:01 in the Emerson data set was based on the HLA annotations from DeWitt et al.(29).

TCR overexpression in PBMC

This well documented technique was employed with slight modifications, as described below(30). CDR3 nucleotide sequences were reconstructed with the appropriate V and J sequences as they appear in the IMGT reference(26), and were joined to mouse constant regions, as previously described(31). Optimized mouse constant-region sequences were kindly provided by Prof. Cyrille J. Cohen (Bar-Ilan University, Ramat-Gan, Israel). Each TCR chain was embedded between *XbaI/NotI* restriction sites. Sequences were ordered as dsDNA from *Twist bioscience,* following sequence optimization for human expression using the vendor's platform. TCR chains were restriction cloned into pGEM-4Z-EGFP-A64. This pGEM-4Z (Promega) based plasmid, was kindly provided by Prof. Zelig Eshhar (Weizmann Institute of Science, Rehovot, Israel and Tel-Aviv Sourasky Medical Center, Tel-Aviv, Israel) under our MTA agreement with the NIH. Sequence-verified cloned plasmids were linearized with *SpeI* digestion, in-vitro transcribed using AmpliCap-Max T7 High Yield Message Maker Kit (#C-ACM04037, CellScript) and purified using RNAcleanup kit (#23600, Norgen Biotek). Formed mRNA was stored in 5μg aliquots at -80ºC. PBMC were electroporated with mixed α/β mRNA, 10μg per $1x10^6$ cells, at 400V/500μs, using an ElectroSquare Porator ECM 830 (BTX). Electroporated cells were rested for at least two hours prior to use in downstream experiments. TCR expression was validated via flow-cytometry using mouse constant TCRβ staining.

Peptide titration assay

HLA-A*01:01+ B-LCL were pulsed with synthetic peptide at concentrations ranging from 10^{-11}M to 10^{-5}M, as described above, and were subsequently co-incubated at 1:1 ratio with either TIL or electroporated lymphocytes for 16-20 hours in 96-well U-bottom plates, at 37˚C 5% CO_2 in a humidified incubator. Following co-incubation, plates were centrifuged

at 300g. For 4-1BB readout, the cells pellets were stained for CD19, CD3, CD8 and 4-1BB and analyzed via flow-cytometry. The percentage of 4-1BB+ cells out of the CD8+ population was compared for the different conditions. For secreted IFNγ readout, the supernatant was collected and analyzed using the Human IFNγ ELISA MAX Deluxe (Biolegend, #430106), as above.

Caspase-3 cleavage assay

Intracellular staining of cleaved caspase-3 was utilized to measure cytotoxic T-cell-induced apoptosis of melanoma target cells as previously described(32). Briefly, melanoma cells were stained with CellTrace Far Red (Invitrogen, #C34564), according to the manufacturer's protocol. $1x10^5$ labeled melanoma cells were then co-cultured with lymphocytes at effector:target ratio of 3:1 in U-bottom 96-well plates for three hours at 37ºC, 5% CO_2 in a humidified incubator. Following incubation, the cells were washed, fixed, permeabilized and labeled with an anti-cleaved caspase-3-PE antibody using the *Caspase 3 apoptosis PE kit* (BD, #550914) according to the manufacturer's protocol. Washed cells were analyzed by flow cytometry, to determine the percent of caspase-3+ cells out of CellTrace+ target cells. Donor derived lymphocytes electroporated with the TCR of interest were compared to negative controls of either lymphocytes electroporated with no mRNA or the melanoma cells alone. Experiment were conducted in biological triplicates.

Statistical analysis

Statistical analysis was executed using GraphPad Prism version 9.0.2 for MacOS, base R (version 3.5.0), and Real Statistics Resource Pack software for excel (Release 7.7.1, www.real-statistics.com). Comparison of HLA-allele frequencies between the pan-cancer, melanoma and RAS.Q61-mutated TCGA populations was conducted using Fisher's exact test with FDR correction. IFNγ ELISA, 4-1BB based reactivity and cleaved caspase-3 assays

were analyzed using one-way ANOVA, with Tukey's multiple comparisons test. Where multiple assays were conducted concurrently, and could therefore reliably compare, two-way ANOVA was utilized. Peptide-titration assays were analyzed via two-way ANOVA with Sidak's multiple comparisons test. Comparison of single-cell phenotypic proportions was conducted using Chi-squared test. Differences in activation scores between TCR clones were analyzed using Wilcoxon rank sum test with Bonferroni multiple hypothesis testing correction. Corrected P-values ≤ 0.05 were considered significant.

Study approval

Metastatic melanoma cell-lines 17T, 135T, 108T, and their cognate TIL products, were established as previously described(33), with informed patient consent under a protocol approved by the NIH Institutional Review Board (IRB) Ethics Committee.

References

1. Toor JS et al. A Recurrent Mutation in Anaplastic Lymphoma Kinase with Distinct Neoepitope Conformations. *Front. Immunol.* 2018;9:99.
2. London N, Raveh B, Cohen E, Fathi G, Schueler-Furman O. Rosetta FlexPepDock web server--high resolution modeling of peptide-protein interactions.. *Nucleic Acids Res.* 2011;39(Web Server issue):W249-53.
3. Vajda S et al. New Additions to the ClusPro Server Motivated by CAPRI doi:10.1002/prot.25219
4. Antunes DA et al. DINC 2.0: A New Protein–Peptide Docking Webserver Using an Incremental Approach. *Cancer Res.* 2017;77(21):e55–e57.
5. Páll S, Abraham MJ, Kutzner C, Hess B, Lindahl E. Tackling Exascale Software Challenges in Molecular Dynamics Simulations with GROMACS. In: Springer, Cham; 2015:3–27
6. Schmid N et al. Definition and testing of the GROMOS force-field versions 54A7 and 54B7. *Eur. Biophys. J.* 2011;40(7):843–856.
7. Hess B, Bekker H, Berendsen HJC, Fraaije JGEM. LINCS: A linear constraint solver for molecular simulations. *J. Comput. Chem.* 1997;18(12):1463–1472.
8. Bussi G, Donadio D, Parrinello M. Canonical sampling through velocity rescaling. *J. Chem. Phys.* 2007;126(1):014101.
9. Parrinello M, Rahman A. Polymorphic transitions in single crystals: A new molecular dynamics method. *J. Appl. Phys.* 1981;52(12):7182–7190.
10. Essmann U et al. A smooth particle mesh Ewald method. *J. Chem. Phys.* 1995;103(19):8577–8593.

11. Schrodinger LLC. The PyMOL Molecular Graphics System, Version 1.82015;
12. Wernet P et al. The Structure of the First Coordination Shell in Liquid Water. *Science (80-.).* 2004;304(5673):995 LP – 999.
13. McGibbon RT et al. MDTraj: A Modern Open Library for the Analysis of Molecular Dynamics Trajectories. *Biophys. J.* 2015;109(8):1528–1532.
14. Shukla SA et al. Comprehensive analysis of cancer-associated somatic mutations in class I HLA genes. *Nat. Biotechnol.* 2015;33(11):1152–1158.
15. Scholtalbers J et al. TCLP: an online cancer cell line catalogue integrating HLA type, predicted neo-epitopes, virus and gene expression. *Genome Med.* 2015;7(1):118.
16. IHWG FRED HUTCH Cell Lines & Genes [Internet]https://www.fredhutch.org/en/labs/clinical/projects/ihwg/cell-lines-genes.html. cited March 4, 2018
17. Milner E et al. The Effect of Proteasome Inhibition on the Generation of the Human Leukocyte Antigen (HLA) Peptidome. *Mol. Cell. Proteomics* 2013;12(7):1853–1864.
18. Bassani-Sternberg M et al. Soluble plasma HLA peptidome as a potential source for cancer biomarkers. *Proc. Natl. Acad. Sci.* 2010;107(44):18769–18776.
19. Ishihama Y, Rappsilber J, Andersen JS, Mann M. Microcolumns with self-assembled particle frits for proteomics.. *J. Chromatogr. A* 2002;979(1–2):233–9.
20. Cox J, Mann M. MaxQuant enables high peptide identification rates, individualized p.p.b.-range mass accuracies and proteome-wide protein quantification. *Nat. Biotechnol.* 2008;26(12):1367–1372.
21. UniProt: a worldwide hub of protein knowledge. *Nucleic Acids Res.* 2019;47(D1):D506–D515.
22. Cox J et al. Andromeda: A Peptide Search Engine Integrated into the MaxQuant Environment. *J. Proteome Res.* 2011;10(4):1794–1805.
23. Riaz N et al. Tumor and Microenvironment Evolution during Immunotherapy with Nivolumab. *Cell* 2017;171(4):934-949.e16.
24. Steff A-M, Fortin M, Arguin C, Hugo P. Detection of a decrease in green fluorescent protein fluorescence for the monitoring of cell death: An assay amenable to high-throughput screening technologies. *Cytometry* 2001;45(4):237–243.
25. Bosselut R et al. Quantitative Characterization of the t Cell Receptor Repertoire of Naïve and Memory subsets Using an Integrated experimental and Computational Pipeline Which Is Robust, economical, and Versatile. *Immunol* 2017;8:1267.
26. Greiff V, Miho E, Menzel U, Reddy ST. Bioinformatic and Statistical Analysis of Adaptive Immune Repertoires. *Trends Immunol.* 2015;36(11):738–749.
27. Emerson RO et al. Immunosequencing identifies signatures of cytomegalovirus exposure history and HLA-mediated effects on the T cell repertoire. *Nat. Genet.* 2017;49(5):659–665.
28. Sethna Z, Elhanati Y, Callan CG, Walczak AM, Mora T. OLGA: fast computation of generation probabilities of B- and T-cell receptor amino acid sequences and motifs.. *Bioinformatics* 2019;35(17):2974–2981.
29. DeWitt WS et al. Human T cell receptor occurrence patterns encode immune history, genetic background, and receptor specificity. *Elife* 2018;7. doi:10.7554/eLife.38358
30. Zhao Y et al. High-efficiency transfection of primary human and mouse T lymphocytes using RNA electroporation. *Mol. Ther.* 2006;13(1):151–159.
31. Cohen CJ, Zhao Y, Zheng Z, Rosenberg SA, Morgan RA. Enhanced antitumor activity of murine-human hybrid T-cell receptor (TCR) in human lymphocytes is associated with improved pairing and TCR/CD3 stability. *Cancer Res.* 2006;66(17):8878–8886.
32. He L et al. A sensitive flow cytometry-based cytotoxic T-lymphocyte assay through detection of cleaved caspase 3 in target cells. *J. Immunol. Methods* 2005;304(1–2):43–59.
33. Lu Y-C et al. Mutated PPP1R3B is recognized by T cells used to treat a melanoma patient

who experienced a durable complete tumor regression.. *J. Immunol.* 2013;190(12):6034–42.

Supplementary Figures

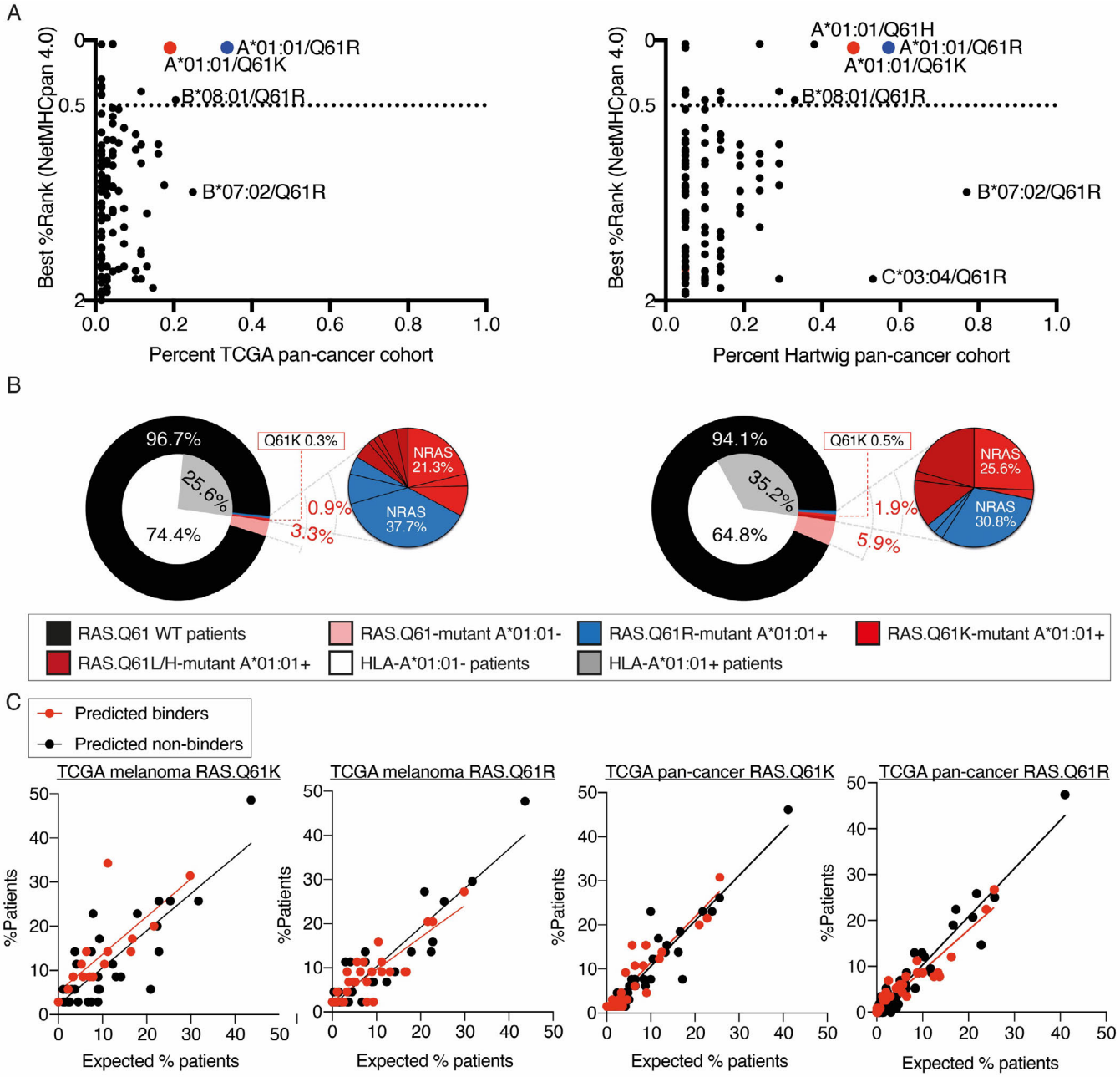

Supplementary figure 1: Additional aspects of patient-cohorts RAS.Q61/HLA data-analysis
(A) X axis: percent of patients with HLA/RAS.Q61 combination in pan-cancer patient cohorts. Y axis: NetMHCpan 4.0 binding predictions best %Rank. %Rank ≤0.5 are considered strong binders; 0.5<%Rank≤2 are considered weak binders. Left – TCGA; right - Hartwig. **(B)** Frequency of A*01:01/RAS.Q61-mutant combinations in pan-cancer cohorts. Left – TCGA; Right – Hartwig. **(C)** Expexted vs. actual HLA frequencies in the TCGA cohort. Comparison of TCGA HLA-allele frequencies between RAS.Q61-mutant and -wild-type melanoma patients did not reveal significant prevalence skews (Fisher's exact test with false-discovery-rate (FDR) correction, see also table S1).

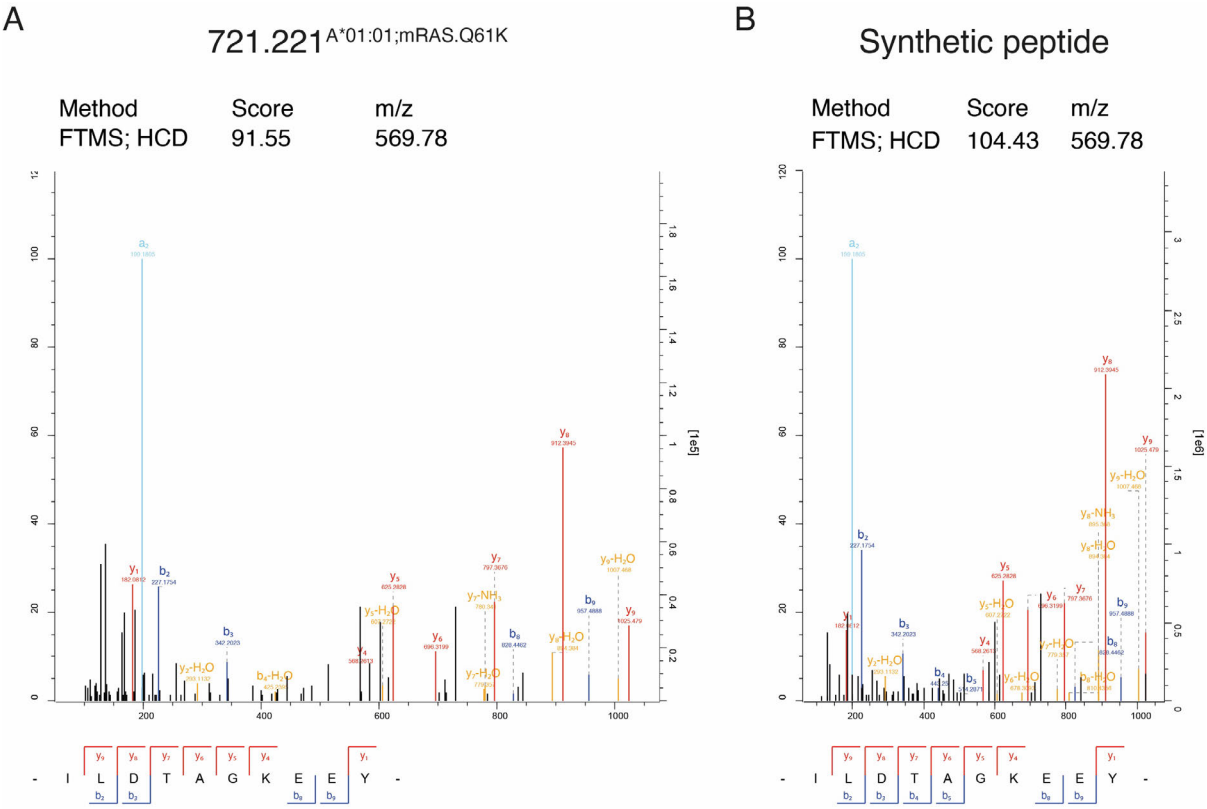

Supplementary figure 2: Tandem mass spectra of the ILDTAG<u>K</u>EEY neopeptide. (A) As it was identified in discovery-mode HLA-peptidomics of mono-allelic 721.221$^{A*01:01;mRAS.Q61K}$ cells overexpressing HLA-allele A*01:01 and the RAS.Q61K minigene. **(B)** Synthetic peptide validation. Images were produced using the MaxQuant software.

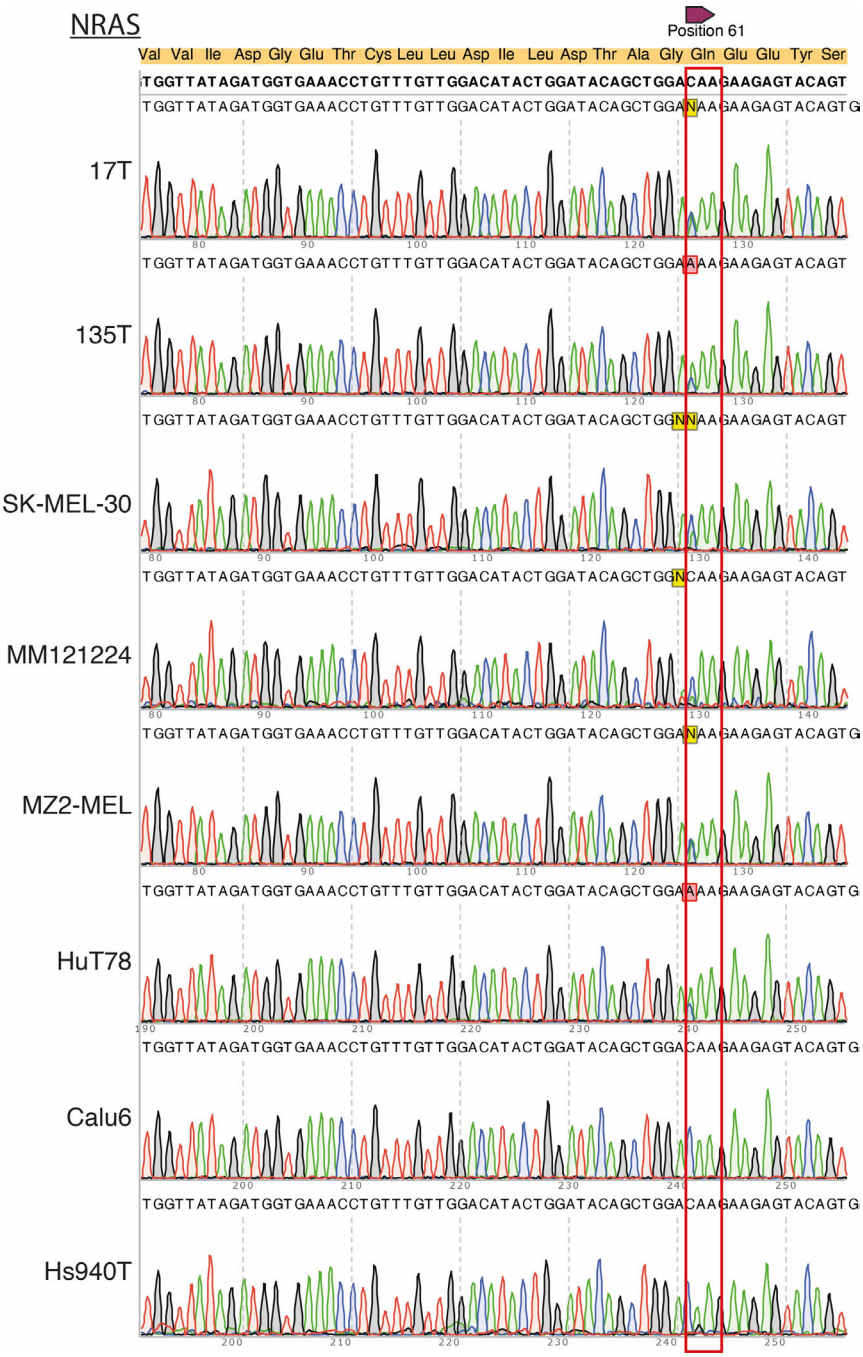

Supplementary figure 3: NRAS.Q61K mutation is expressed in NRAS mutant tumor cell-lines harboring HLA-A*01:01. The area surrounding position 61 was sequenced from extracted cDNA, to examine if the mutated allele of the gene is expressed. Calu6 is NRAS wild-type (KRAS.Q61 mutant), Hs940T is NRAS.Q61R.

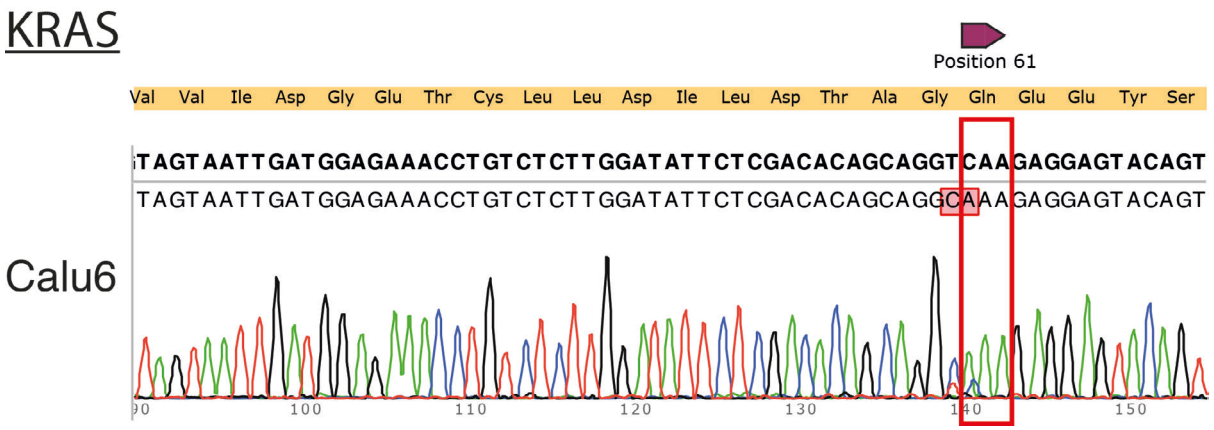

Supplementary figure 4: KRAS.Q61K mutation is expressed in KRAS-mutant lung adenocarcinoma cell-line Calu6, harboring the HLA-A*01:01 allele. cDNA was extracted from Calu6 cells, and the area surrounding position 61 was Sanger sequenced.

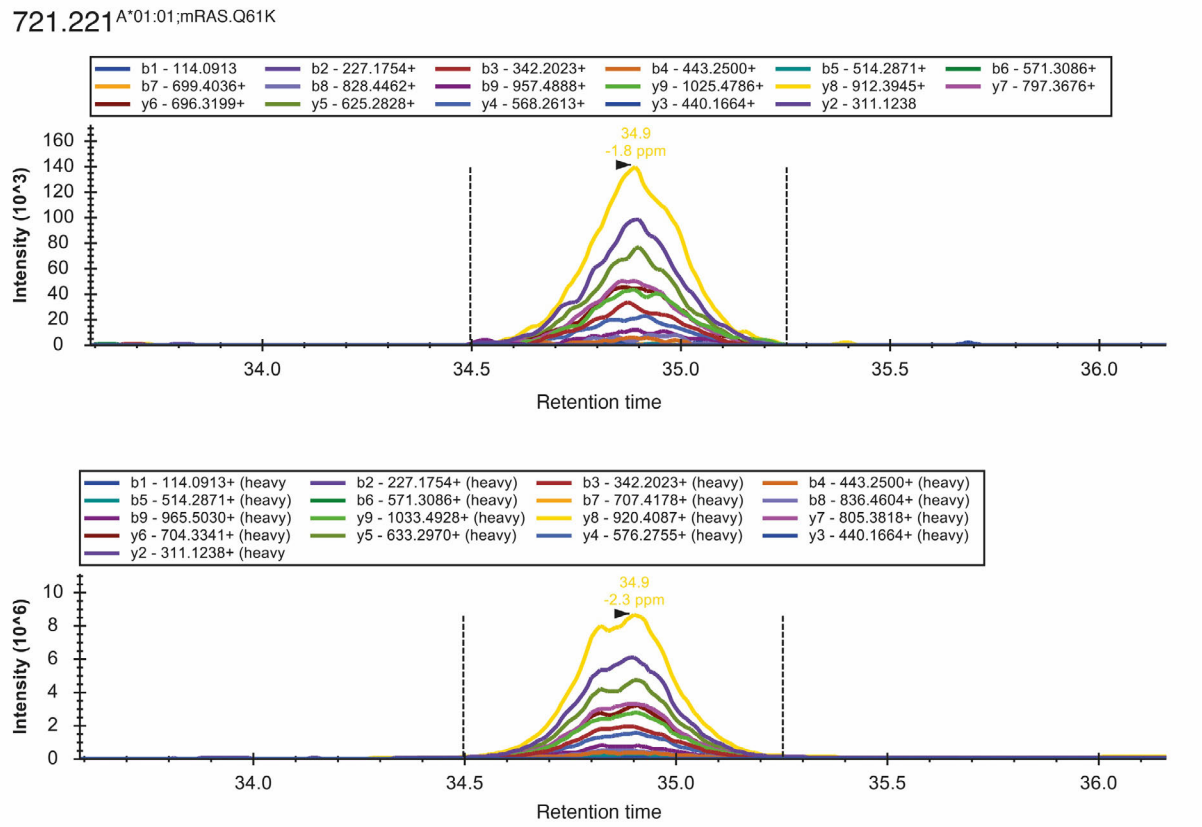

Supplementary figure 5: Overlaid extracted ion chromatograms for both endogenous and heavy-peptide spike-in *ILDTAG<u>K</u>EEY* peptides, as they were identified in targeted HLA-peptidomics of 721.221 B-LCL overexpressing both HLA allele and a 25-mer RAS.Q61K minigene. Images were produced using the Skyline software.

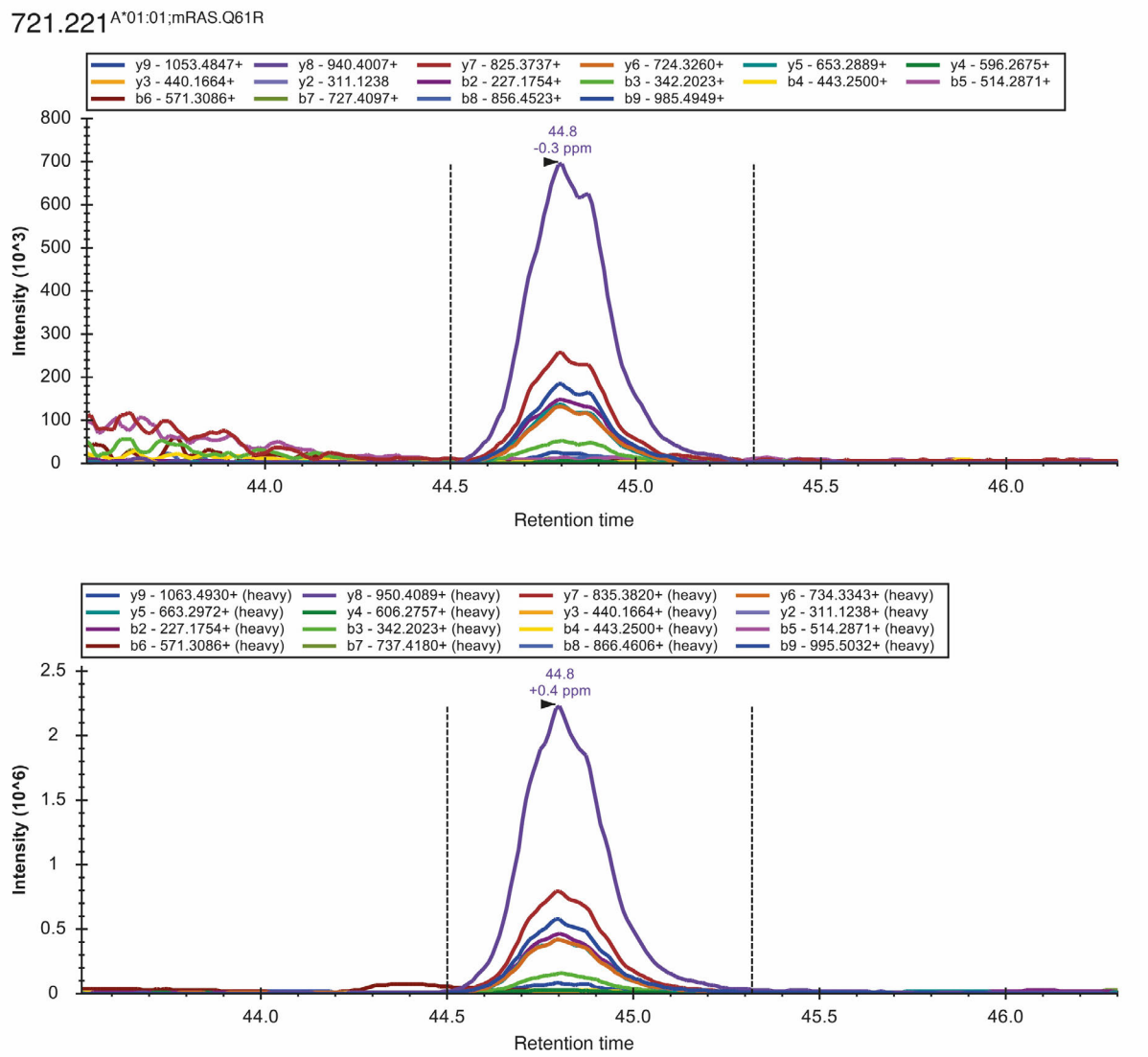

Supplementary figure 6: Overlaid extracted ion chromatograms for both endogenous and heavy-peptide spike-in *ILDTAGREEY* peptides, as they were identified in targeted HLA-peptidomics of 721.221 B-LCL overexpressing both HLA allele and a 25-mer RAS.Q61R minigene. Images were produced using the Skyline software.

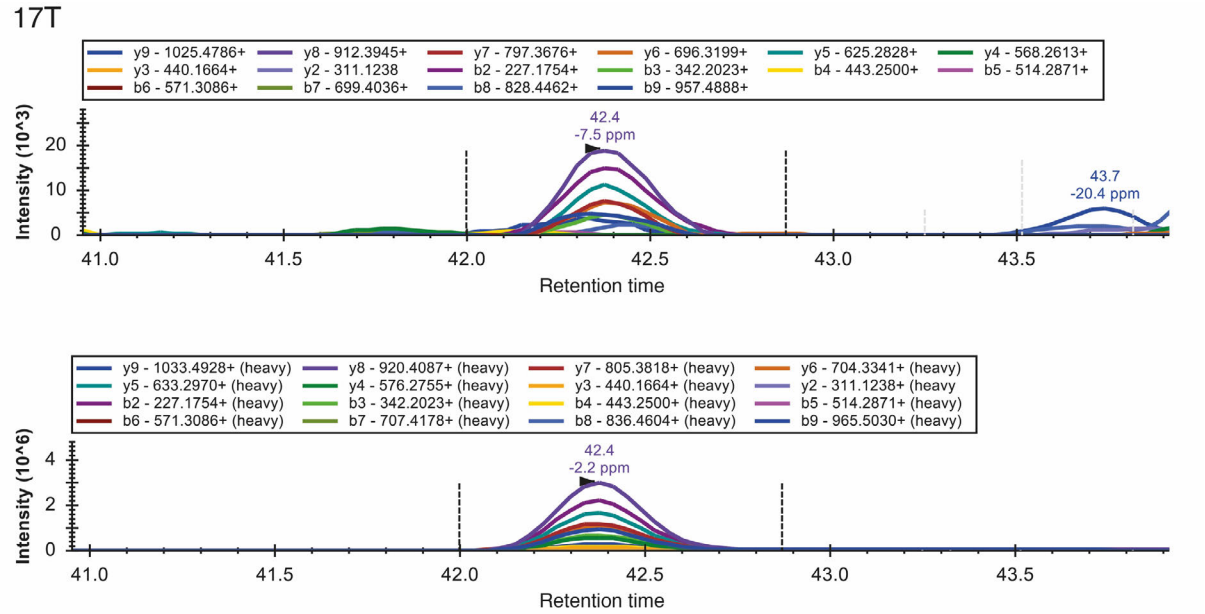

Supplementary figure 7: Overlaid extracted ion chromatograms for both endogenous and heavy-peptide spike-in *ILDTAG<u>K</u>EEY* peptides, as they were identified in targeted HLA-peptidomics of the 17T melanoma cell-line bearing the HLA A*01:01/NRAS.Q61K combination. Images were produced using the Skyline software.

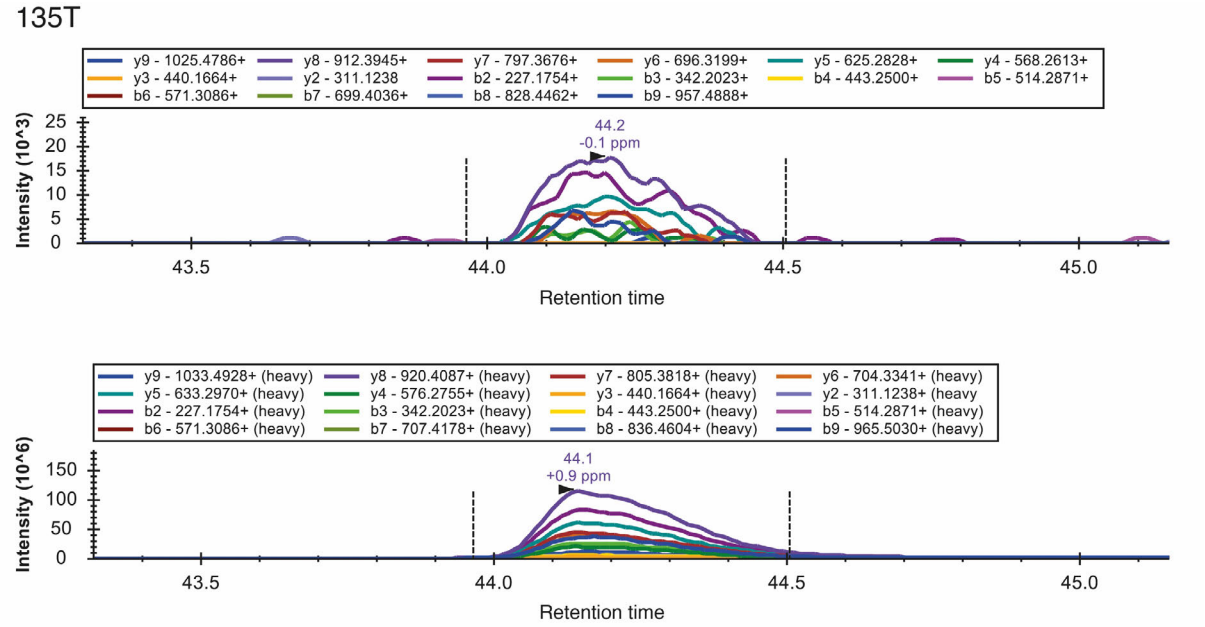

Supplementary figure 8: Overlaid extracted ion chromatograms for both endogenous and heavy-peptide spike-in *ILDTAG<u>K</u>EEY* peptides, as they were identified in targeted HLA-peptidomics of the 135T melanoma cell-line bearing the HLA A*01:01/NRAS.Q61K combination. Images were produced using the Skyline software.

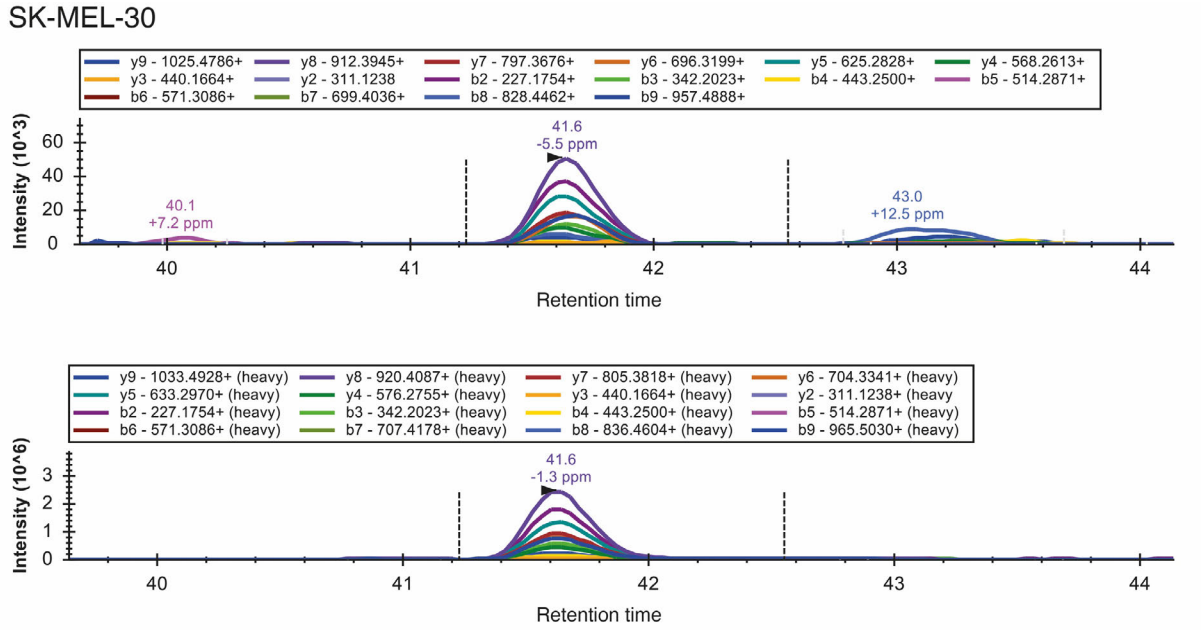

Supplementary figure 9: Overlaid extracted ion chromatograms for both endogenous and heavy-peptide spike-in *ILDTAGKEEY* peptides, as they were identified in targeted HLA-peptidomics of the SK-MEL-30 melanoma cell-line bearing the HLA A*01:01/NRAS.Q61K combination. Images were produced using the Skyline software.

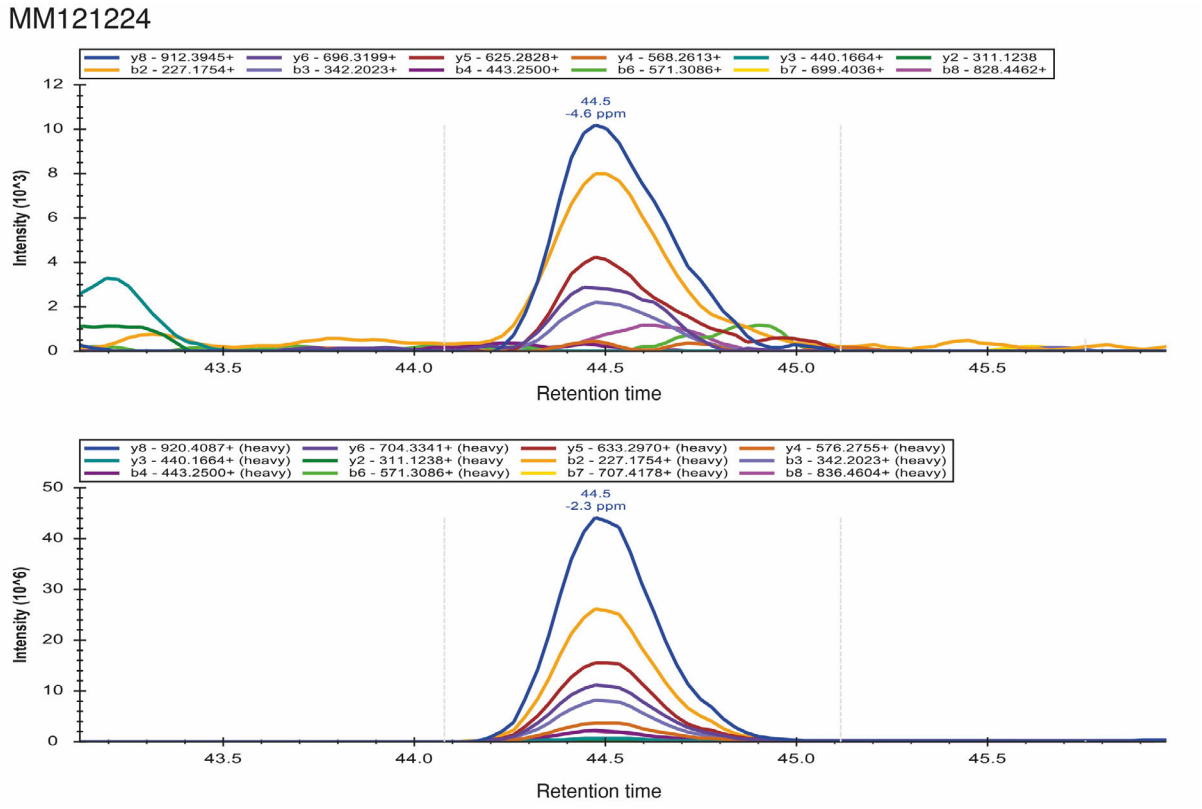

Supplementary figure 10: Overlaid extracted ion chromatograms for both endogenous and heavy-peptide spike-in *ILDTAGKEEY* peptides, as they were identified in targeted HLA-peptidomics of the MM121224 melanoma cell-line bearing the HLA A*01:01/NRAS.Q61K combination. Images were produced using the Skyline software.

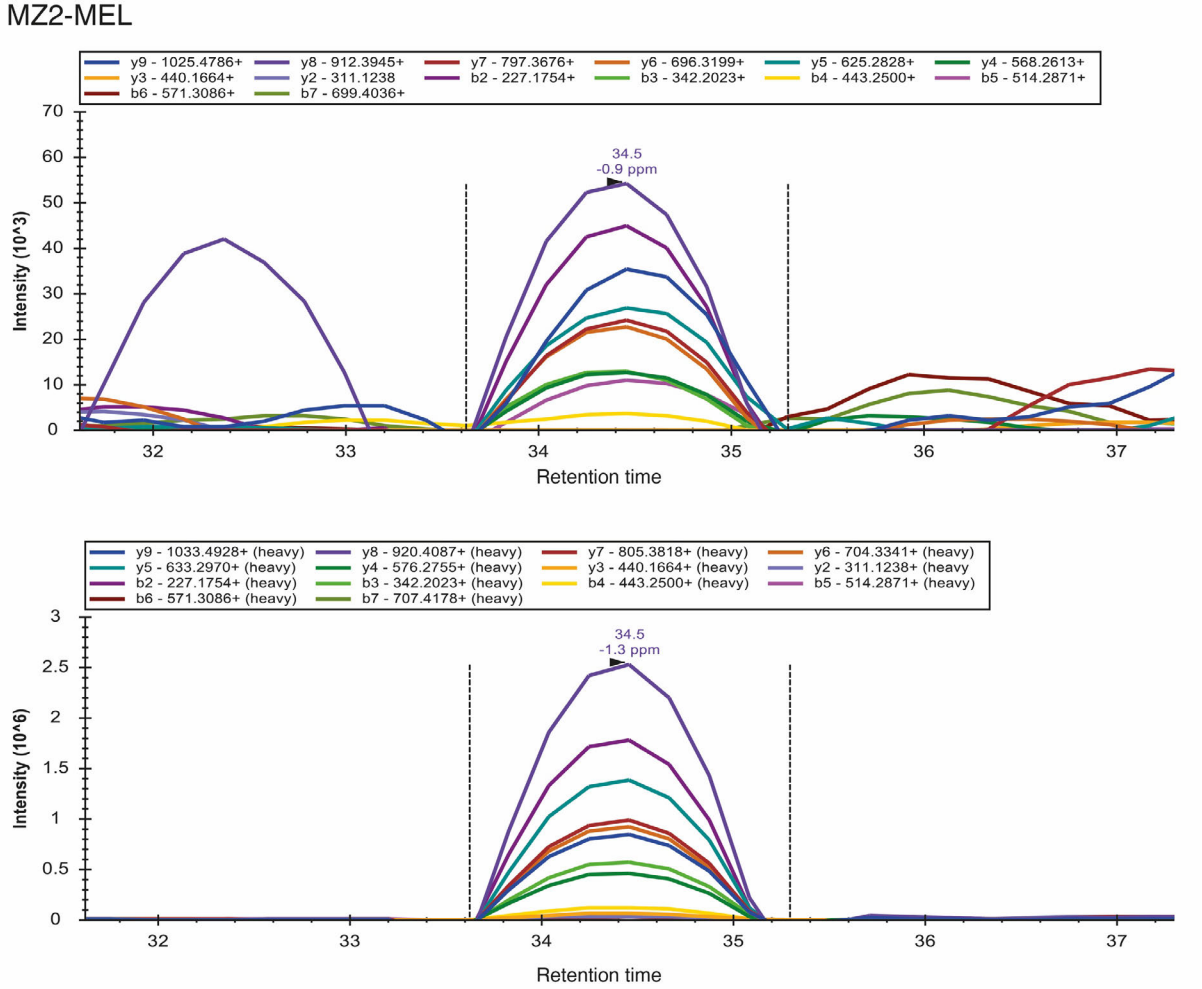

Supplementary figure 11: Overlaid extracted ion chromatograms for both endogenous and heavy-peptide spike-in *ILDTAGKEEY* peptides, as they were identified in targeted HLA-peptidomics of the MZ2-MEL melanoma cell-line bearing the HLA A*01:01/NRAS.Q61K combination. Images were produced using the Skyline software.

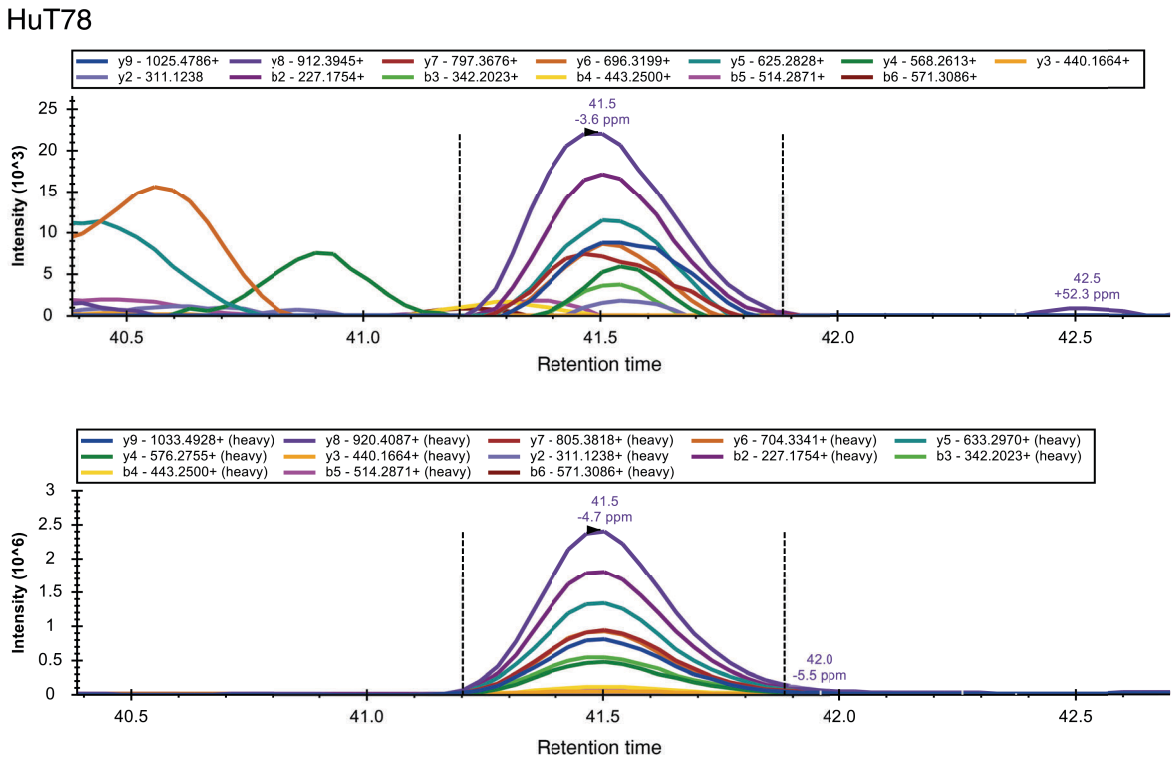

Supplementary figure 12: Overlaid extracted ion chromatograms for both endogenous and heavy-peptide spike-in *ILDTAG<u>K</u>EEY* peptides, as they were identified in targeted HLA-peptidomics of the HuT78 cutaneous T-cell lymphoma cell-line bearing the HLA A*01:01/NRAS.Q61K combination. Images were produced using the Skyline software.

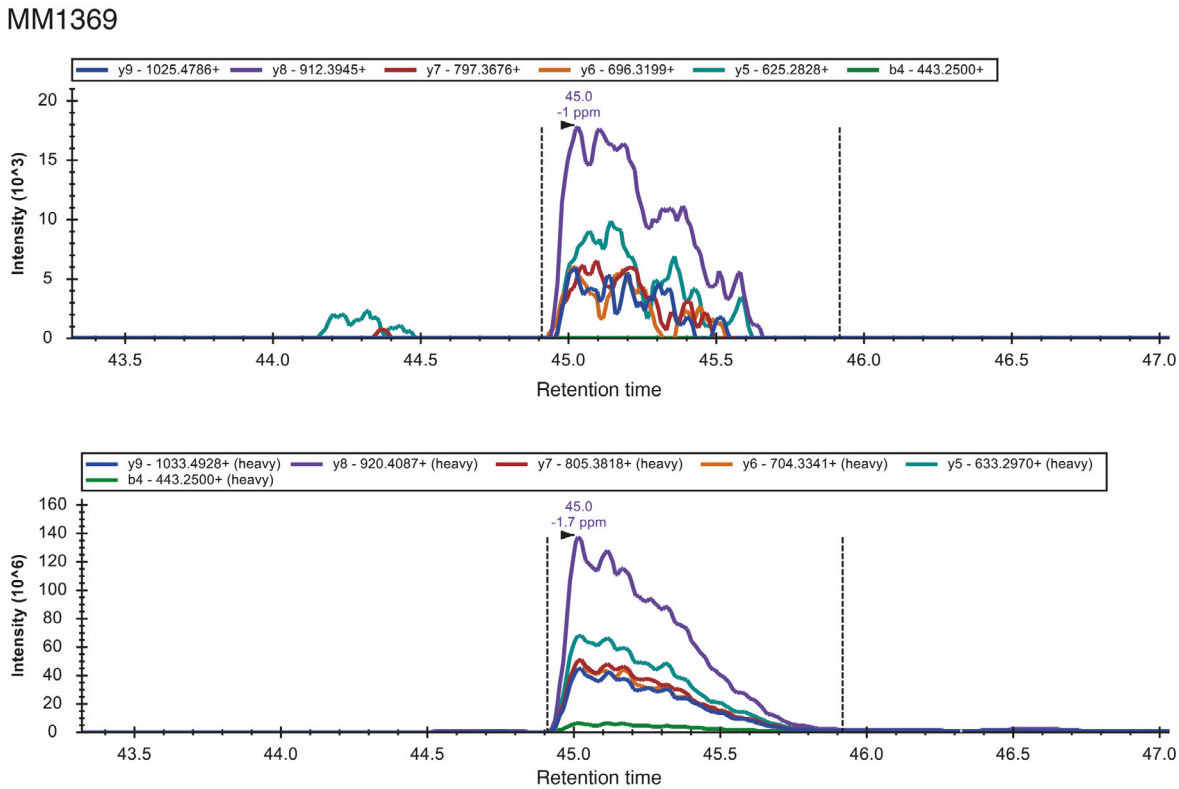

Supplementary figure 13: Overlaid extracted ion chromatograms for both endogenous and heavy-peptide spike-in *ILDTAG<u>K</u>EEY* peptides, as they were identified in targeted HLA-peptidomics of the MM1369 melanoma tumor bearing the HLA A*01:01/NRAS.Q61K combination. Images were produced using the Skyline software.

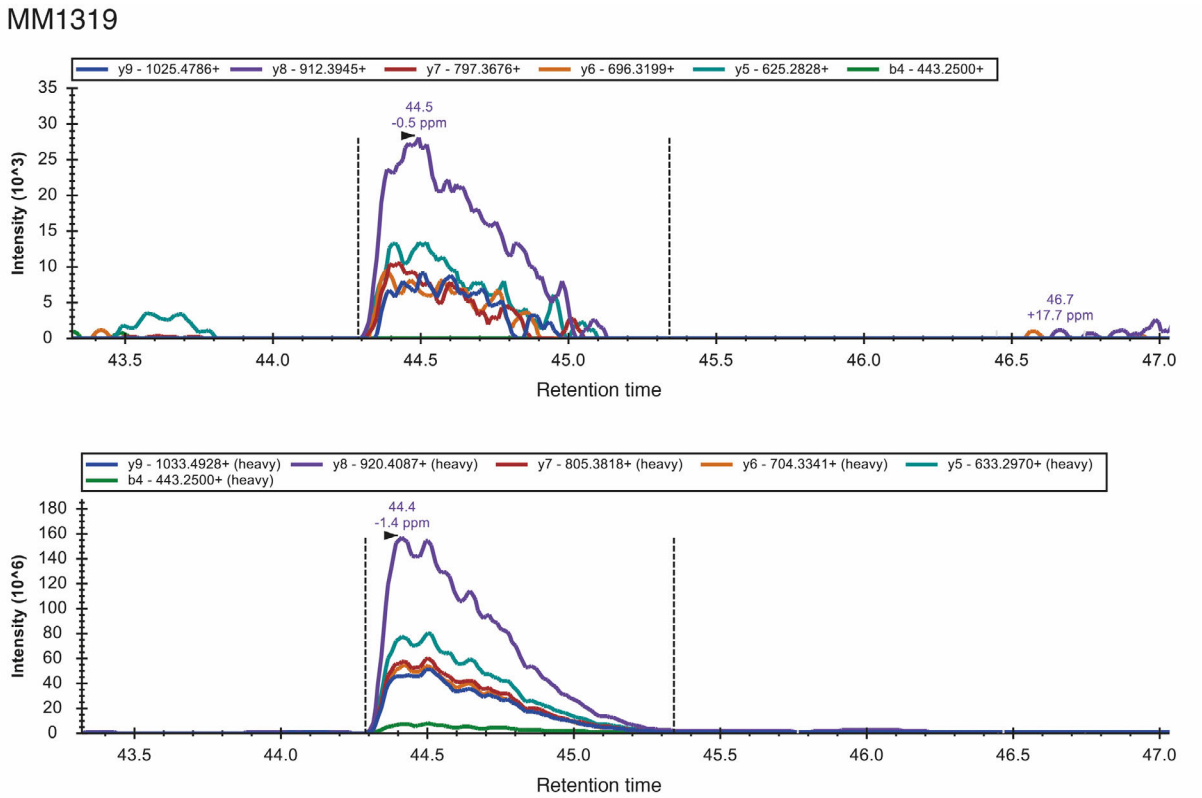

Supplementary figure 14: Overlaid extracted ion chromatograms for both endogenous and heavy-peptide spike-in *ILDTAGKEEY* peptides, as they were identified in targeted HLA-peptidomics of the MM1319 melanoma tumor bearing the HLA A*01:01/NRAS.Q61K combination. Images were produced using the Skyline software.

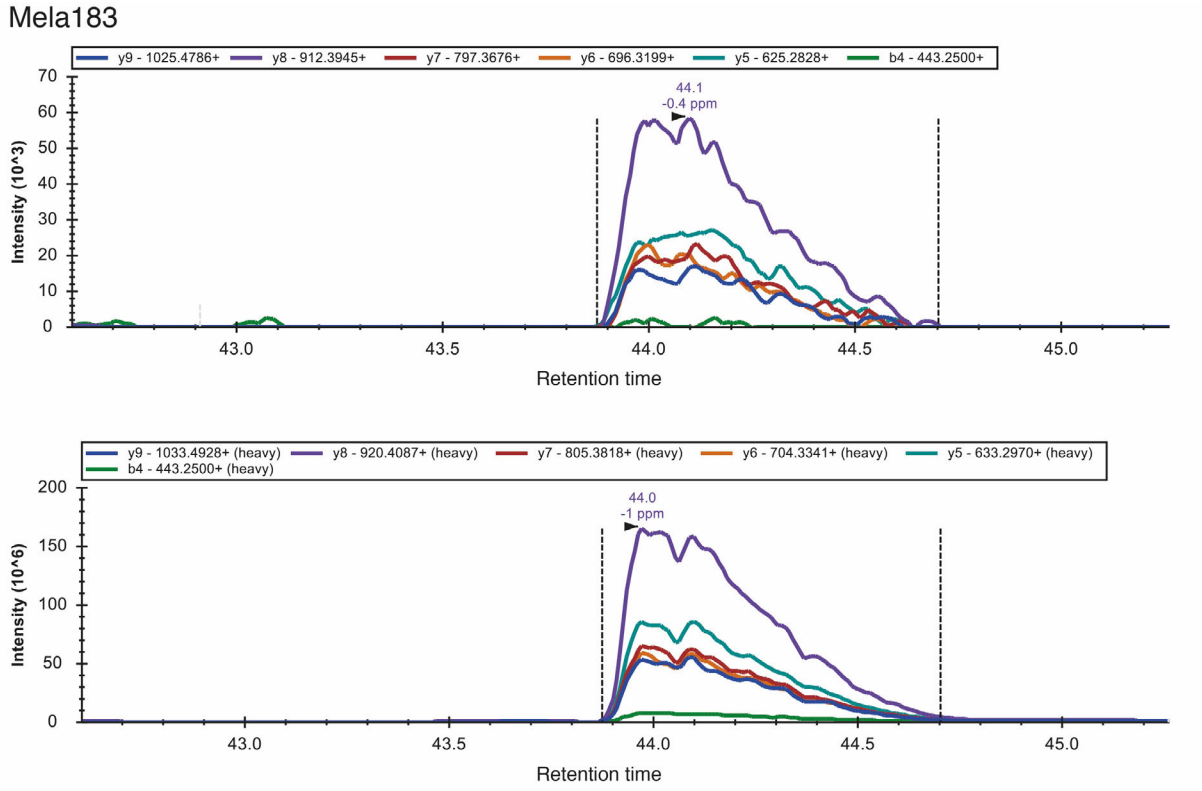

Supplementary figure 15: Overlaid extracted ion chromatograms for both endogenous and heavy-peptide

spike-in *ILDTAGKEEY* peptides, as they were identified in targeted HLA-peptidomics of the Mela183 melanoma tumor bearing the HLA A*01:01/NRAS.Q61K combination. Images were produced using the Skyline software.

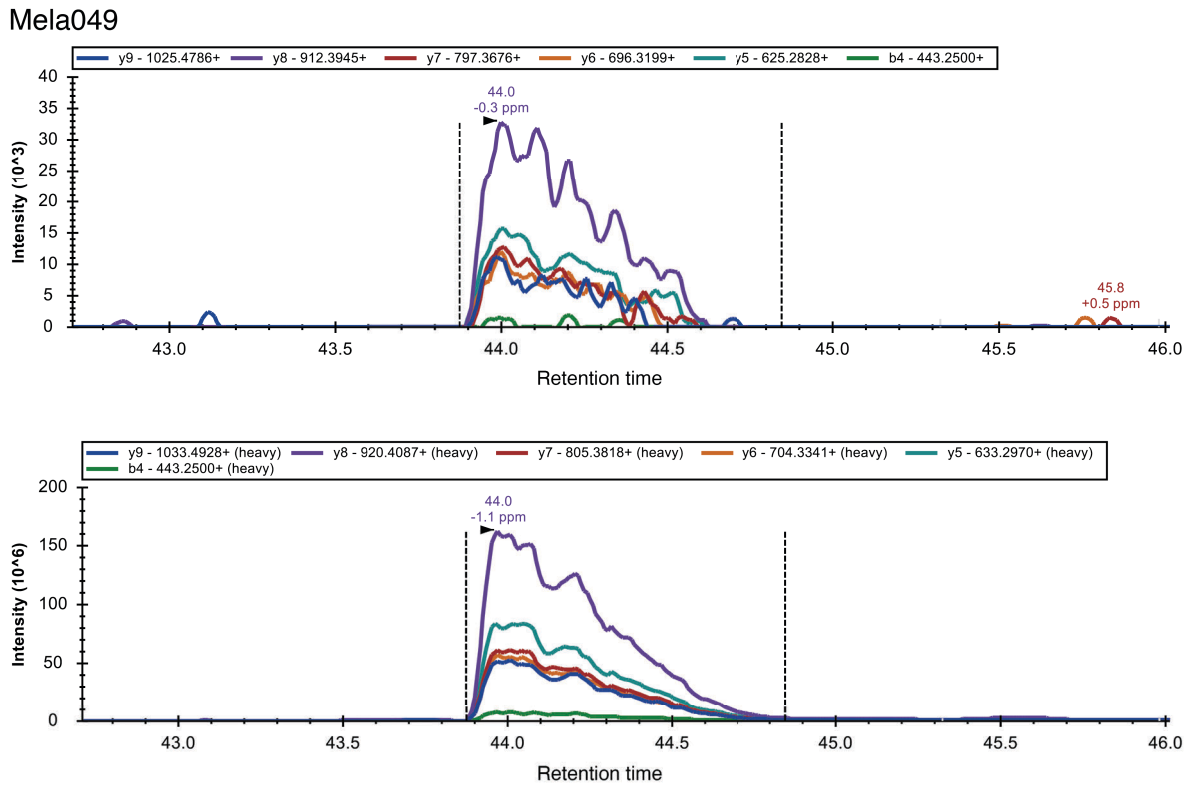

Supplementary figure 16: Overlaid extracted ion chromatograms for both endogenous and heavy-peptide spike-in *ILDTAGKEEY* peptides, as they were identified in targeted HLA-peptidomics of the Mela049 melanoma tumor bearing the HLA A*01:01/NRAS.Q61K combination. Images were produced using the Skyline software.

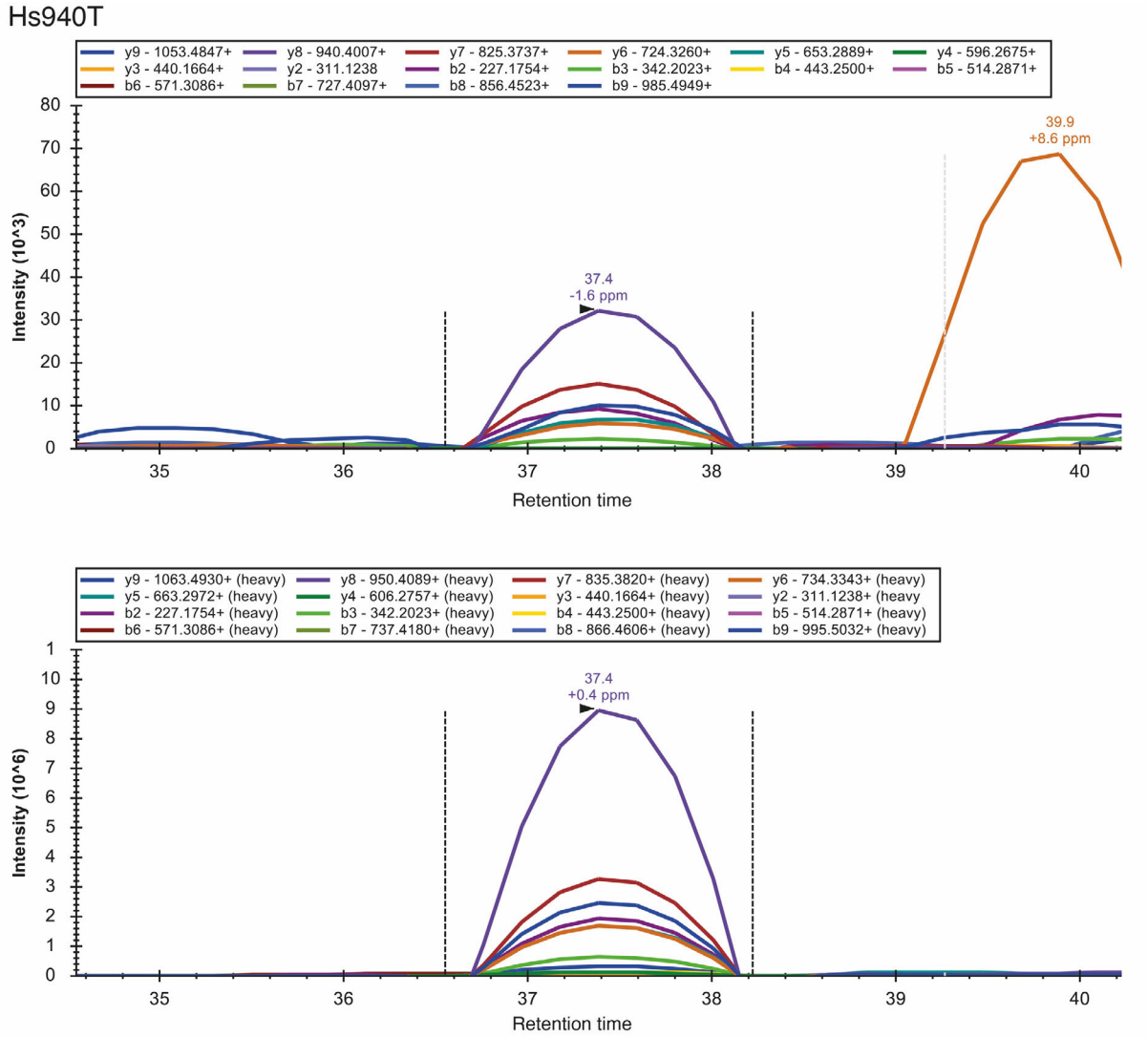

Supplementary figure 17: Overlaid extracted ion chromatograms for both endogenous and heavy-peptide spike-in *ILDTAGREEY* peptides, as they were identified in targeted HLA-peptidomics of the Hs940T melanoma tumor bearing the HLA A*01:01/NRAS.Q61R combination. Images were produced using the Skyline software.

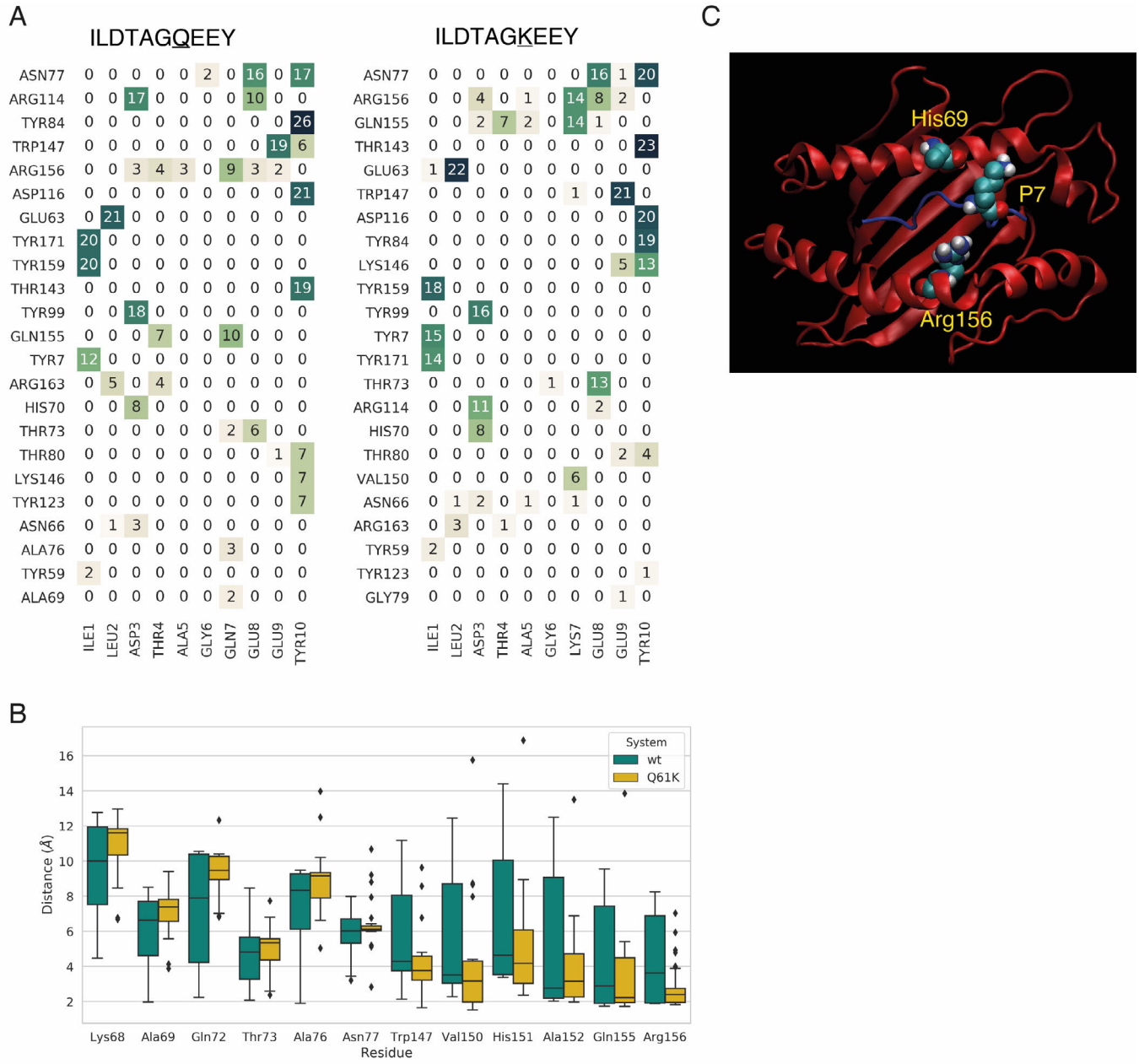

Supplementary figure 18: P7 residue is free to interact with T-cell receptors according to predictions. (A) Hydrogen-bonding interactions between RAS neo-peptides ILDTAGQEEY (wild-type) and ILDTAGKEEY (mutant) and HLA-A*01:01 in cluster centroid structures. Values shown are counts of the number of hydrogen-bonding interactions formed between a given peptide residue (horizontal axis) and a HLA residue (vertical axis). HLA residues shown on the vertical axis are ordered by the total count of hydrogen interactions made with each residue. **(B)** Boxplot depicting the minimal distance between any sidechain atom of P7 and an HLA residue. **(C)** Another view at the modeled HLA-A*01:01/ILDRAGKEEY complex. P7 sidechain faces outwards and is free to interact with the TCR.

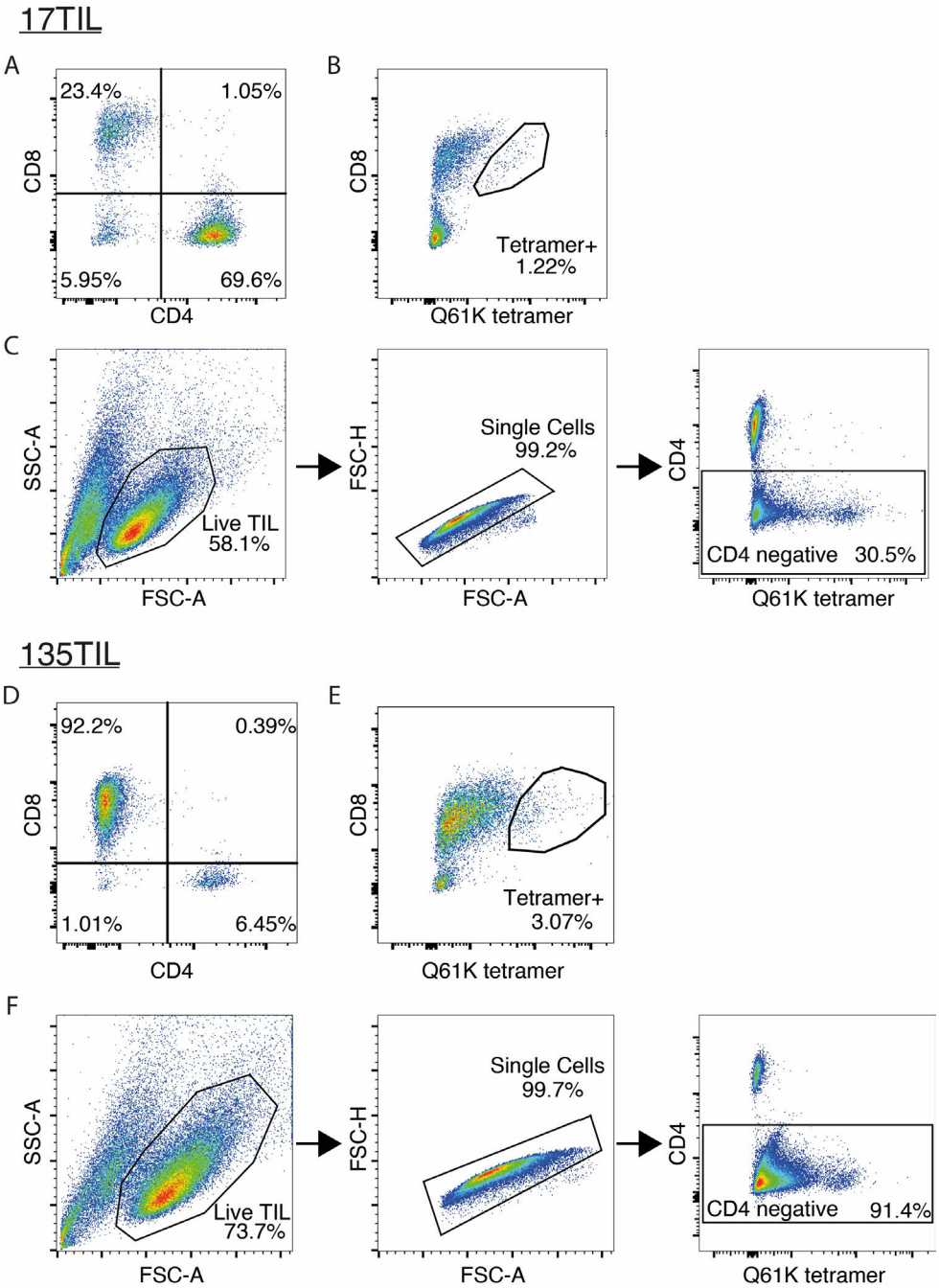

Supplementary figure 19: Flow-cytometry analysis of bulk TIL. Top – 17TIL, bottom – 135TIL. (A) and (D) CD4+/CD8+ distribution of TIL. (B-C) and (E-F) As expected, tetramer+ cells are restricted to the CD8+CD4- subpopulation. Full gating for the experiments presented in (A-B) and (D-E) can be found in supplementary figure 22.

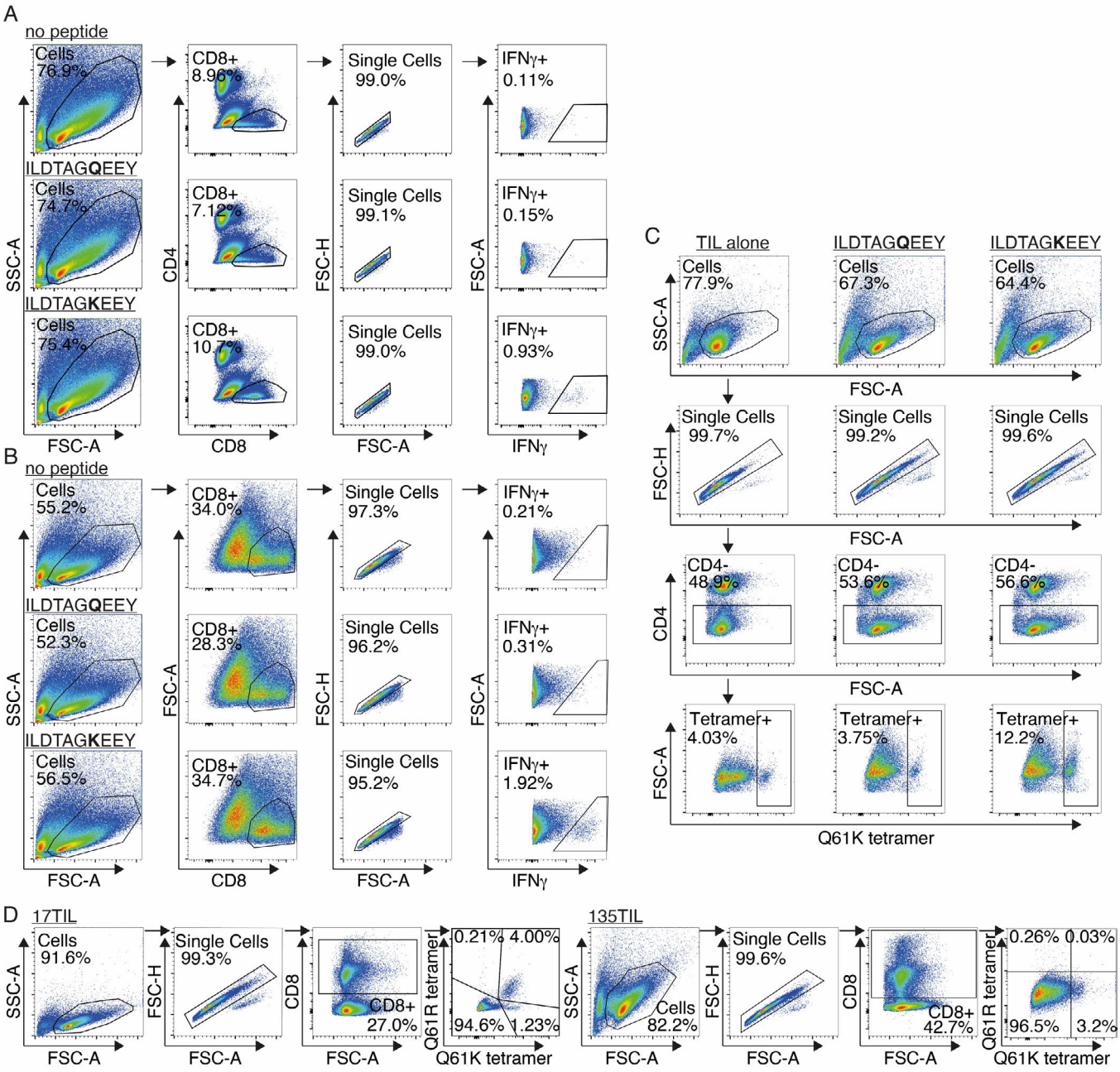

Supplementary figure 20: Gating strategy for the experiments shown in figure 3

(A) IFNγ secretion assay – 17TIL. **(B)** IFNγ secretion assay – 135TIL. **(C)** 17TIL peptide-dependent expansion assay. **(D)** TIL double stained with the Q61K and Q61R tetramers. Left – 17TIL; Right – 135TIL.

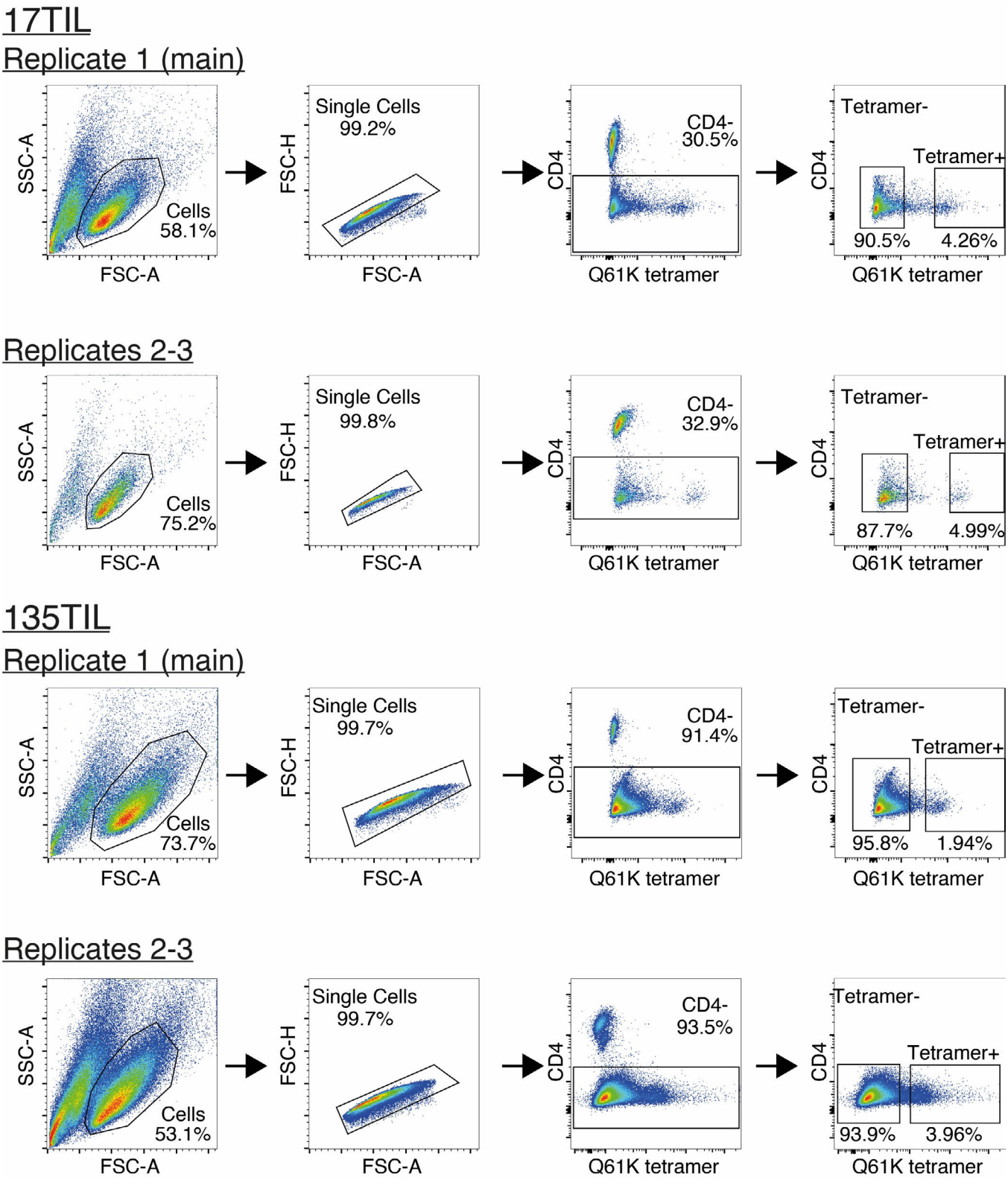

Supplementary figure 21: Tetramer-sorting for bulk TCR sequencing experiments. Top – 17TIL, bottom – 135TIL. Cells were stained with the HLA-A*01:01/*ILDTAGKEEY*-tetramer and subsequently with anti-CD4 antibody. The CD4- gate, and its Tetramer+ and Tetramer- were utilized to obtain the 'bulk CD4-', tetramer+ and tetramer- sorted populations. The second and third replicates were obtained in the same experiment, separate from the first replicate.

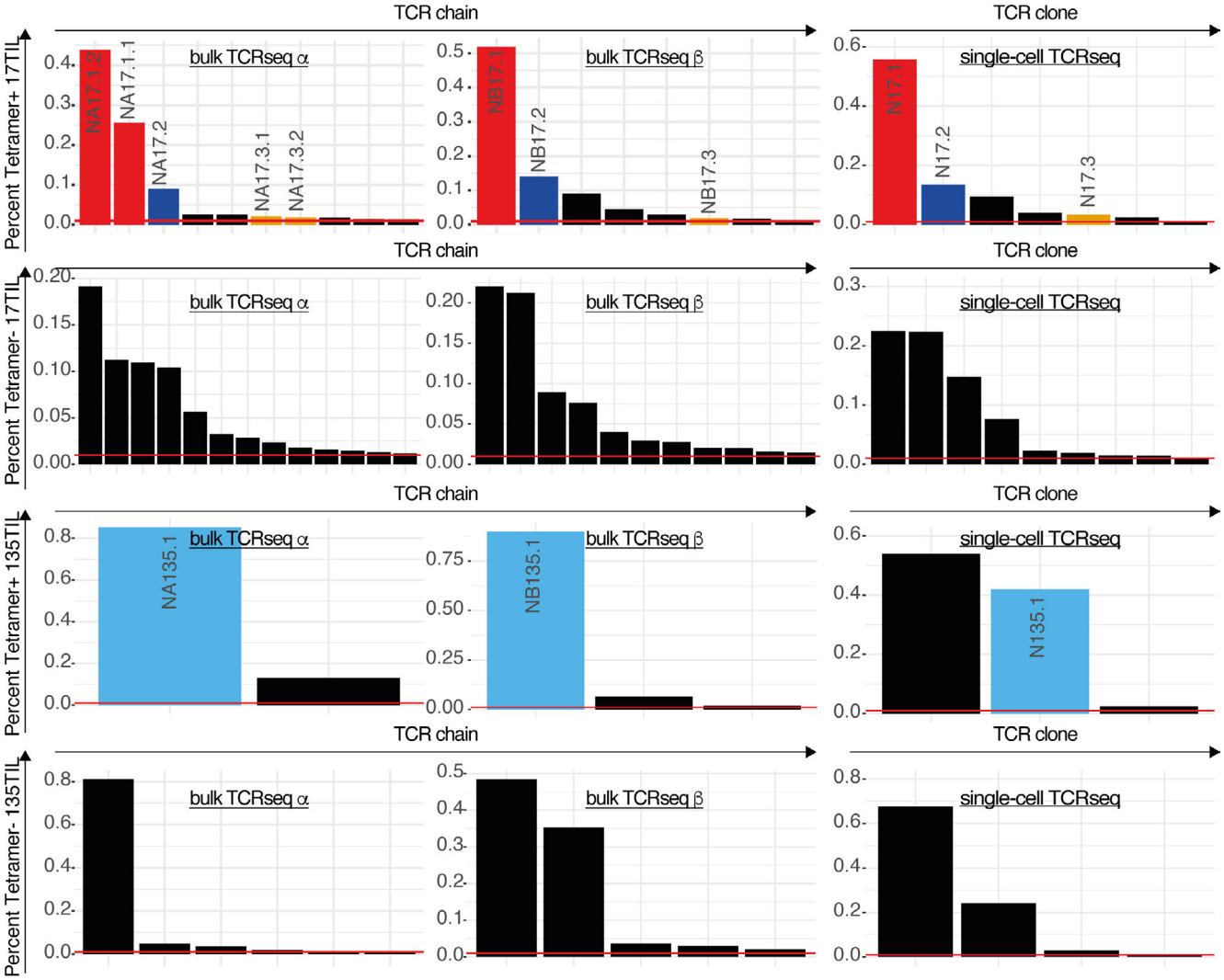

Supplementary figure 22: Tetramer+ and tetramer- 17TIL and 135TIL have oligoclonal distributions. Frequency distributions for tetramer+ and tetramer- 17TIL and 135TIL. Top panel – tetramer+ 17TIL; second panel – tetramer- 17TIL; third panel – tetramer+ 135TIL; bottom panel – tetramer- 135TIL. Left panel – TCR α and β chain frequencies from bulk TCR-sequencing; Right panel – single-cell TCR-sequencing. Only chains/clones with frequency of at least 1% are depicted. A representative of three replicates is shown for the bulk TCR-sequencing. Tetramer-specific clones/chains are colored and labeled, other clones/chains are shown in black.

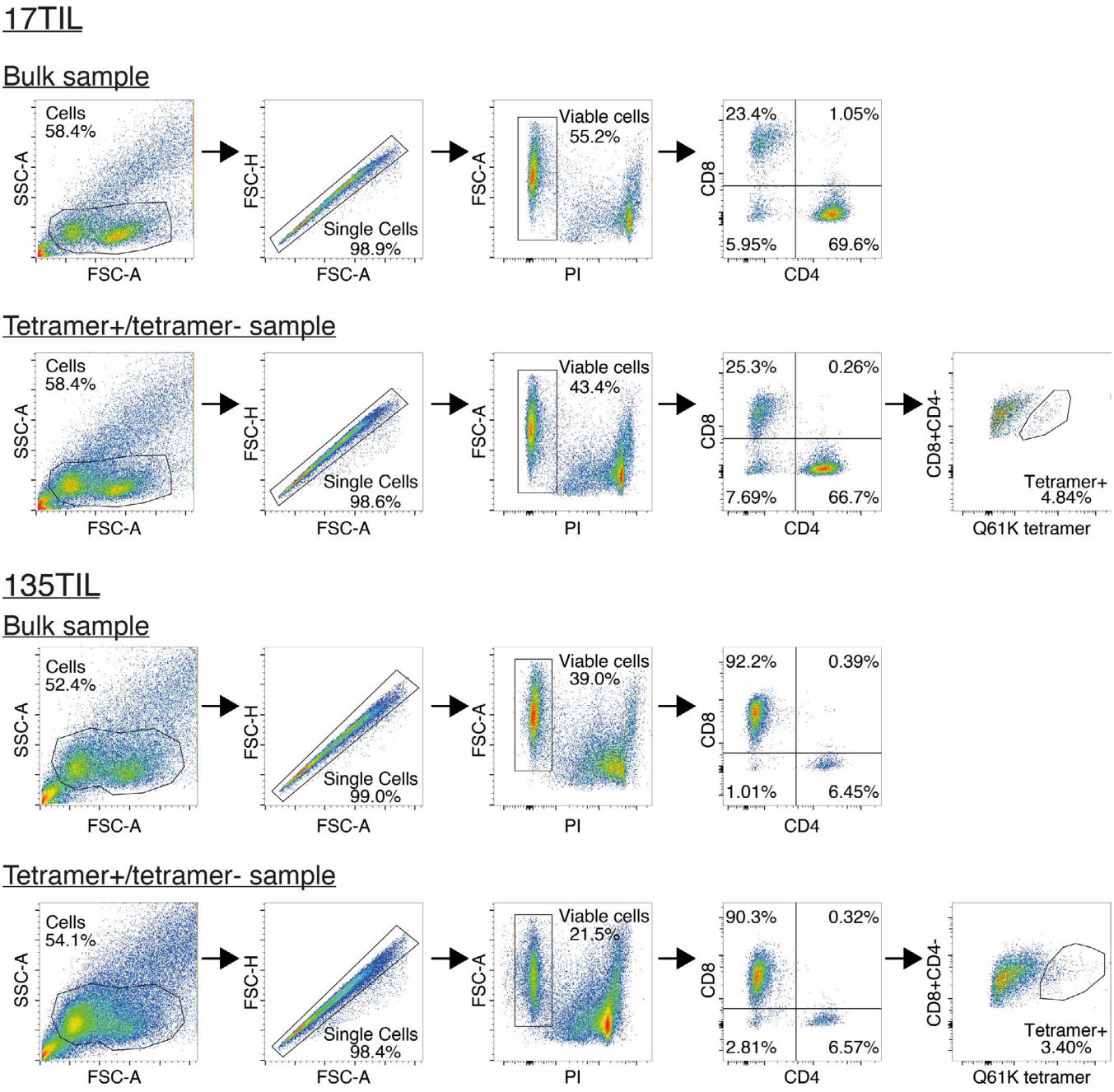

Supplementary figure 23: Tetramer-sorting for single-cells sequencing experiment. Top – 17TIL, bottom – 135TIL. In order to obtain the 'bulk CD8+' samples, bulk TIL were stained for CD8 and CD4, and the CD8+CD4- population was sorted. To obtain the tetramer+ and tetramer- subpopulations, bulk TIL samples were stained with the HLA-A*01:01/*ILDTAGKEEY*-tetramer prior to CD8/CD4 staining; tetramer+ and tetramer- populations were sorted out of CD8+CD4- cells. Proprium Iodide was used to gate on viable cells.

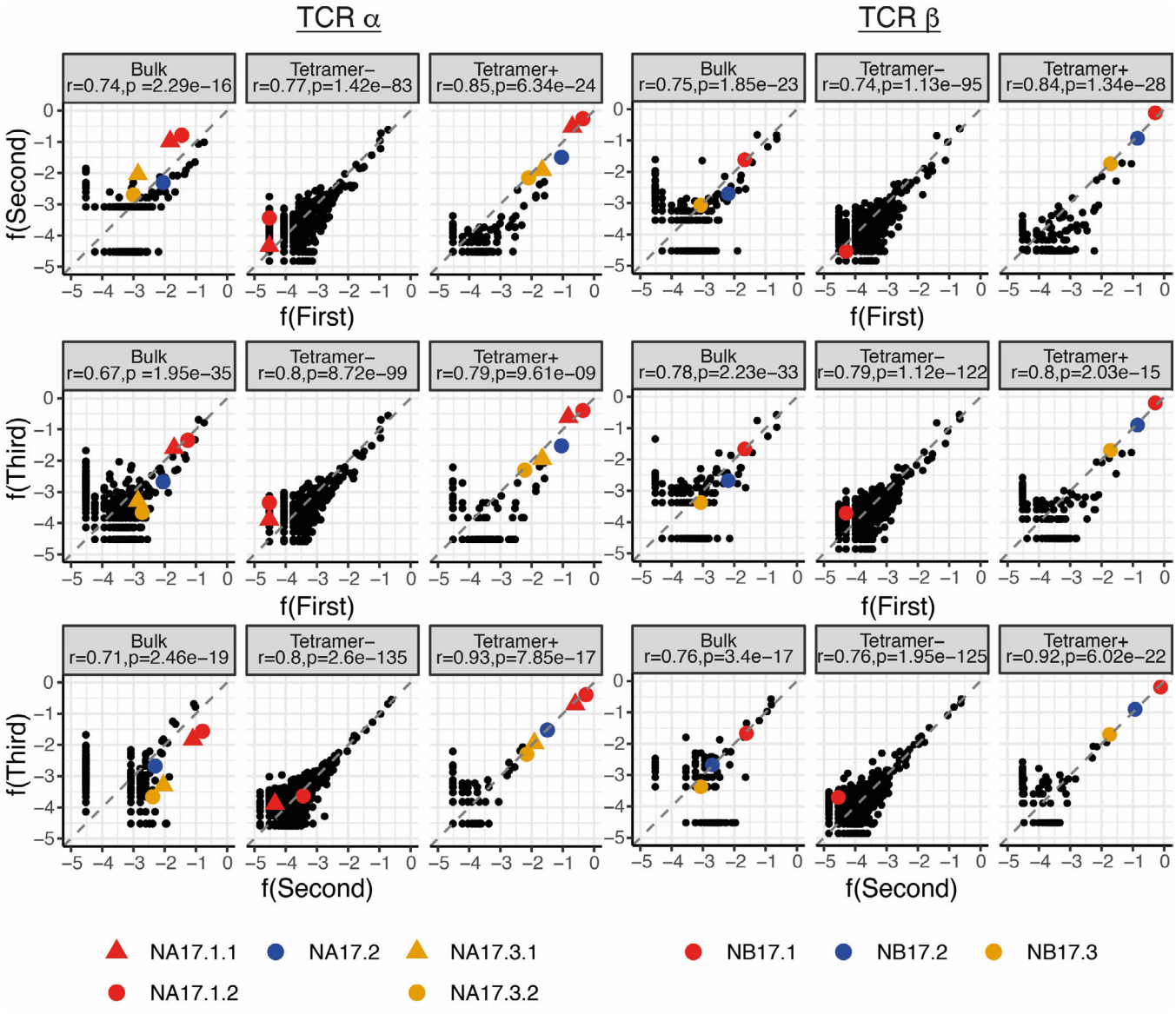

Supplementary figure 24: Comparing 17TIL TCR chain frequencies between the three bulk-TCR-sequencing replicates. Left panels – TCR α chains, right panels – TCR β chains.

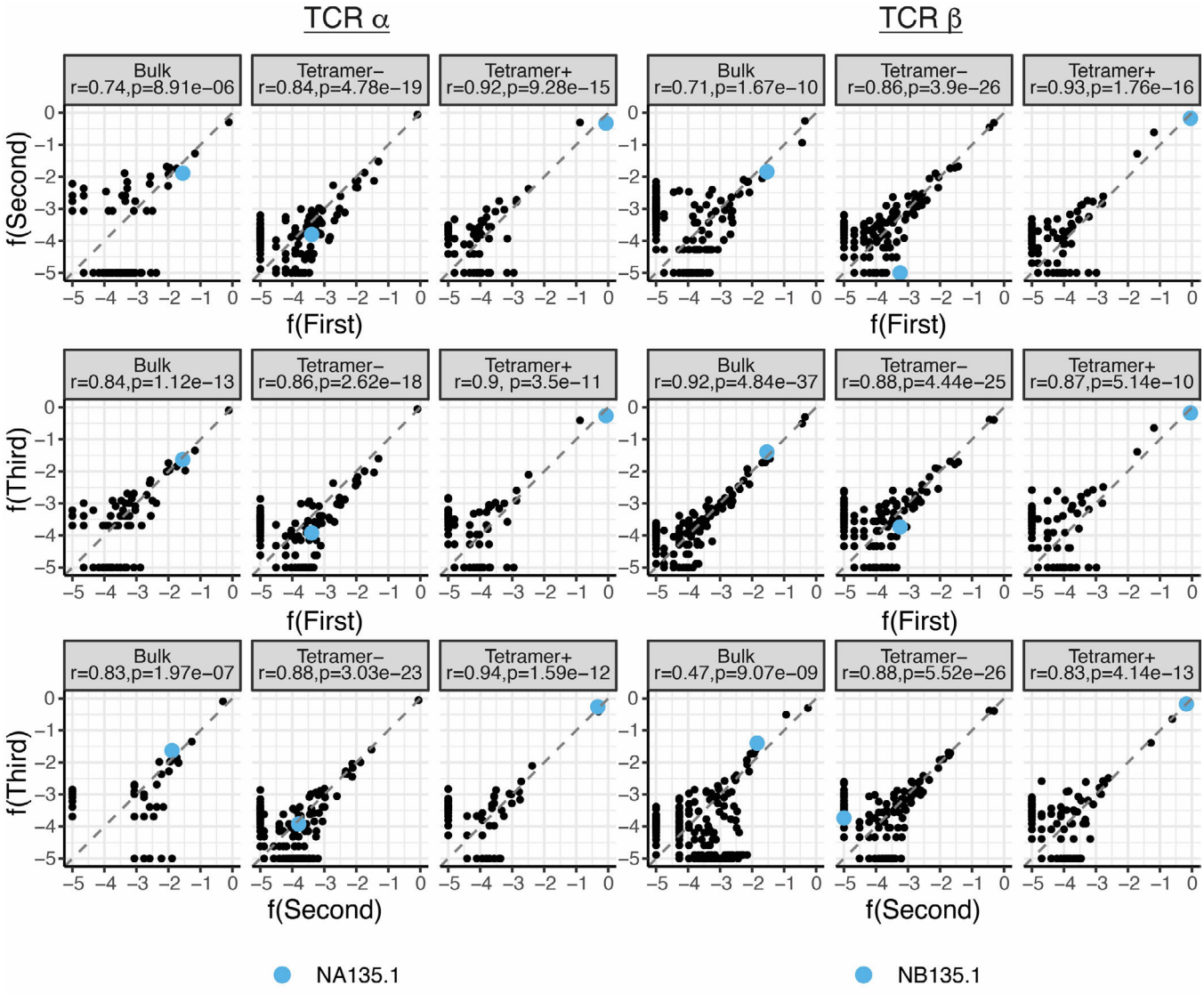

Supplementary figure 25: Comparing 135TIL TCR chain frequencies between the three bulk-TCR-sequencing replicates. Left panels – TCR α chains, right panels – TCR β chains.

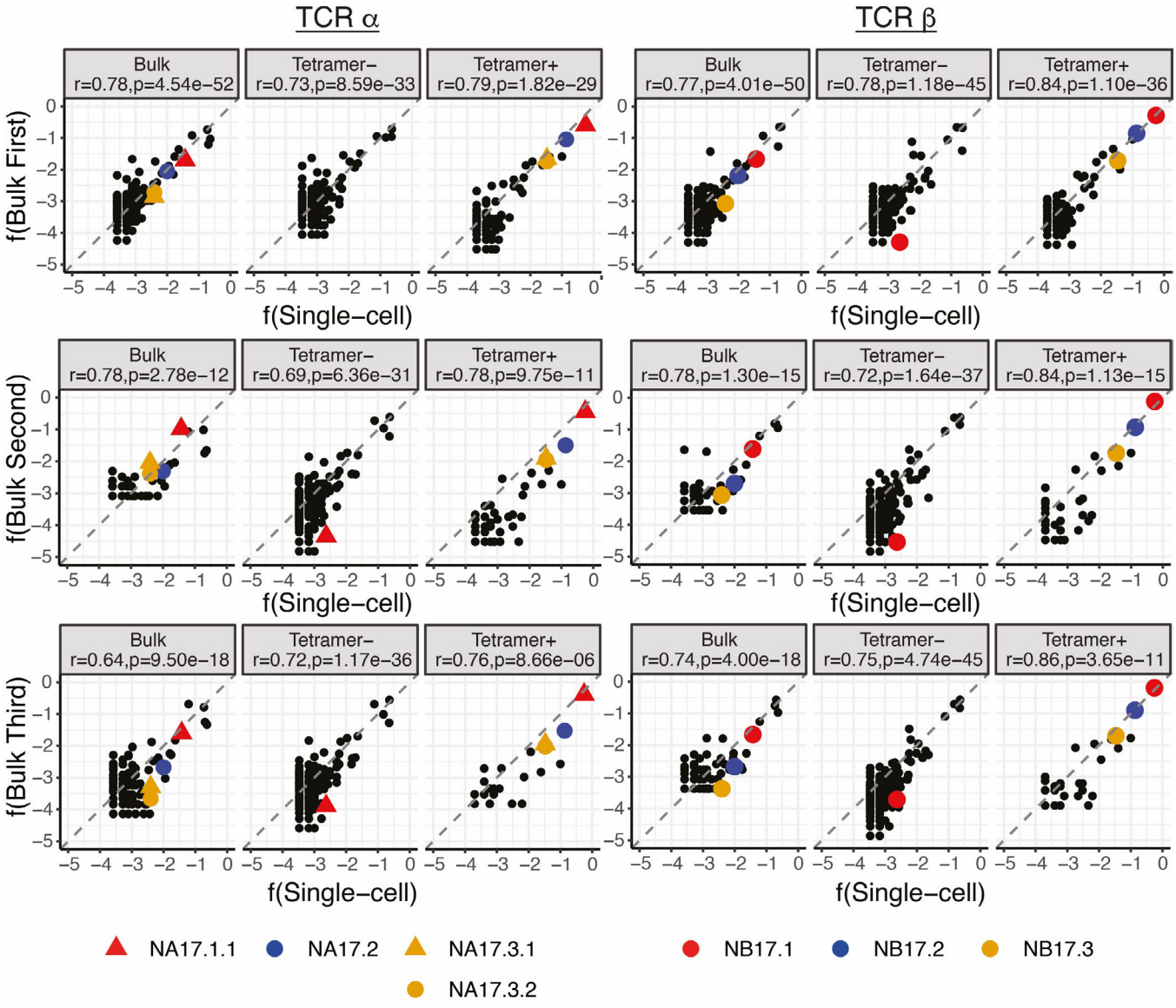

Supplementary figure 26: Comparing 17TIL TCR chain frequencies between the single-cell experiment and the three bulk-TCR-sequencing replicates. Left panels – TCR α chains, right panels – TCR β chains.

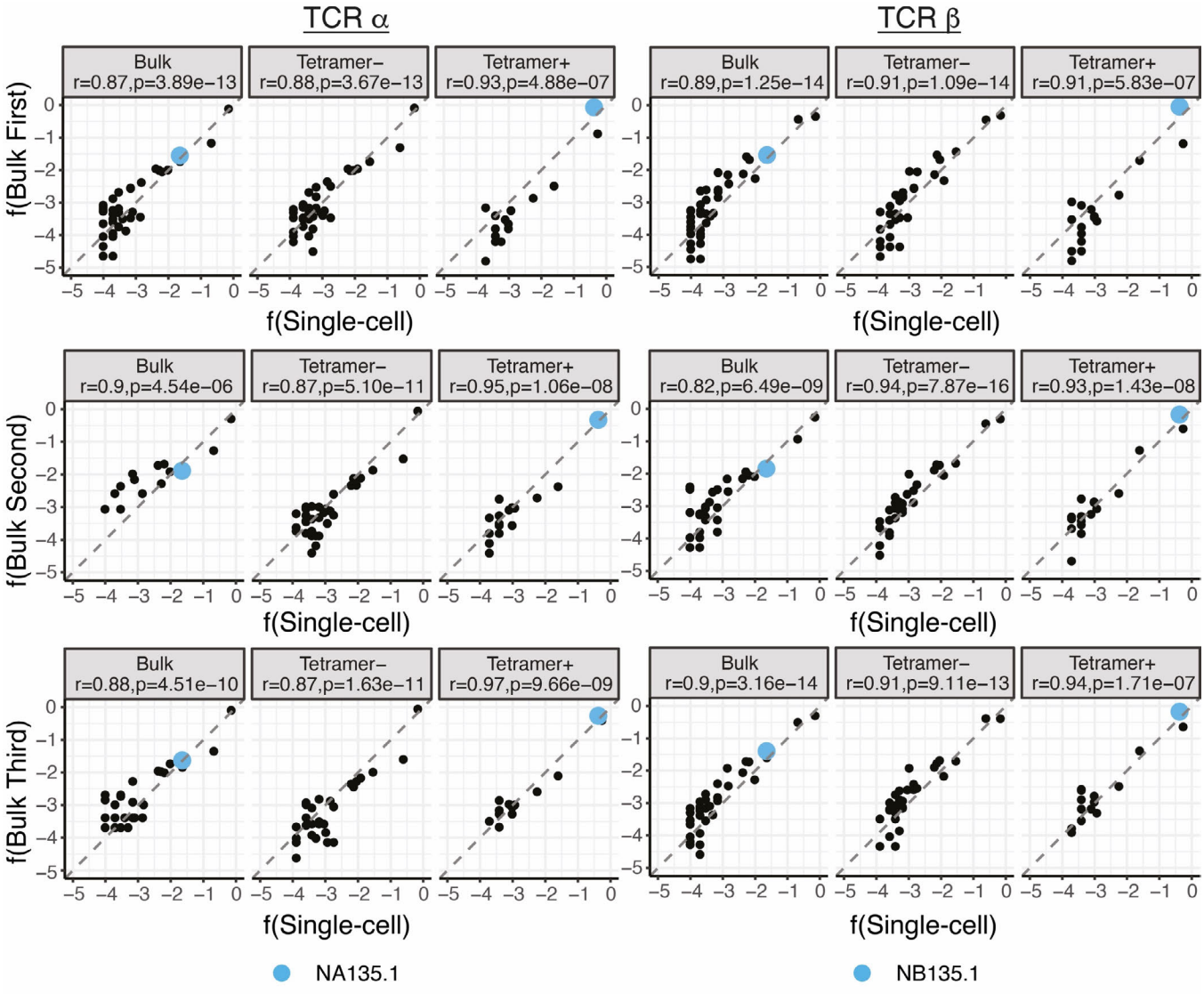

Supplementary figure 27: Comparing 135TIL TCR chain frequencies between the single-cell experiment and the three bulk-TCR-sequencing replicates. Left panels – TCR α chains, right panels – TCR β chains.

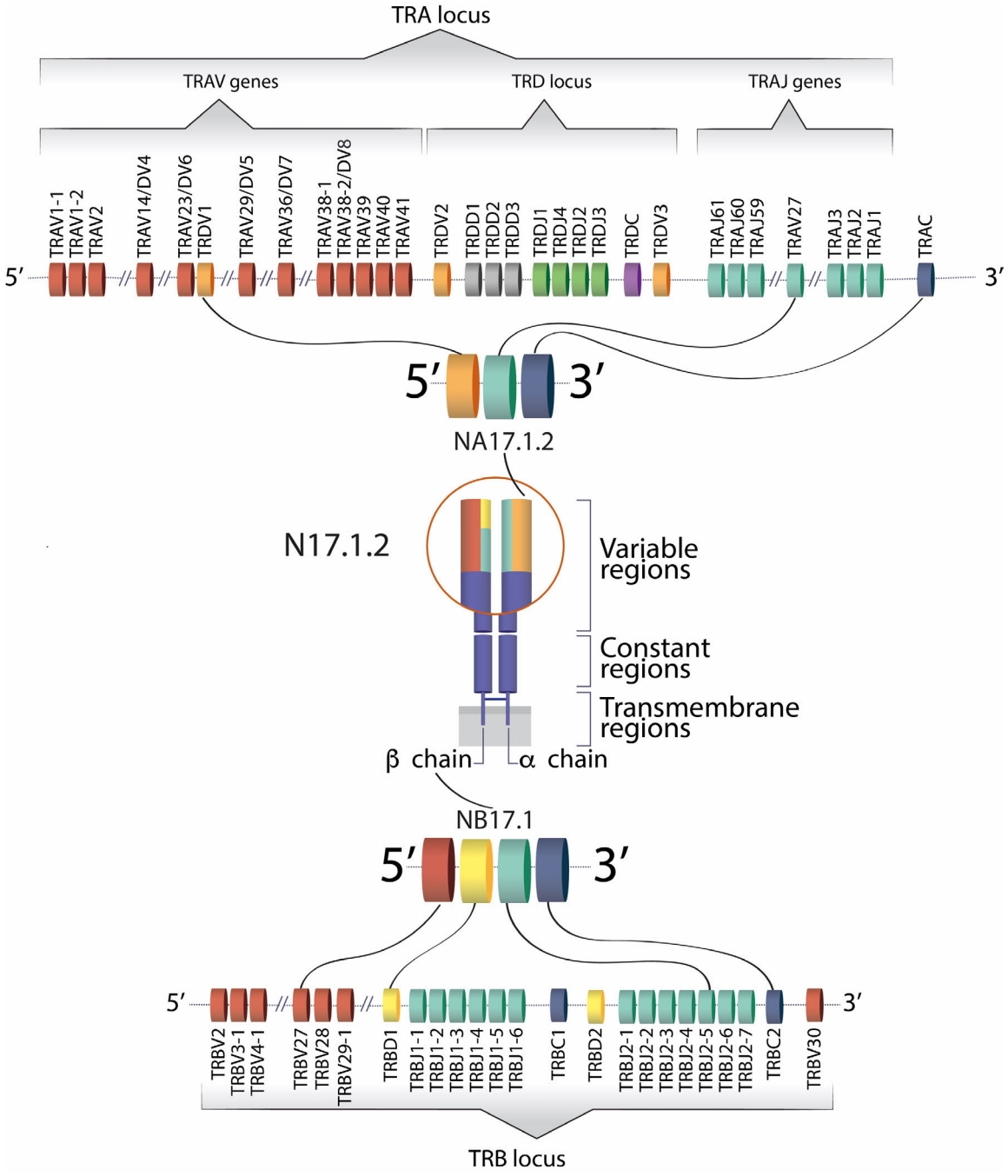

Supplementary figure 28: VDJ rearrangement resulting in TCR N17.1.2.
TCR N17.1.2 of clone N17.1 pairs α chain NA17.1.2 with β chain NB17.1. Standard β chain VDJ recombination joins a TRBD gene (either TRBD1 or TRBD2, this not annotated by our pipeline) to TRBJ2-5; then joins V-gene TRBV27 to the already formed D-J segment. Junctional variation forms CDR3 sequence CASSLVSTPLPKETQYF for NB17.1. The NA17.1.2 α chain forms in less of a 'mainstream' recombination, where J-gene TRAV27 recombines with the δ V-gene TRDV1.
Some V-genes outside the TRD locus are known to rearrange into α and δ chain interchangeably, and are named accordingly (TRAV14/DV4, TRAV23/DV6, TRAV29/DV5, TRAV36/DV7, TRAV38-2/DV8). Other V-genes, that are located within the TRD locus, are considered strictly δ (TRDV2, TRDV2). While TRDV1, which notably resides outside the TRD locus, was previously described to recombine also into α chains, this is not accounted for in α/β annotation procedures of standard TCR-sequencing platforms. Junctional variation forms CDR3 sequence CALGDTAGKSTF for NA17.1.2.

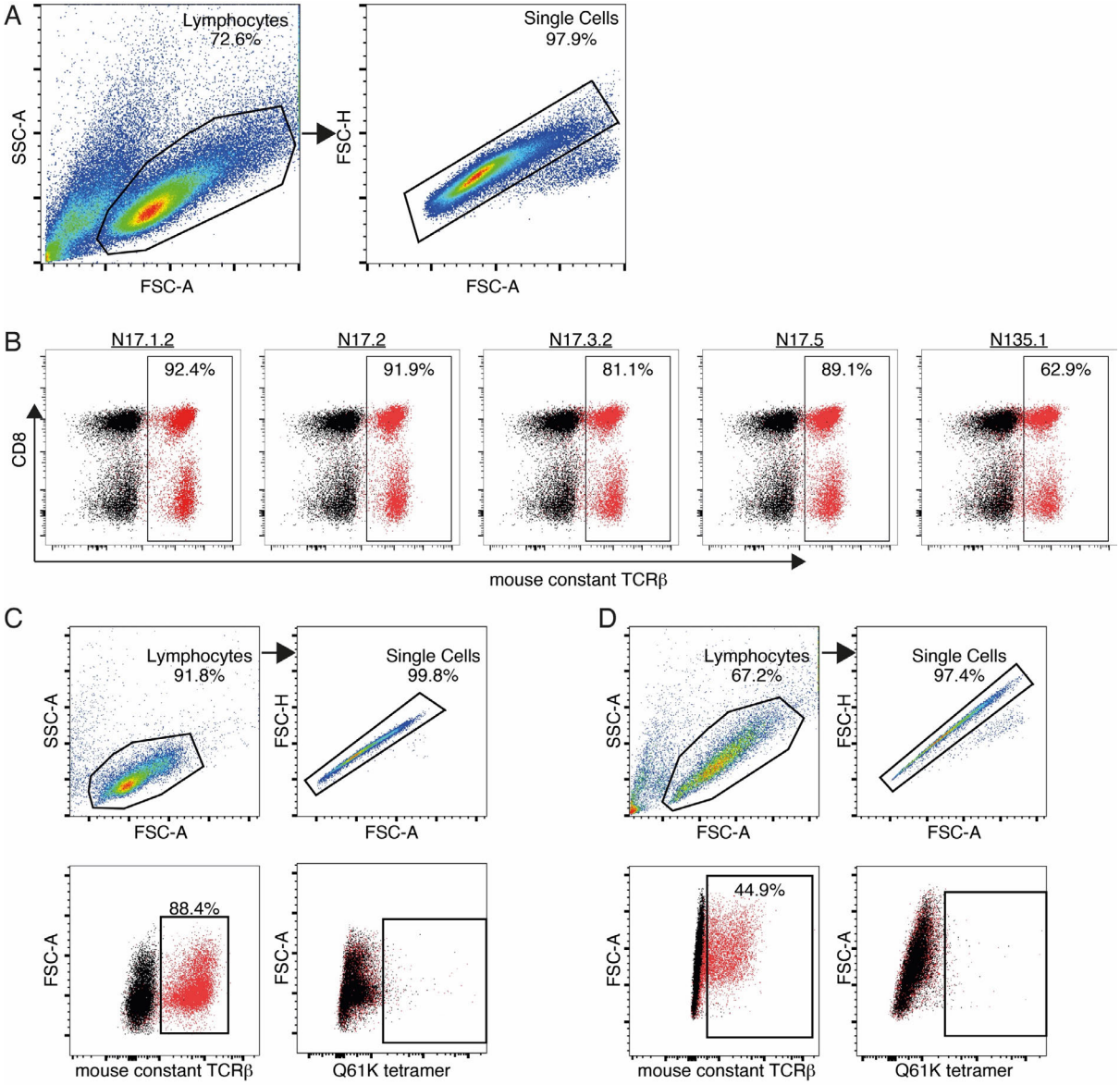

Supplementary figure 29: Electroporation of healthy-donor T-cells to express candidate neoantigen-specific TCRs. (A) Gating strategy for the plots presented in (B) and in main figure 5A. **(B)** Electroporated T-cells as presented in main figure 5A, stained for mouse constant TCRβ. **(C)** TCR N17.1.1 does not bind the neoantigen. Top – gating strategy, bottom – mouse constant TCRβ and tetramer staining. **(D)** TCR N17.3.1 does not bind the neoantigen. Top – gating strategy, bottom – mouse constant TCRβ and tetramer staining. Red – TCR electroporated cells. Black – negative control: cells electroporated without mRNA ('electroporated nothing', EN, control).

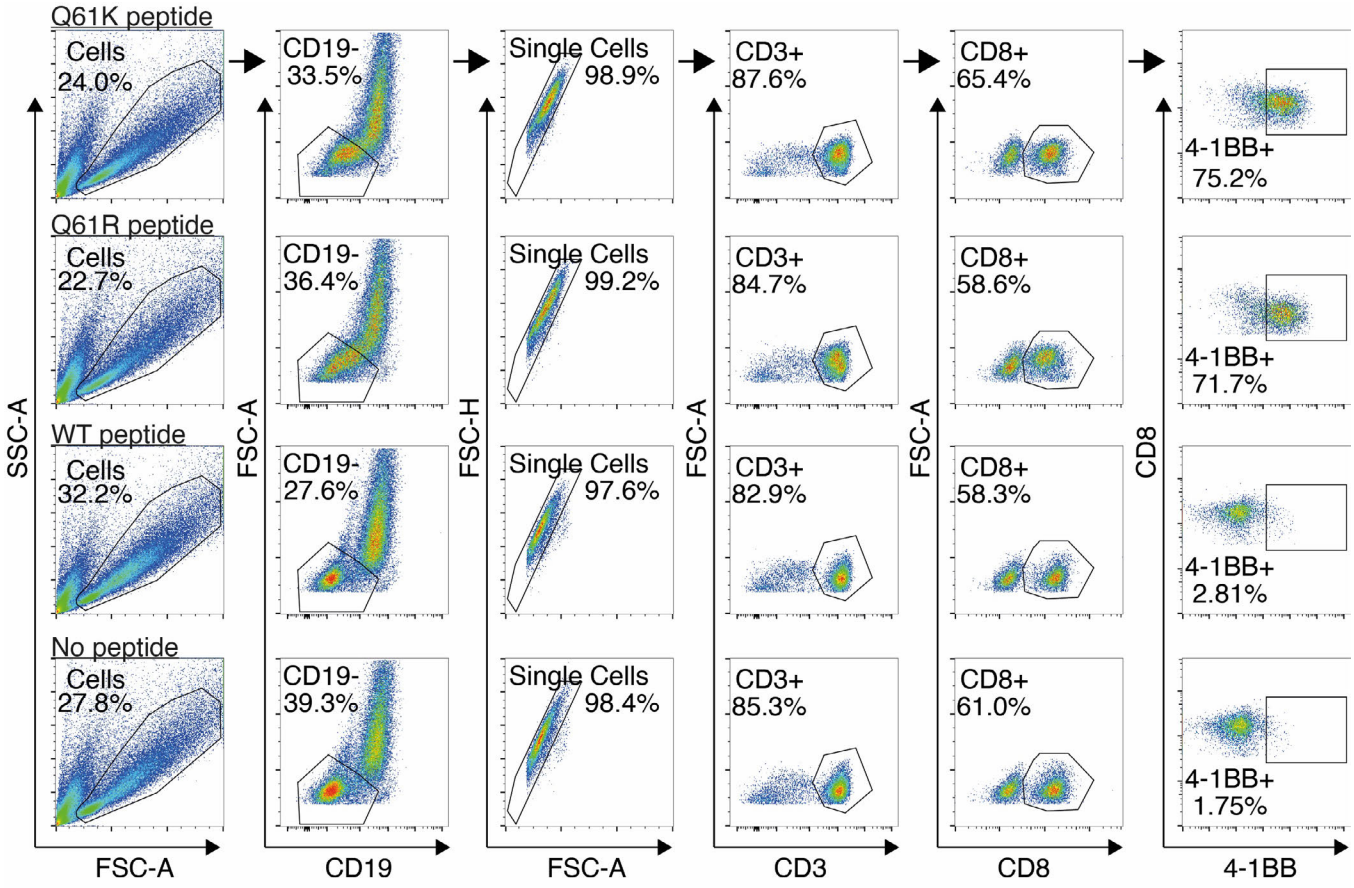

Supplementary figure 30: Flow-cytometry gating strategy for 4-1BB peptide-titration assay of healthy-donor T-cells electroporated with TCR N17.1.2. Representative replicates are shown for each of the *ILDTAGKEEY*, *ILDTAGREEY*, *ILDTAGQEEY* and 'no peptide' conditions.

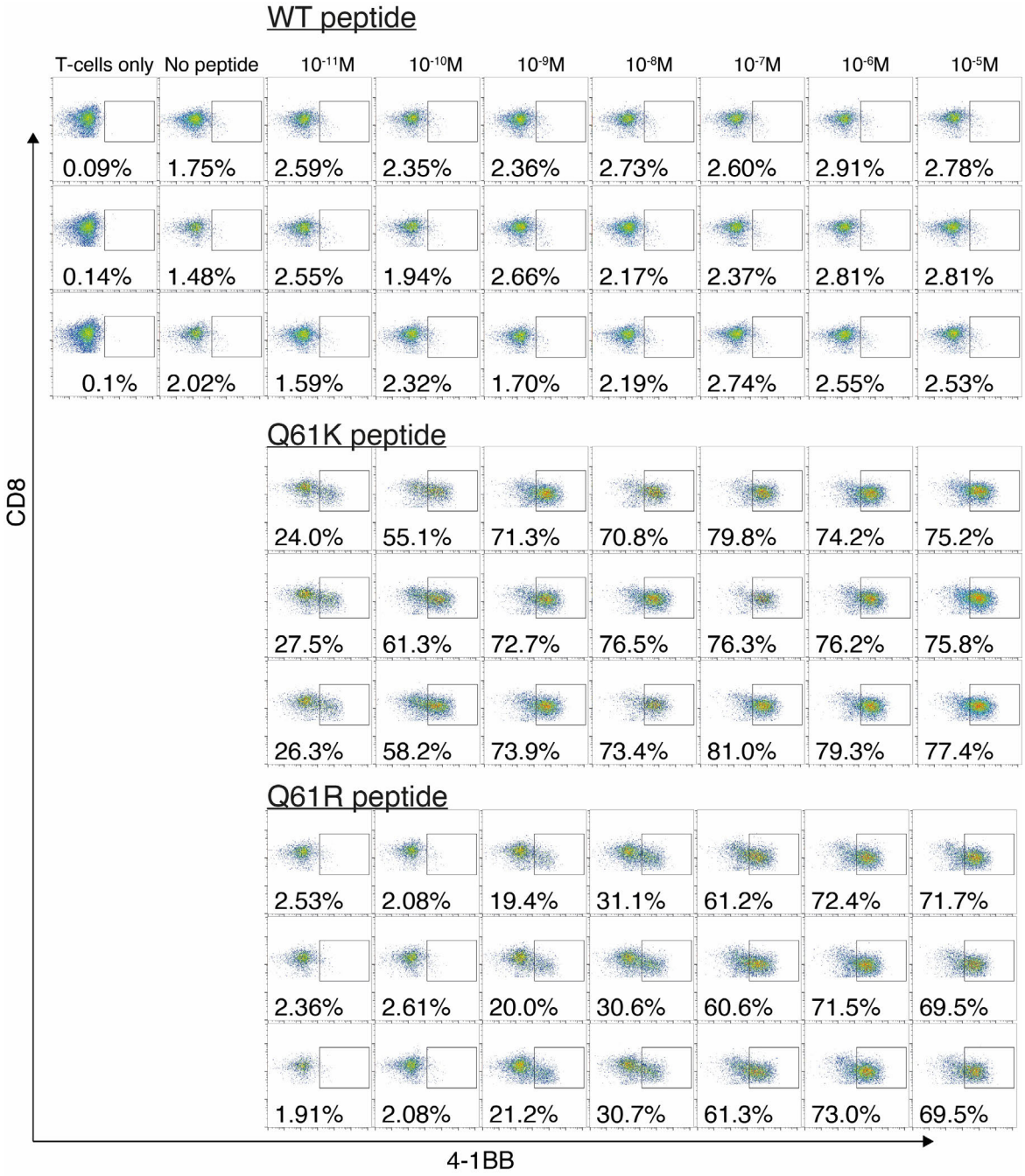

Supplementary figure 31: Flow-cytometry 4-1BB gating for peptide-titration assay of healthy-donor T-cells electroporated with TCR N17.1.2. Samples were gated as shown in supplementary figure 30; HLA-A*01:01+ B-LCL IHW01161 were pulsed with different concentrations of the *ILDTAGKEEY*, *ILDTAGREEY* or wild-type *ILDTAGQEEY,* and were co-incubated with the electroporated T-cells. For the 'no peptide' control and equal volume of the DMSO vehicle was utilized. Biological triplicates were prepared for each condition.

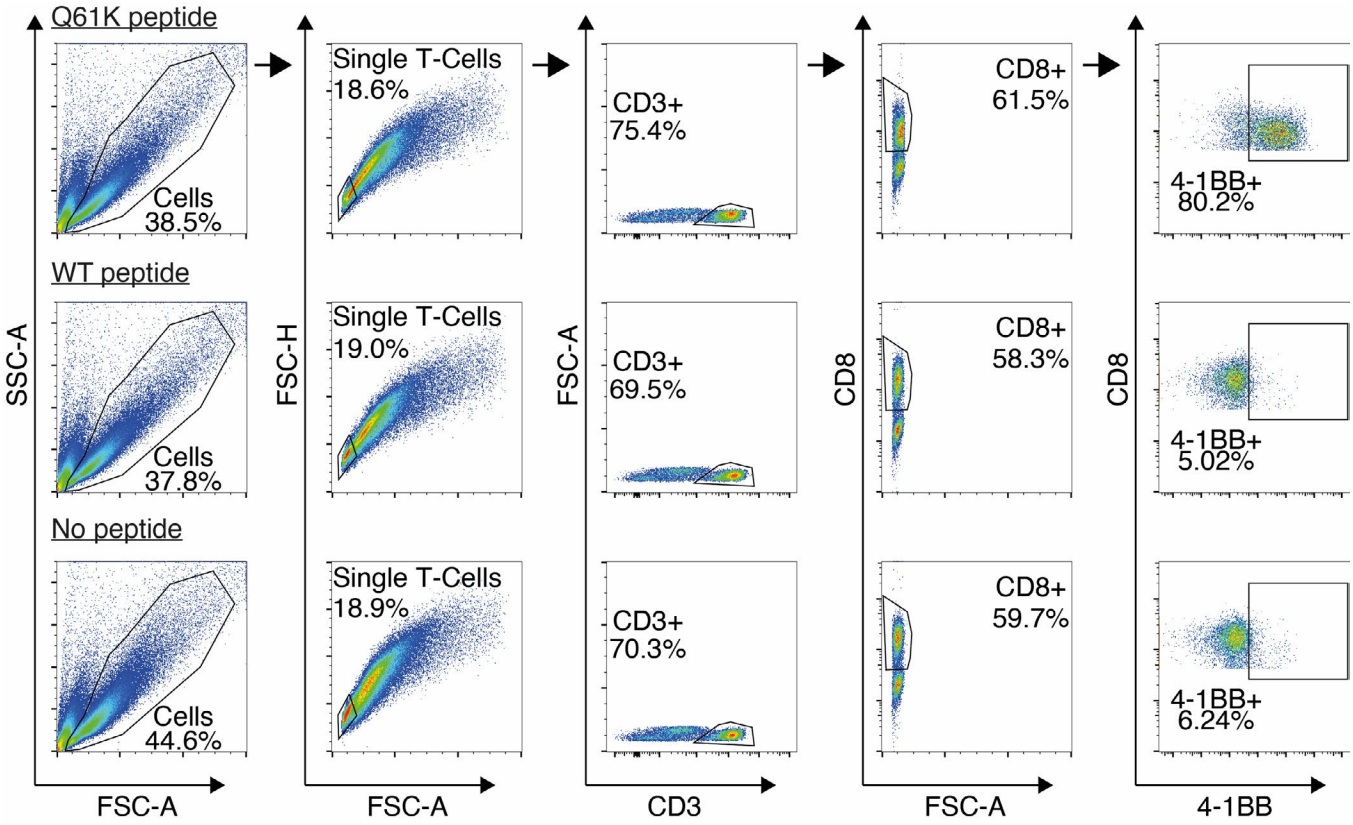

Supplementary figure 32: Flow-cytometry gating strategy for 4-1BB peptide-titration assay of healthy-donor T-cells electroporated with TCR N17.2. Representative replicates are shown for each of the *ILDTAG<u>K</u>EEY*, *ILDTAGQEEY* and 'no peptide' conditions.

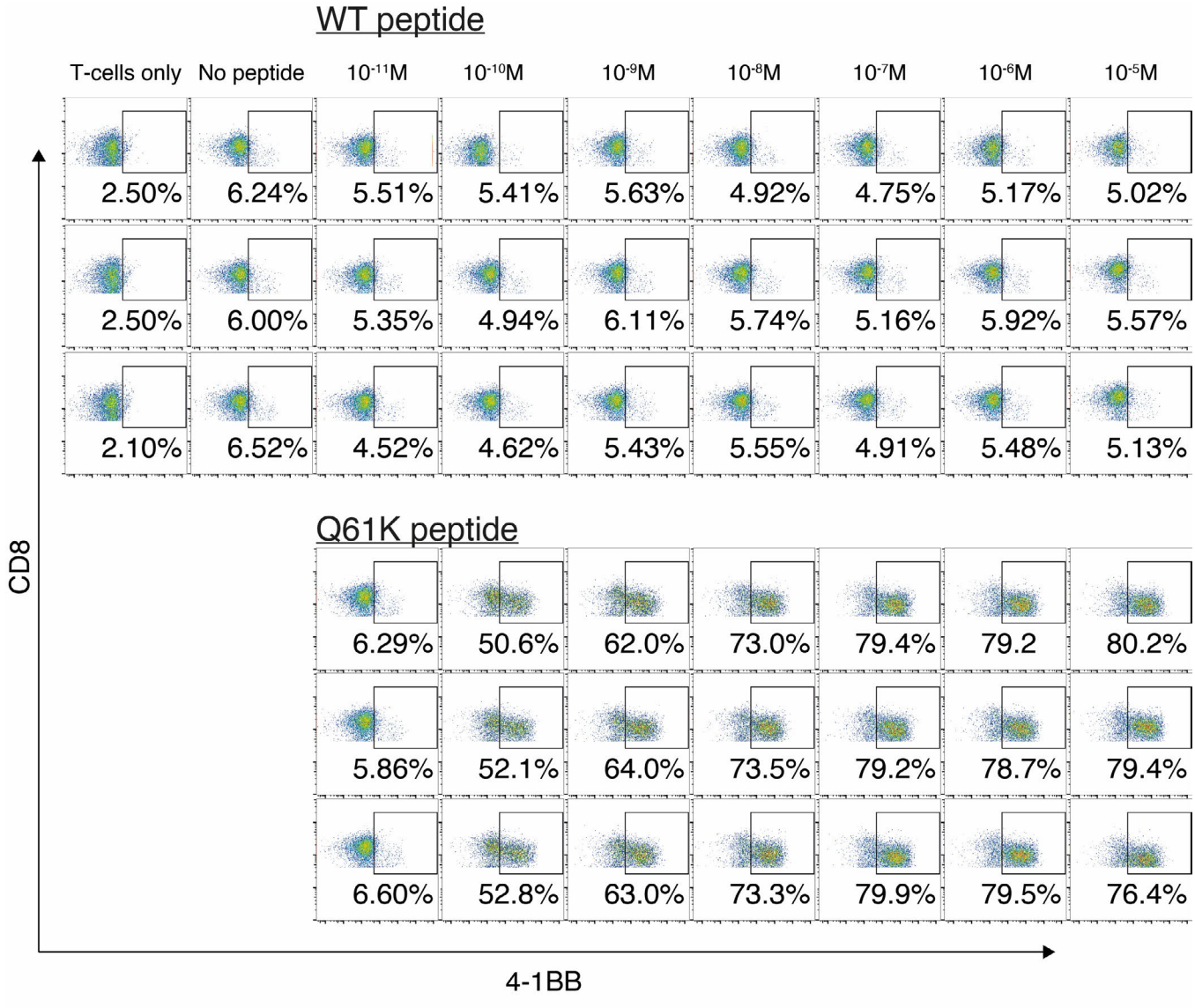

Supplementary figure 33: Flow-cytometry 4-1BB gating for peptide-titration assay of healthy-donor T-cells electroporated with TCR N17.2. Samples were gated as shown in supplementary figure 32; HLA-A*01:01+ B-LCL IHW01161 were pulsed with different concentrations of the *ILDTAG<u>K</u>EEY* or wild-type *ILDTAGQEEY,* and were co-incubated with the electroporated T-cells. For the 'no peptide' control and equal volume of the DMSO vehicle was utilized. Biological triplicates were prepared for each condition.

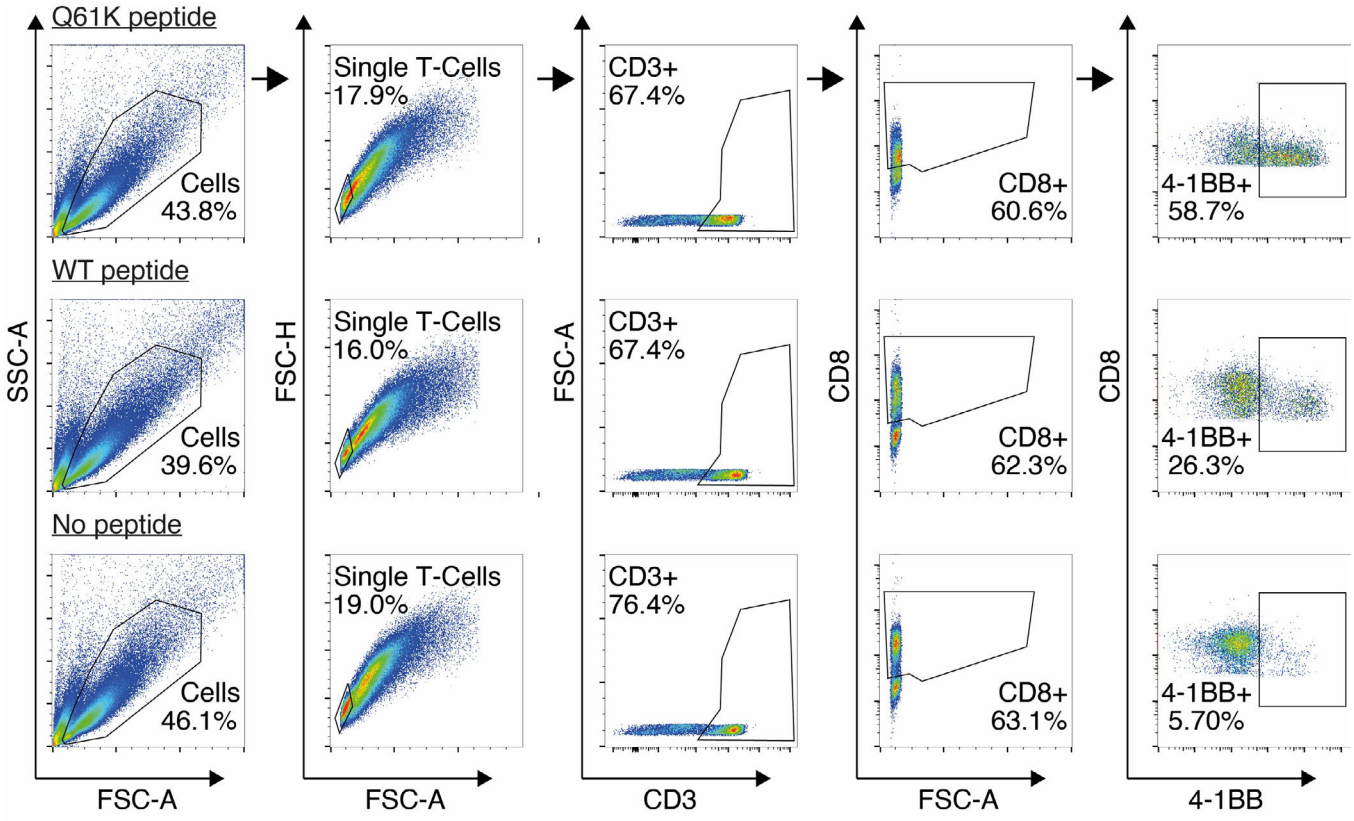

Supplementary figure 34: Flow-cytometry gating strategy for 4-1BB peptide-titration assay of healthy-donor T-cells electroporated with TCR N17.3.2. Representative replicates are shown for each of the *ILDTAG<u>K</u>EEY*, *ILDTAGQEEY* and 'no peptide' conditions.

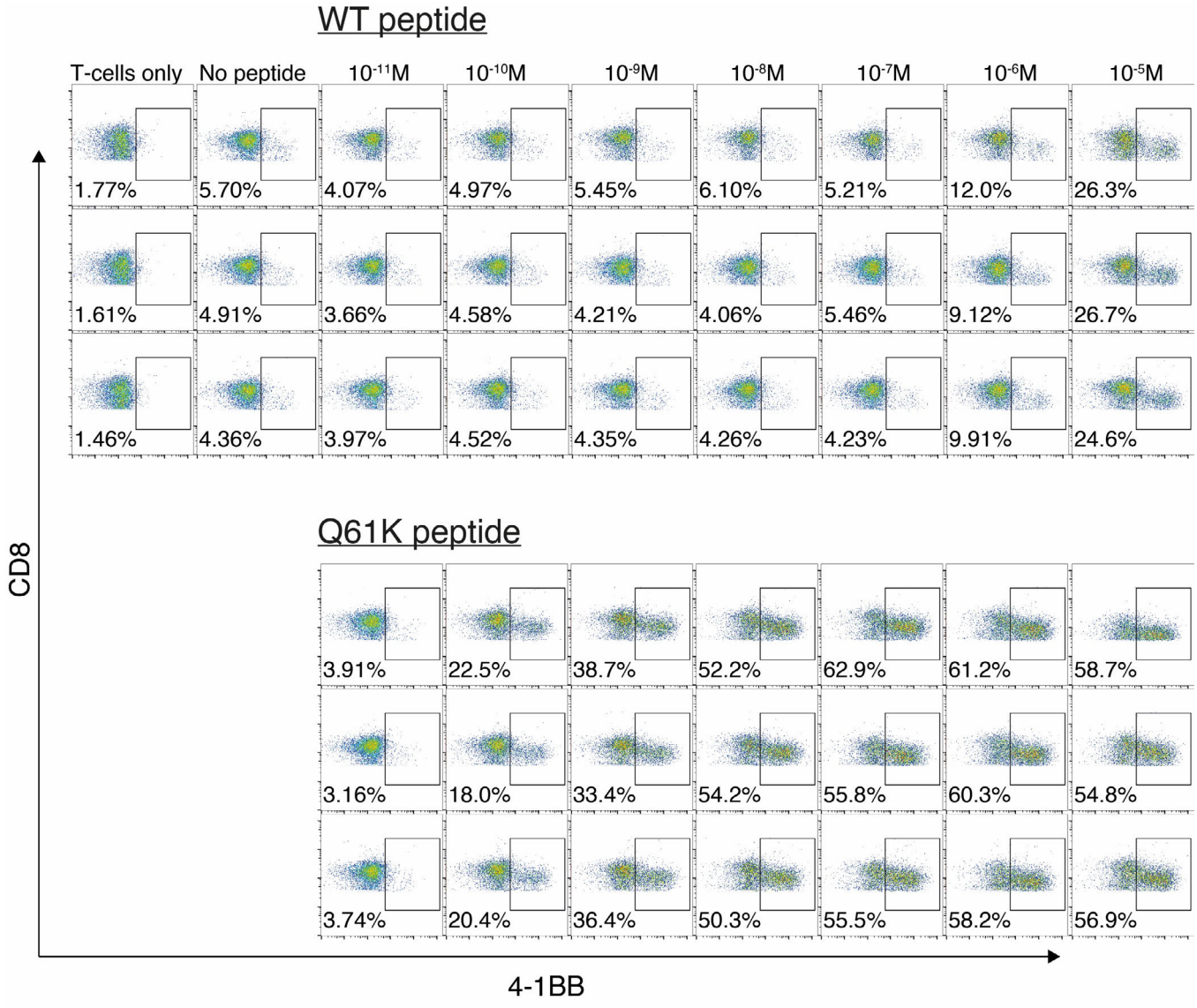

Supplementary figure 35: Flow-cytometry 4-1BB gating for peptide-titration assay of healthy-donor T-cells electroporated with TCR N17.3.2. Samples were gated as shown in supplementary figure 34; HLA-A*01:01+ B-LCL IHW01161 were pulsed with different concentrations of the *ILDTAG<u>K</u>EEY* or wild-type *ILDTAGQEEY,* and were co-incubated with the electroporated T-cells. For the 'no peptide' control and equal volume of the DMSO vehicle was utilized. Biological triplicates were prepared for each condition.

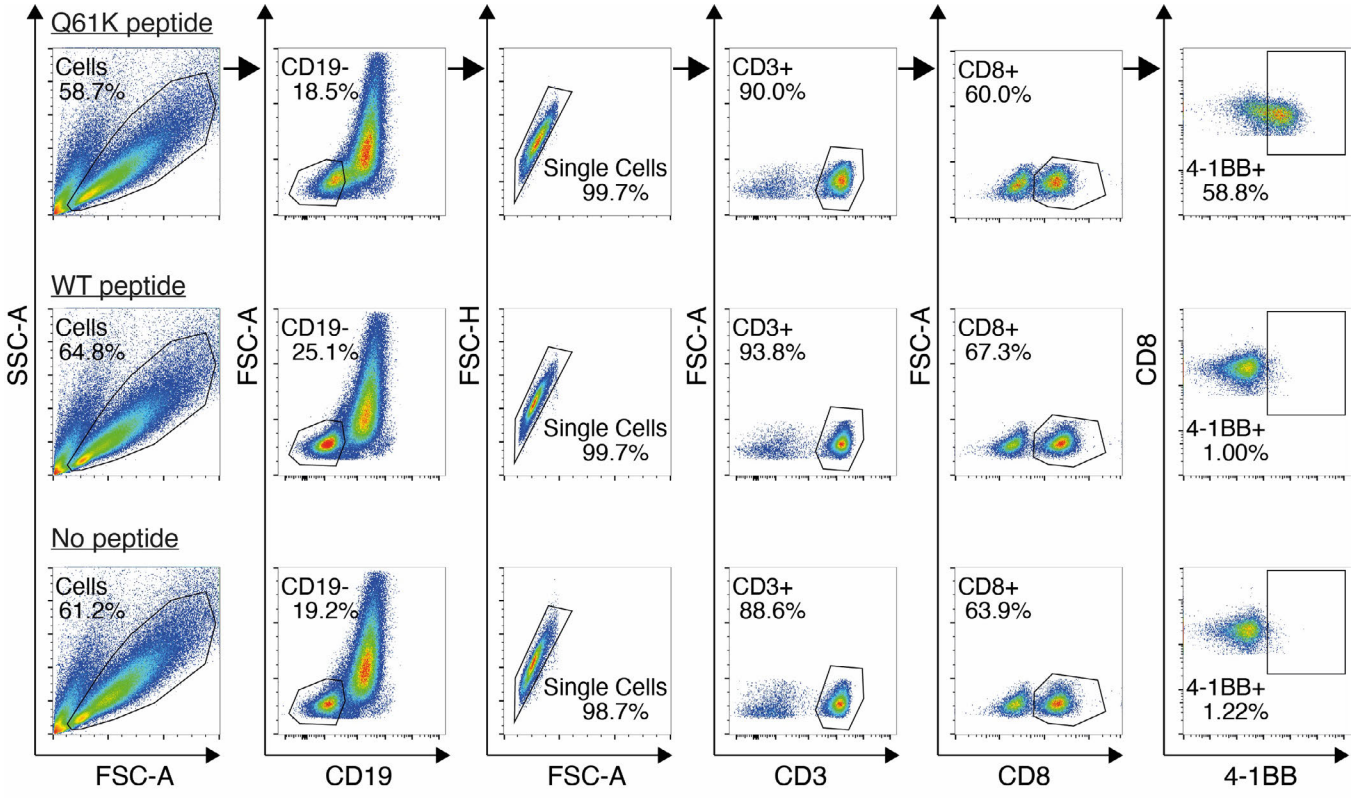

Supplementary figure 36: Flow-cytometry gating strategy for 4-1BB peptide-titration assay of healthy-donor T-cells electroporated with TCR N17.5. Representative replicates are shown for each of the *ILDTAG<u>K</u>EEY*, *ILDTAGQEEY* and 'no peptide' conditions.

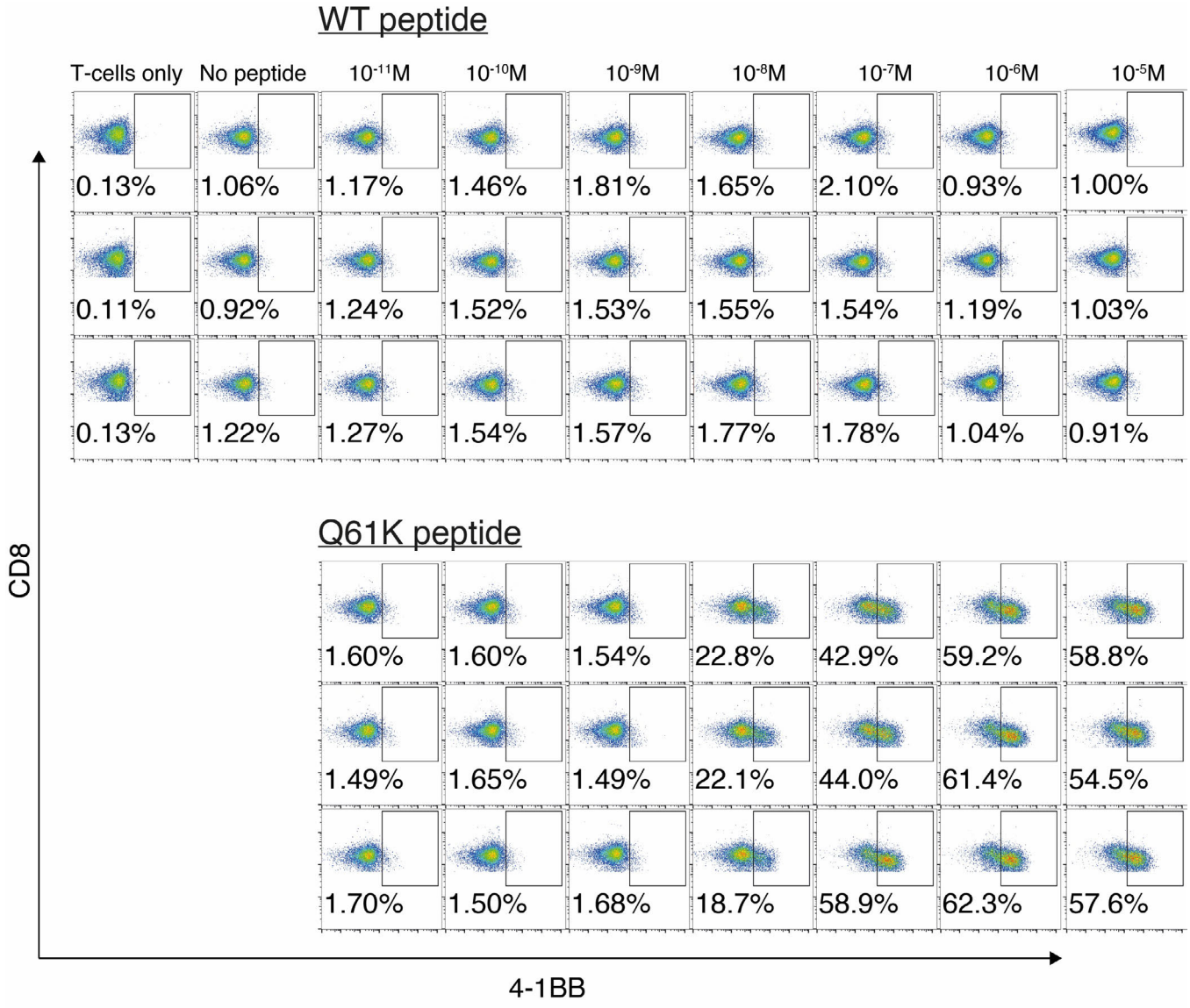

Supplementary figure 37: Flow-cytometry 4-1BB gating for peptide-titration assay of healthy-donor T-cells electroporated with TCR N17.5. Samples were gated as shown in supplementary figure 36; HLA-A*01:01+ B-LCL IHW01161 were pulsed with different concentrations of the *ILDTAGKEEY* or wild-type *ILDTAGQEEY,* and were co-incubated with the electroporated T-cells. For the 'no peptide' control and equal volume of the DMSO vehicle was utilized. Biological triplicates were prepared for each condition.

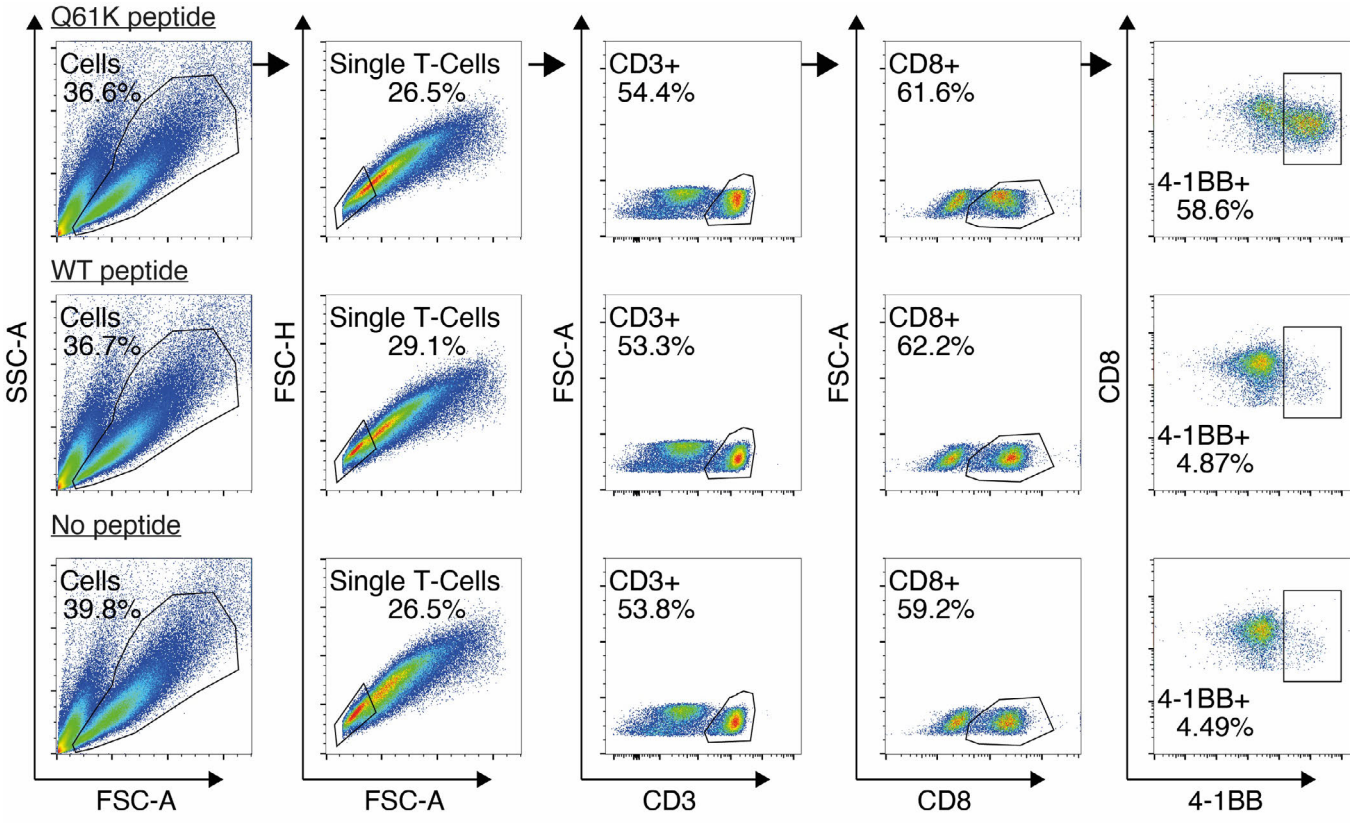

Supplementary figure 38: Flow-cytometry gating strategy for 4-1BB peptide-titration assay of healthy-donor T-cells electroporated with TCR N135.1. Representative replicates are shown for each of the *ILDTAG<u>K</u>EEY*, *ILDTAGQEEY* and 'no peptide' conditions.

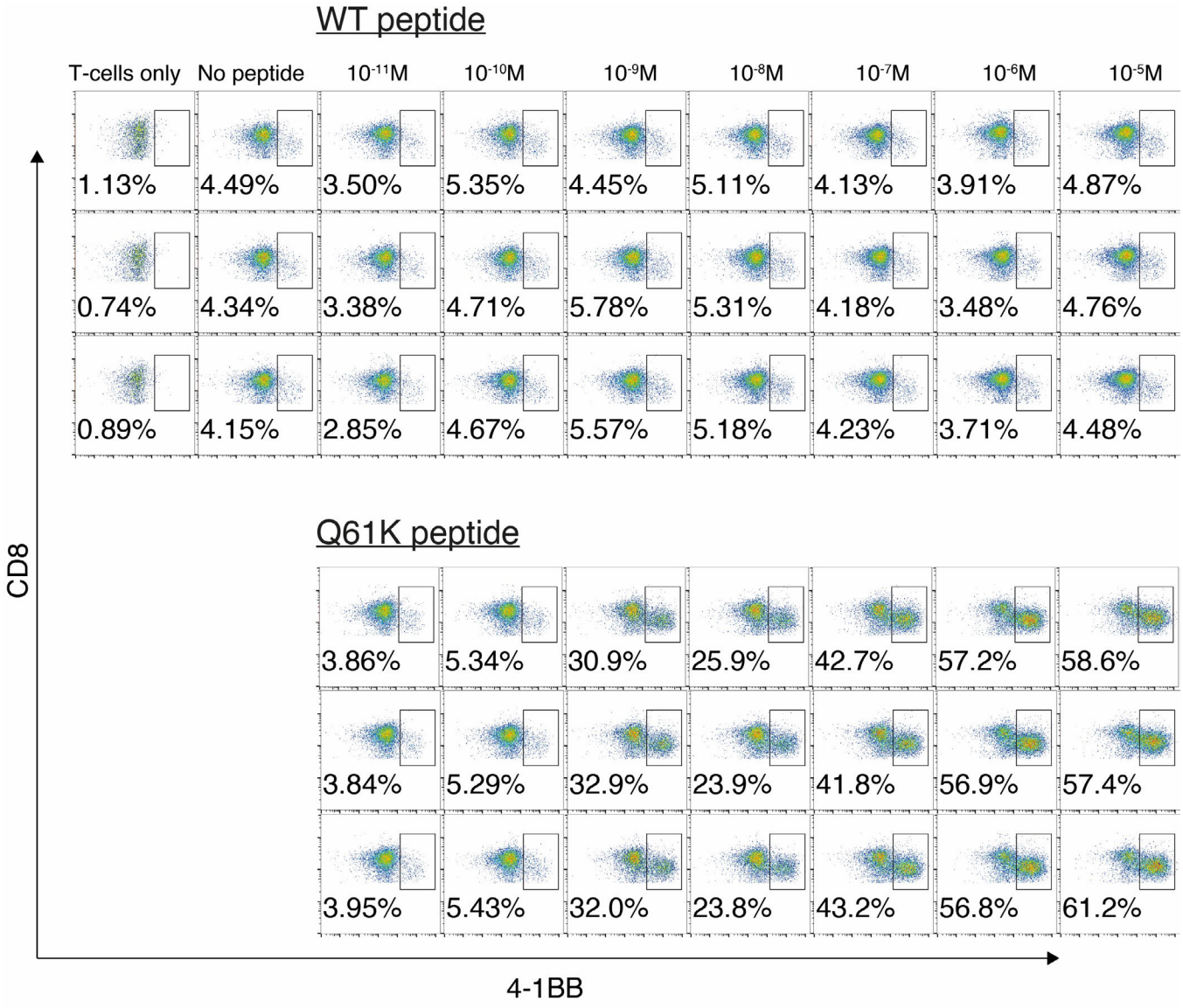

Supplementary figure 39: Flow-cytometry 4-1BB gating for peptide-titration assay of healthy-donor T-cells electroporated with TCR N135.1. Samples were gated as shown in supplementary figure 38; HLA-A*01:01+ B-LCL IHW01161 were pulsed with different concentrations of the *ILDTAGKEEY* or wild-type *ILDTAGQEEY,* and were co-incubated with the electroporated T-cells. For the 'no peptide' control and equal volume of the DMSO vehicle was utilized. Biological triplicates were prepared for each condition.

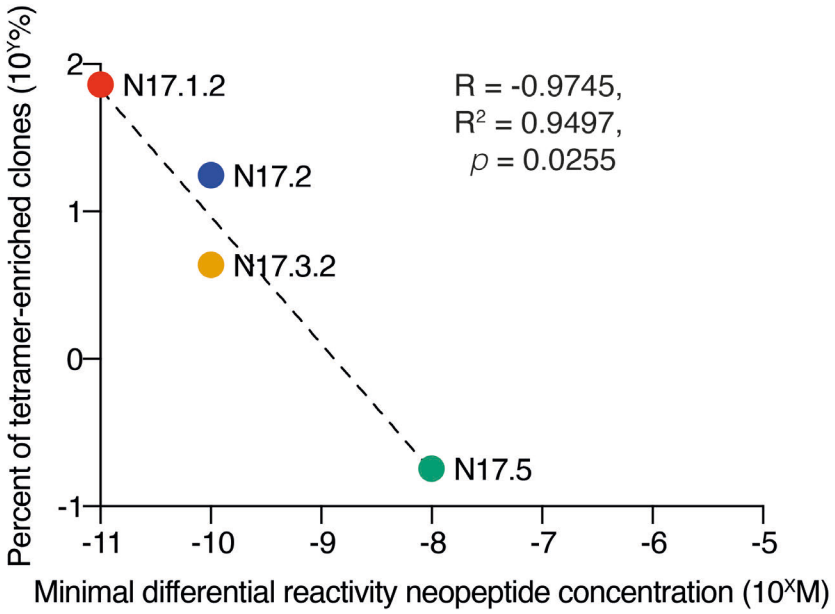

Supplementary figure 40: TCR sensitivity towards the *A*01:01/ILDTAGKEEY* neoantigen correlates with its abundance. For 17TIL, validated TCRs' sensitivity towards the neoantigen, as measures by the minimal peptide concentration required to elicit differential reactivity (see also figure 5), is plotted against the abundance of the cognate T-cell clone in the single-cell tetramer-enriched population. Pearson's correlation was calculated for the power model of the data (i.e. both variables were log-transformed); The linear regression line appears in dashed.

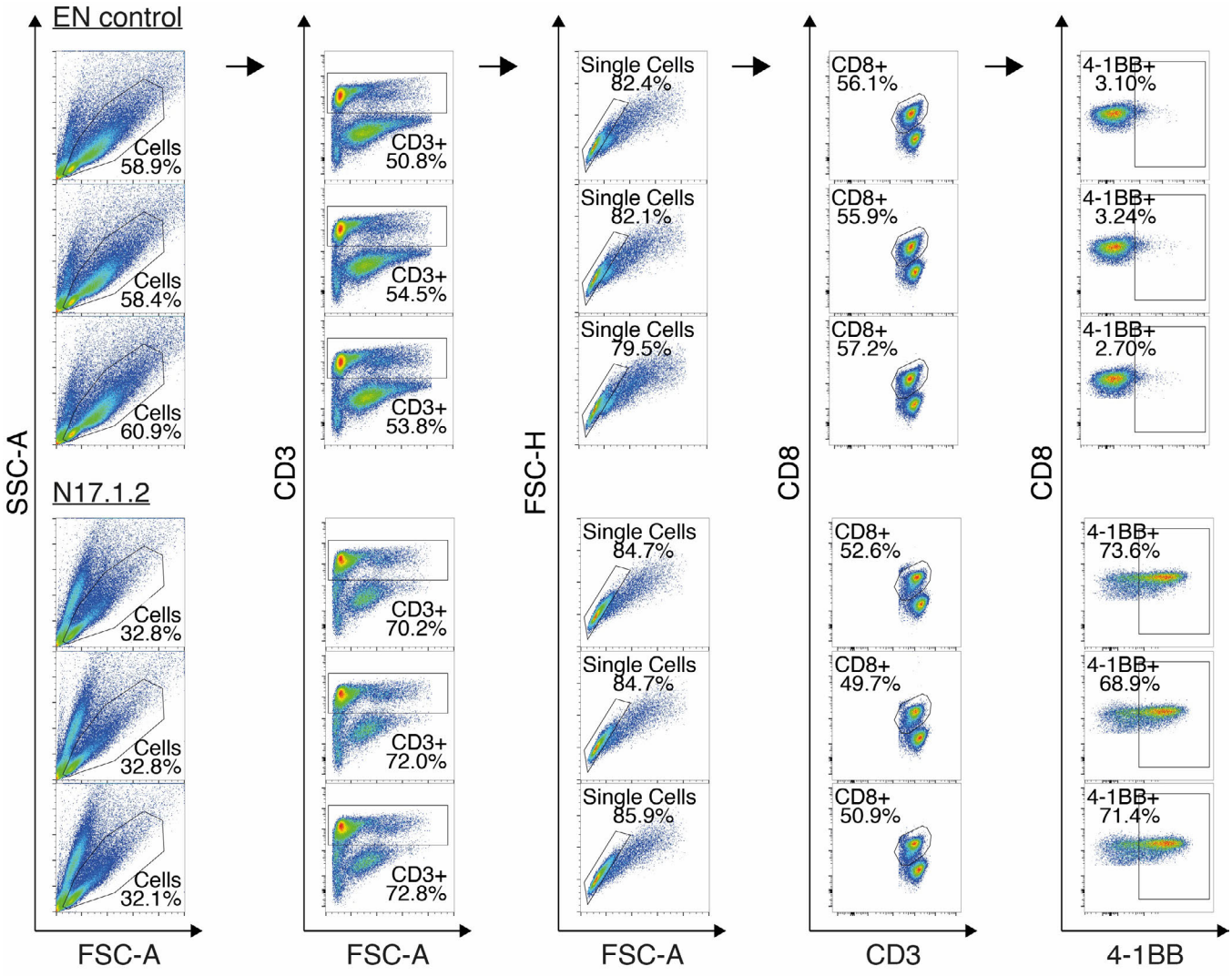

Supplementary figure 41: Flow-cytometry analysis of 4-1BB reactivity assay of N17.1.2-electroporated T-cells co-incubated with 17T melanoma cell-line at 1:1 ratio. 'EN' = 'electroporated nothing'; i.e. a negative control of the same batch of healthy-donor T-cells which went through the same electroporation procedure but without mRNA. Biological triplicates were prepared for each condition.

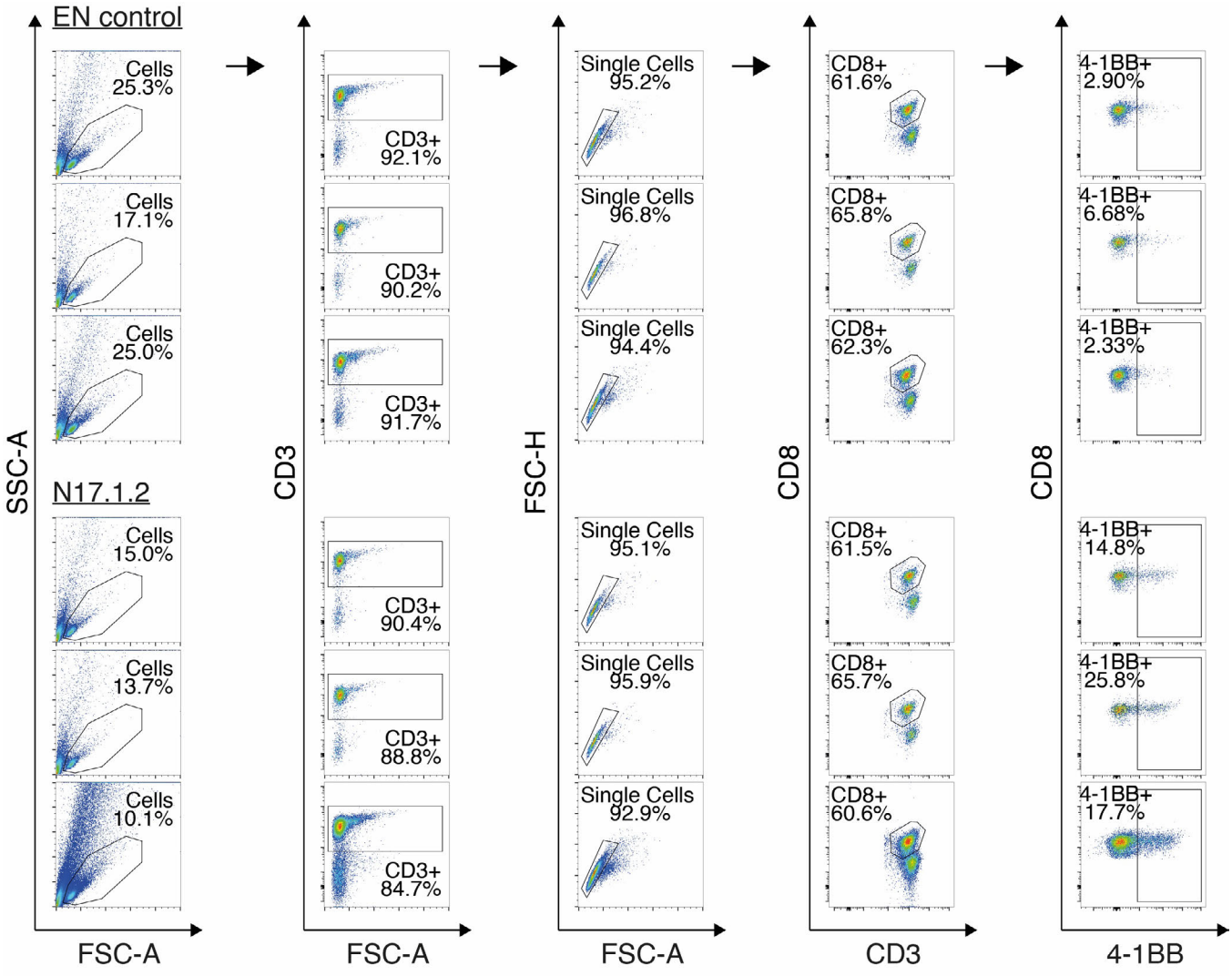

Supplementary figure 42: Flow-cytometry analysis of 4-1BB reactivity assay of N17.1.2-electroporated T-cells co-incubated with 135T melanoma cell-line at 1:1 ratio. 'EN' = 'electroporated nothing'; i.e. a negative control of the same batch of healthy-donor T-cells which went through the same electroporation procedure but without mRNA. Biological triplicates were prepared for each condition.

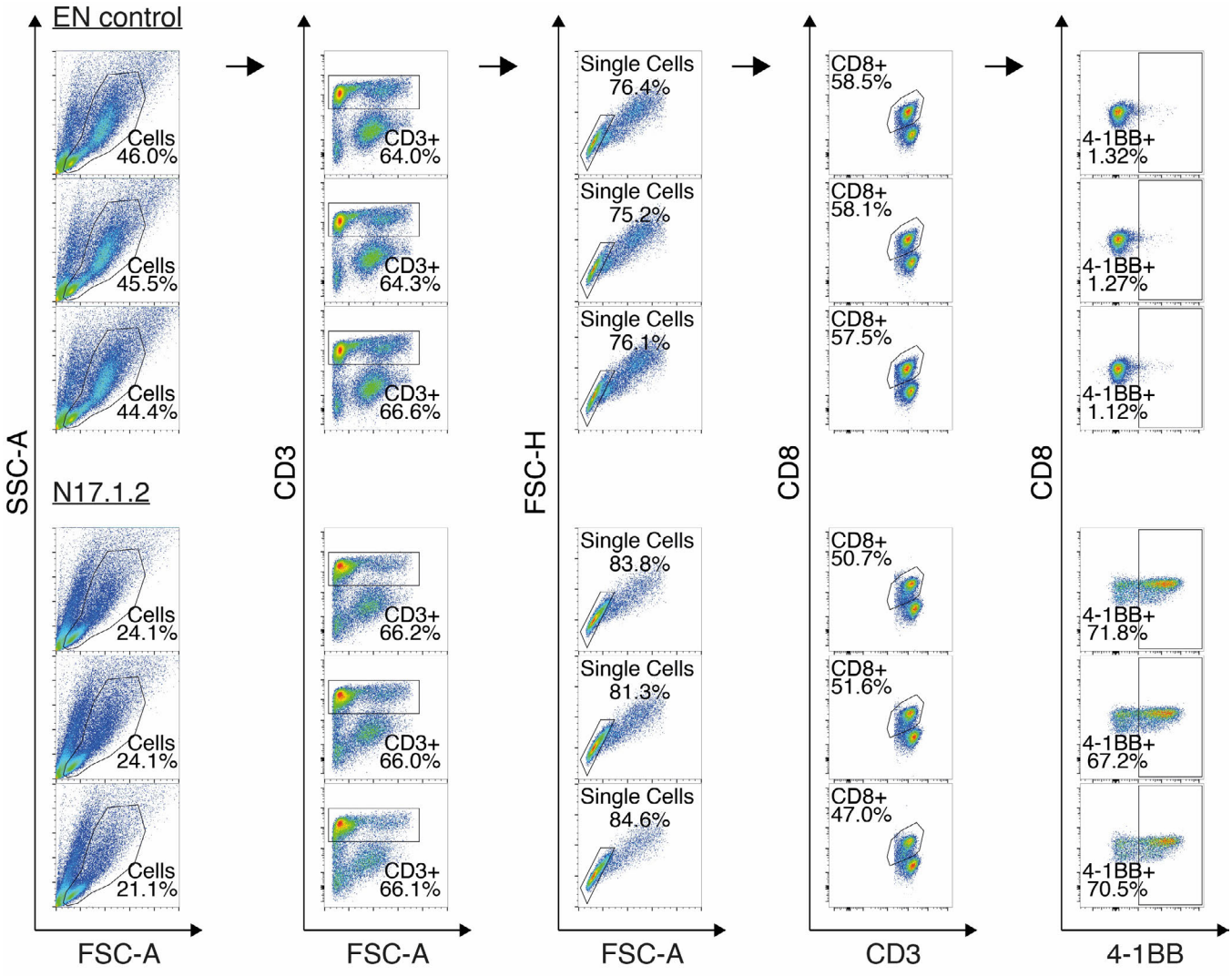

Supplementary figure 43: Flow-cytometry analysis of 4-1BB reactivity assay of N17.1.2-electroporated T-cells co-incubated with SK-MEL-30 melanoma cell-line at 1:1 ratio. 'EN' = 'electroporated nothing'; i.e. a negative control of the same batch of healthy-donor T-cells which went through the same electroporation procedure but without mRNA. Biological triplicates were prepared for each condition.

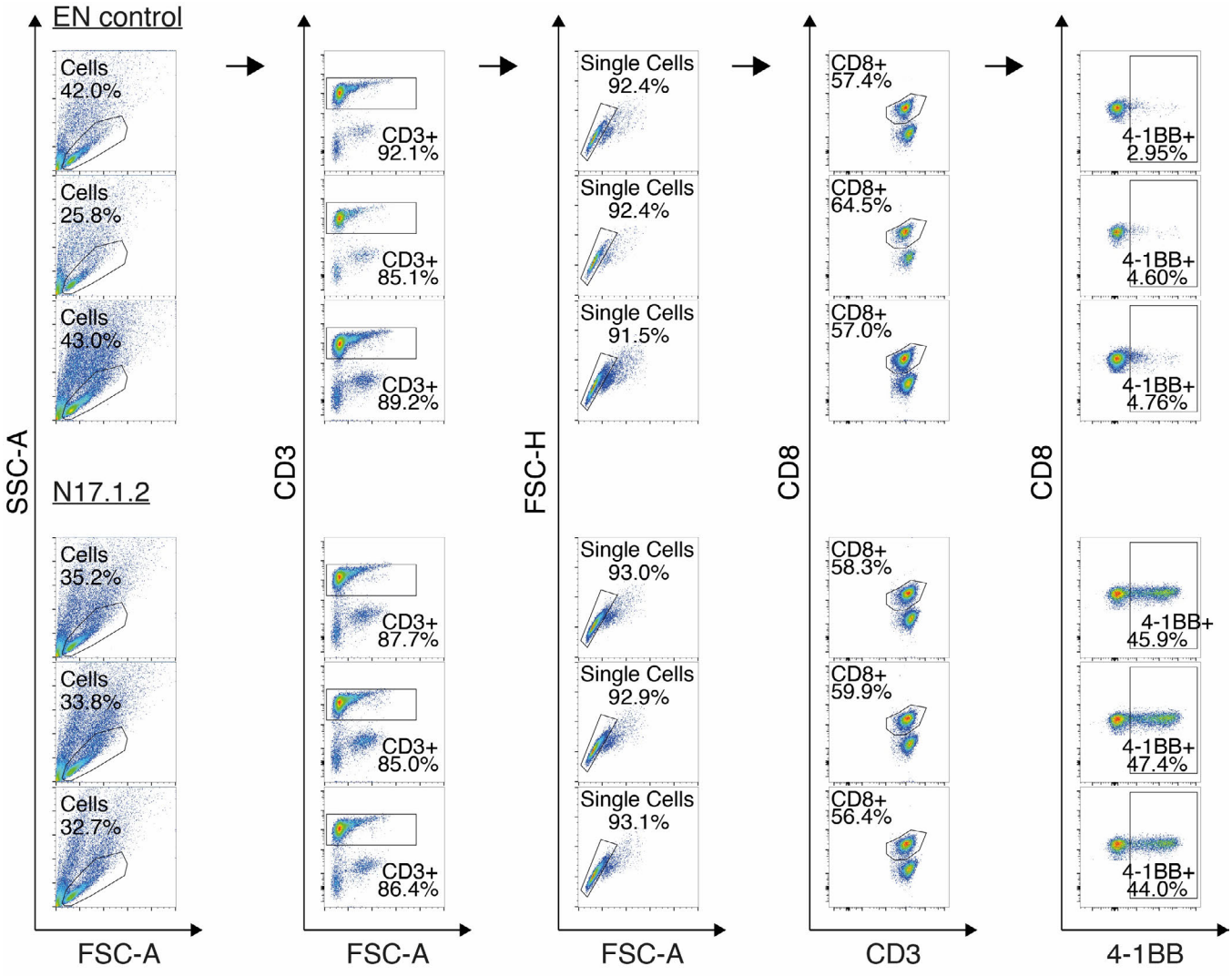

Supplementary figure 44: Flow-cytometry analysis of 4-1BB reactivity assay of N17.1.2-electroporated T-cells co-incubated with MM121224 melanoma cell-line at 1:1 ratio. 'EN' = 'electroporated nothing'; i.e. a negative control of the same batch of healthy-donor T-cells which went through the same electroporation procedure but without mRNA. Biological triplicates were prepared for each condition.

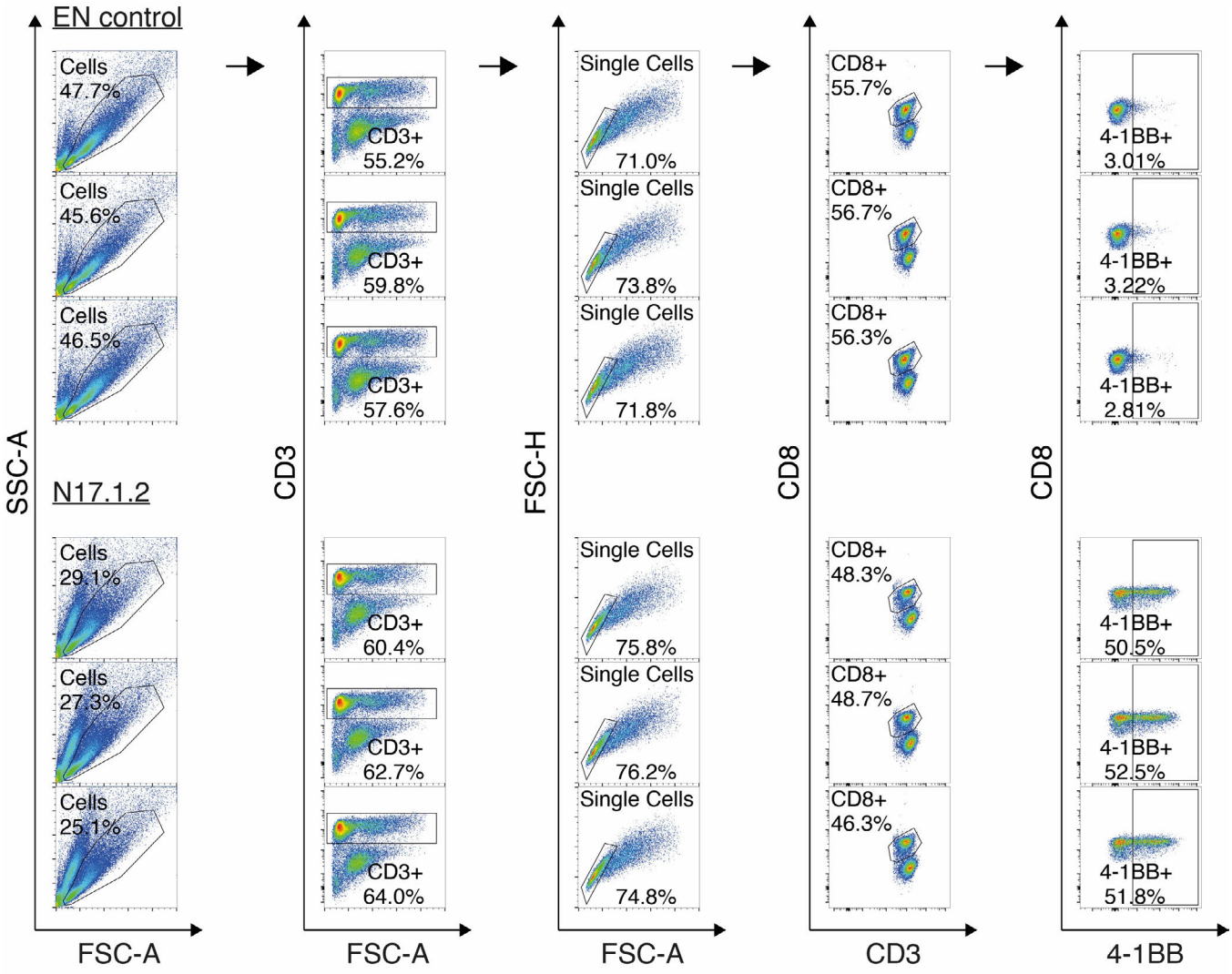

Supplementary figure 45: Flow-cytometry analysis of 4-1BB reactivity assay of N17.1.2-electroporated T-cells co-incubated with MZ2-MEL melanoma cell-line at 1:1 ratio. 'EN' = 'electroporated nothing'; i.e. a negative control of the same batch of healthy-donor T-cells which went through the same electroporation procedure but without mRNA. Biological triplicates were prepared for each condition.

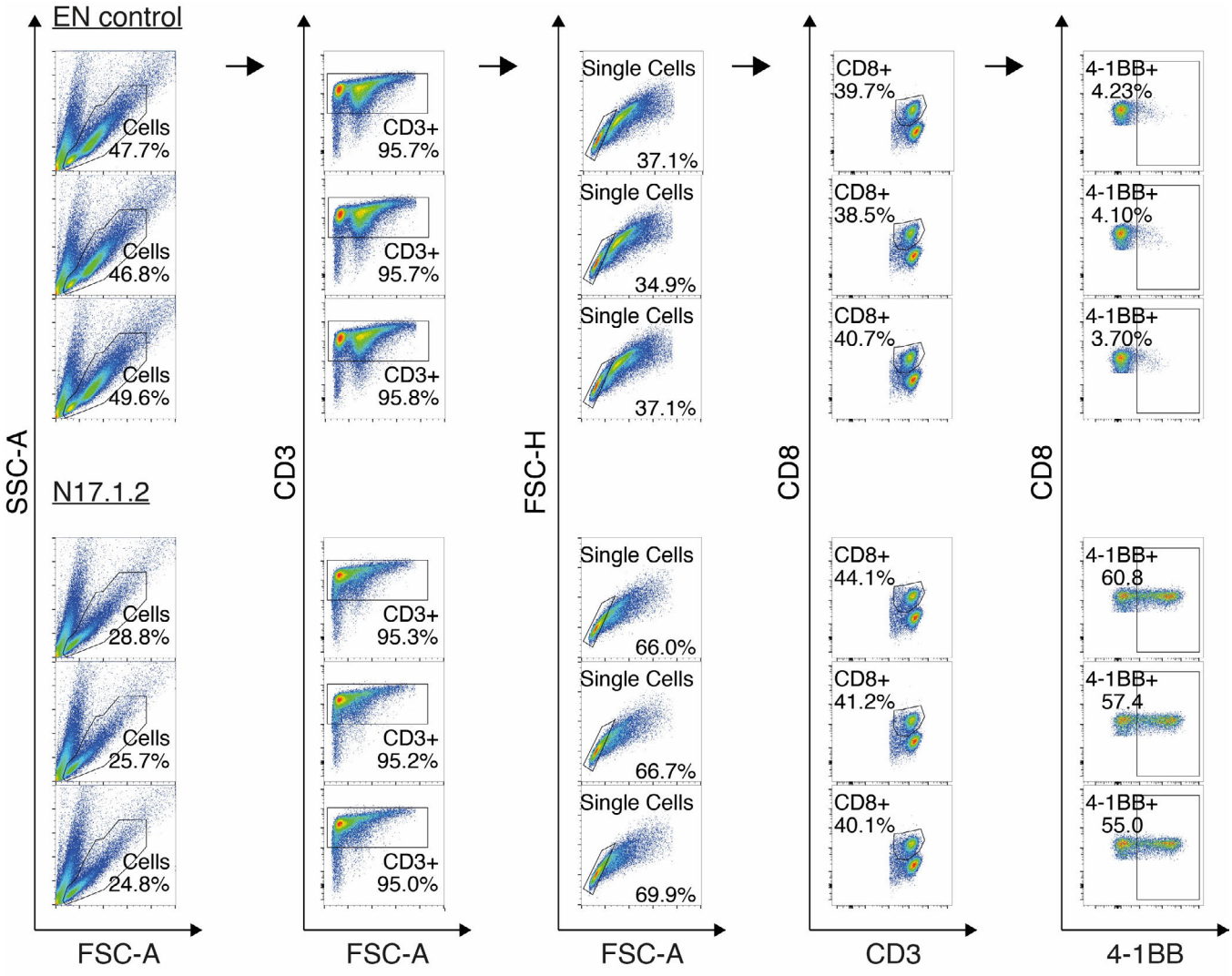

Supplementary figure 46: Flow-cytometry analysis of 4-1BB reactivity assay of N17.1.2-electroporated T-cells co-incubated with HuT78 cutaneous T-cell lymphoma cell-line at 1:1 ratio. 'EN' = 'electroporated nothing'; i.e. a negative control of the same batch of healthy-donor T-cells which went through the same electroporation procedure but without mRNA. Biological triplicates were prepared for each condition.

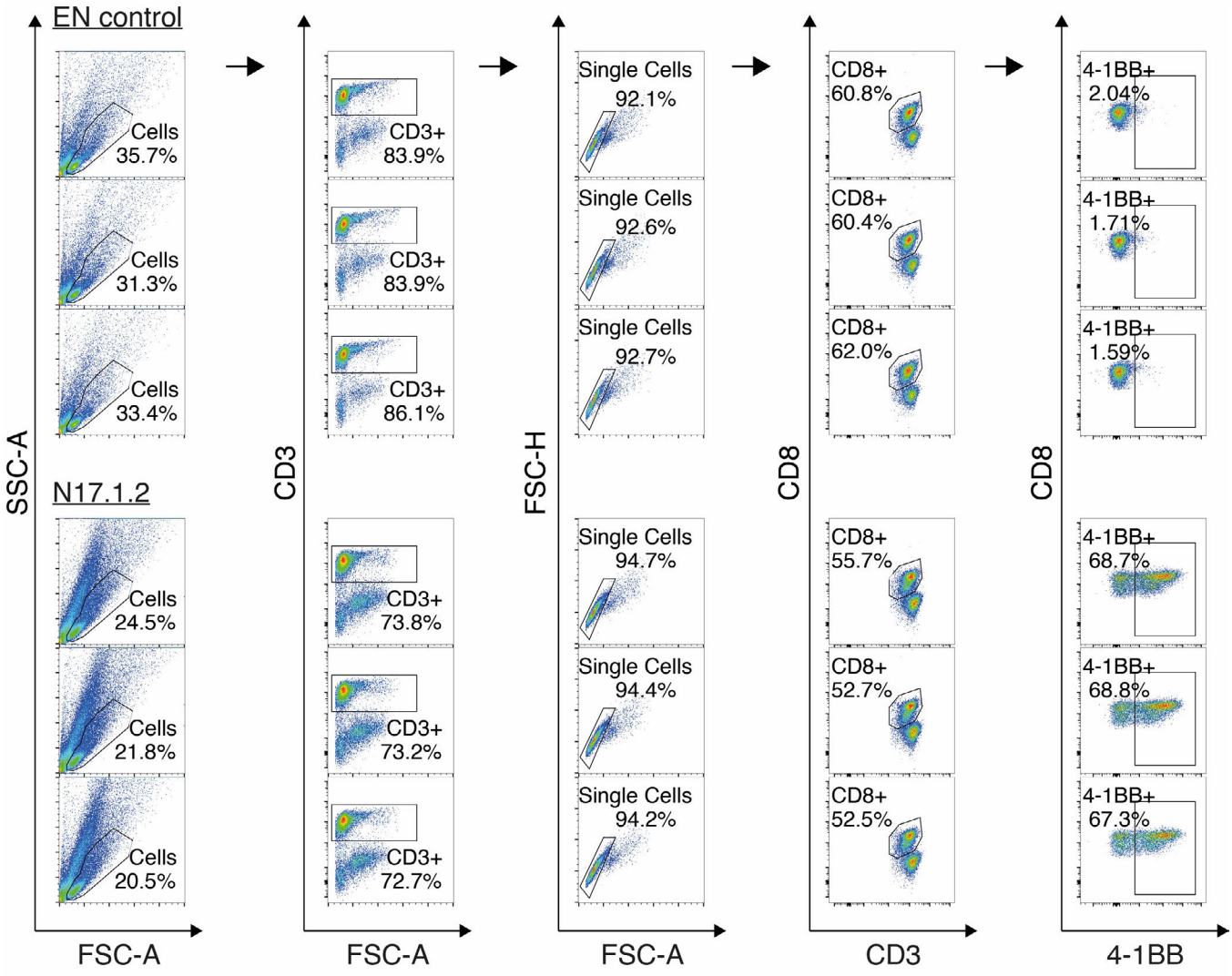

Supplementary figure 47: Flow-cytometry analysis of 4-1BB reactivity assay of N17.1.2-electroporated T-cells co-incubated with Calu6 lung adenocarcinoma cell-line at 1:1 ratio. 'EN' = 'electroporated nothing'; i.e. a negative control of the same batch of healthy-donor T-cells which went through the same electroporation procedure but without mRNA. Biological triplicates were prepared for each condition.

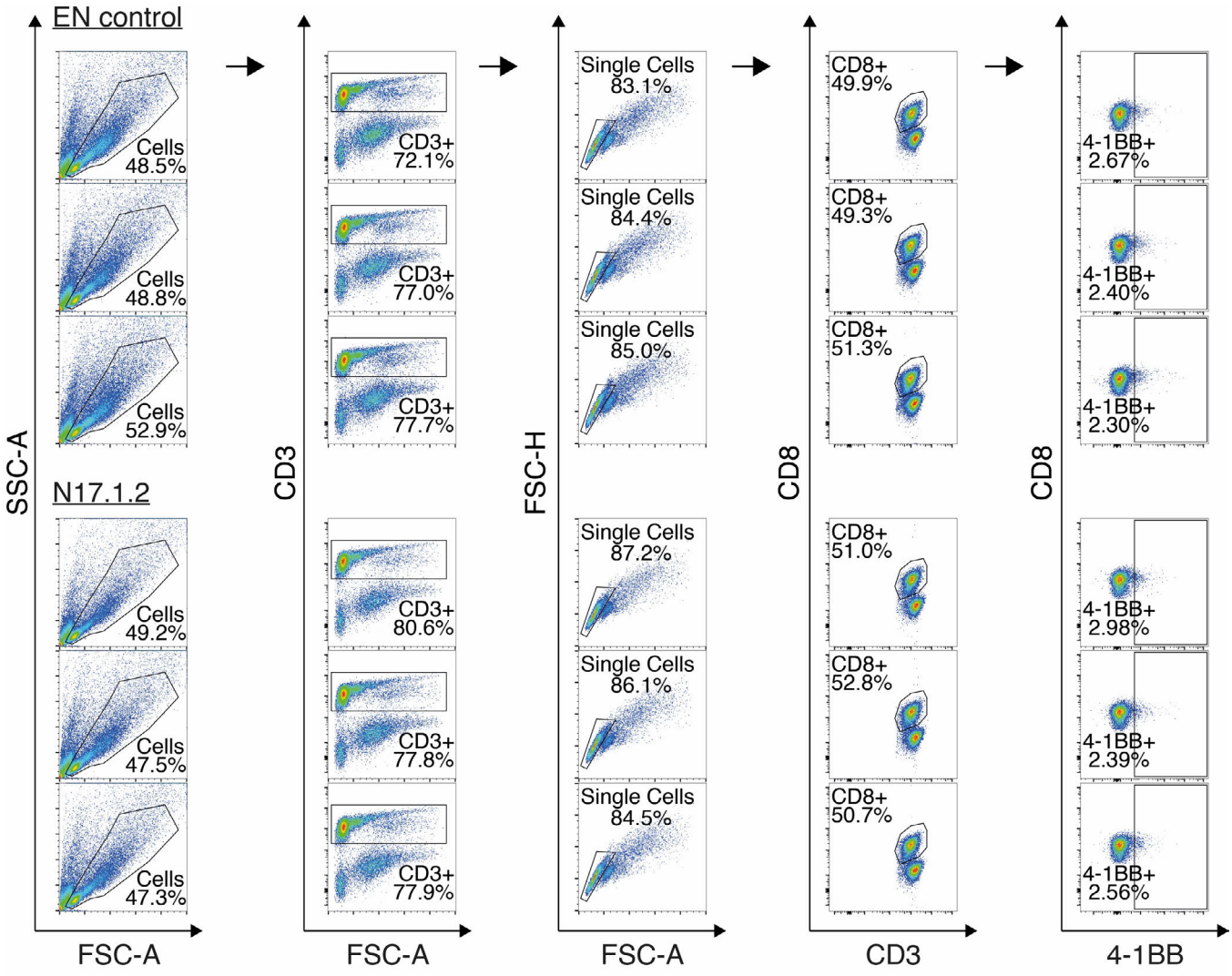

Supplementary figure 48: Flow-cytometry analysis of 4-1BB reactivity assay of N17.1.2-electroporated T-cells co-incubated with 108T melanoma cell-line at 1:1 ratio. 'EN' = 'electroporated nothing'; i.e. a negative control of the same batch of healthy-donor T-cells which went through the same electroporation procedure but without mRNA. Biological triplicates were prepared for each condition.

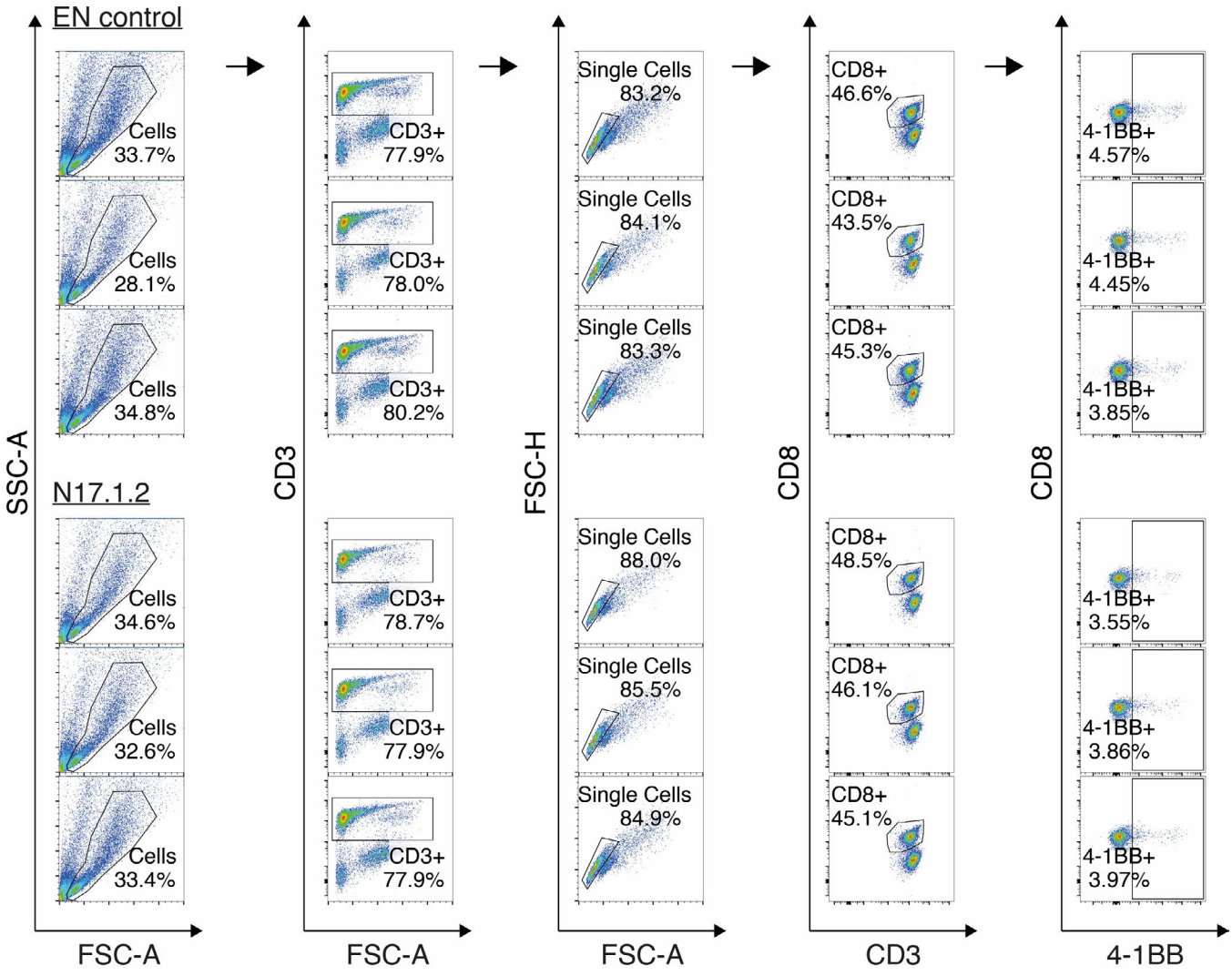

Supplementary figure 49: Flow-cytometry analysis of 4-1BB reactivity assay of N17.1.2-electroporated T-cells co-incubated with MM150414 melanoma cell-line at 1:1 ratio. 'EN' = 'electroporated nothing'; i.e. a negative control of the same batch of healthy-donor T-cells which went through the same electroporation procedure but without mRNA. Biological triplicates were prepared for each condition.

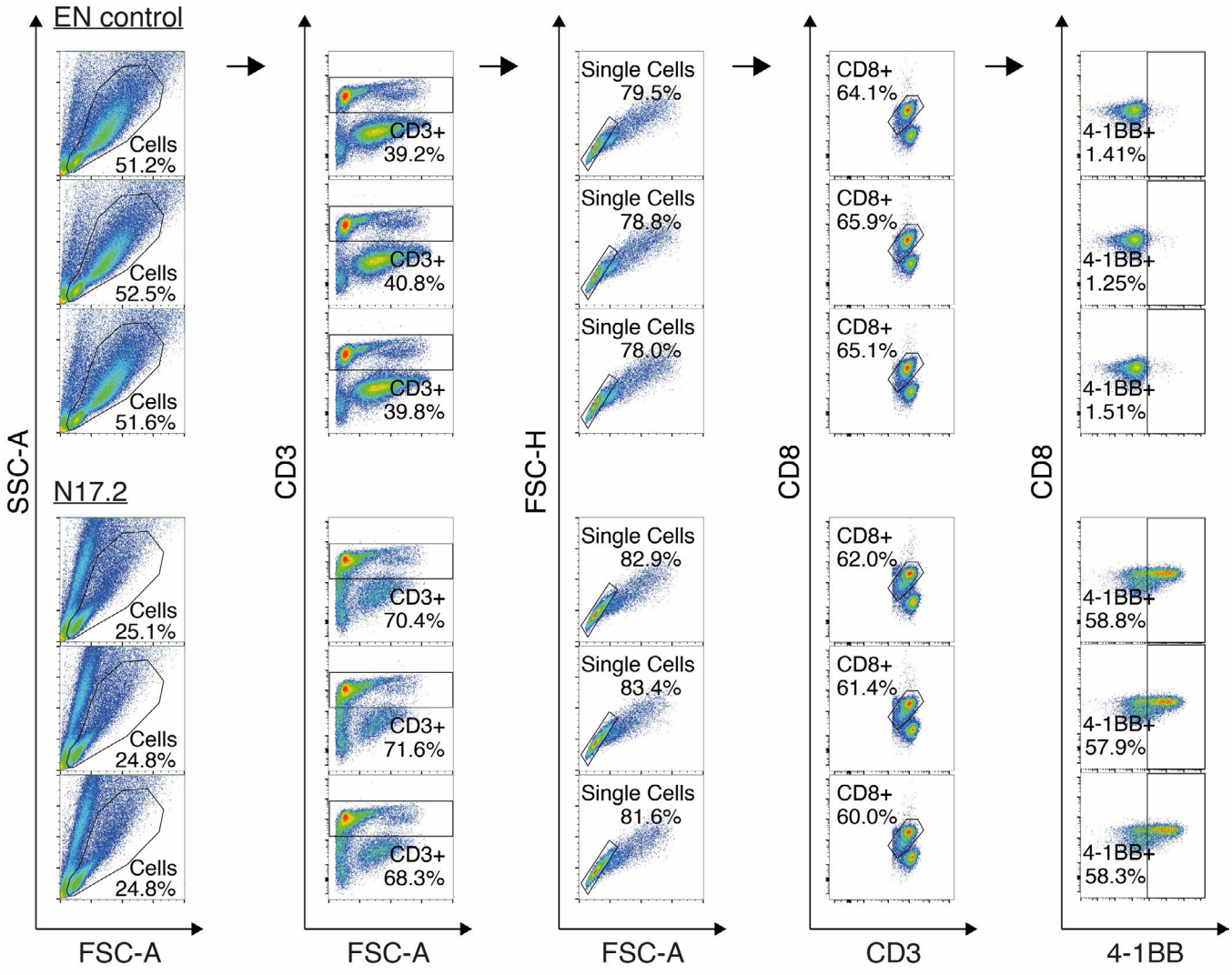

Supplementary figure 50: Flow-cytometry analysis of 4-1BB reactivity assay of N17. 2-electroporated T-cells co-incubated with 17T melanoma cell-line at 1:1 ratio. 'EN' = 'electroporated nothing'; i.e. a negative control of the same batch of healthy-donor T-cells which went through the same electroporation procedure but without mRNA. Biological triplicates were prepared for each condition.

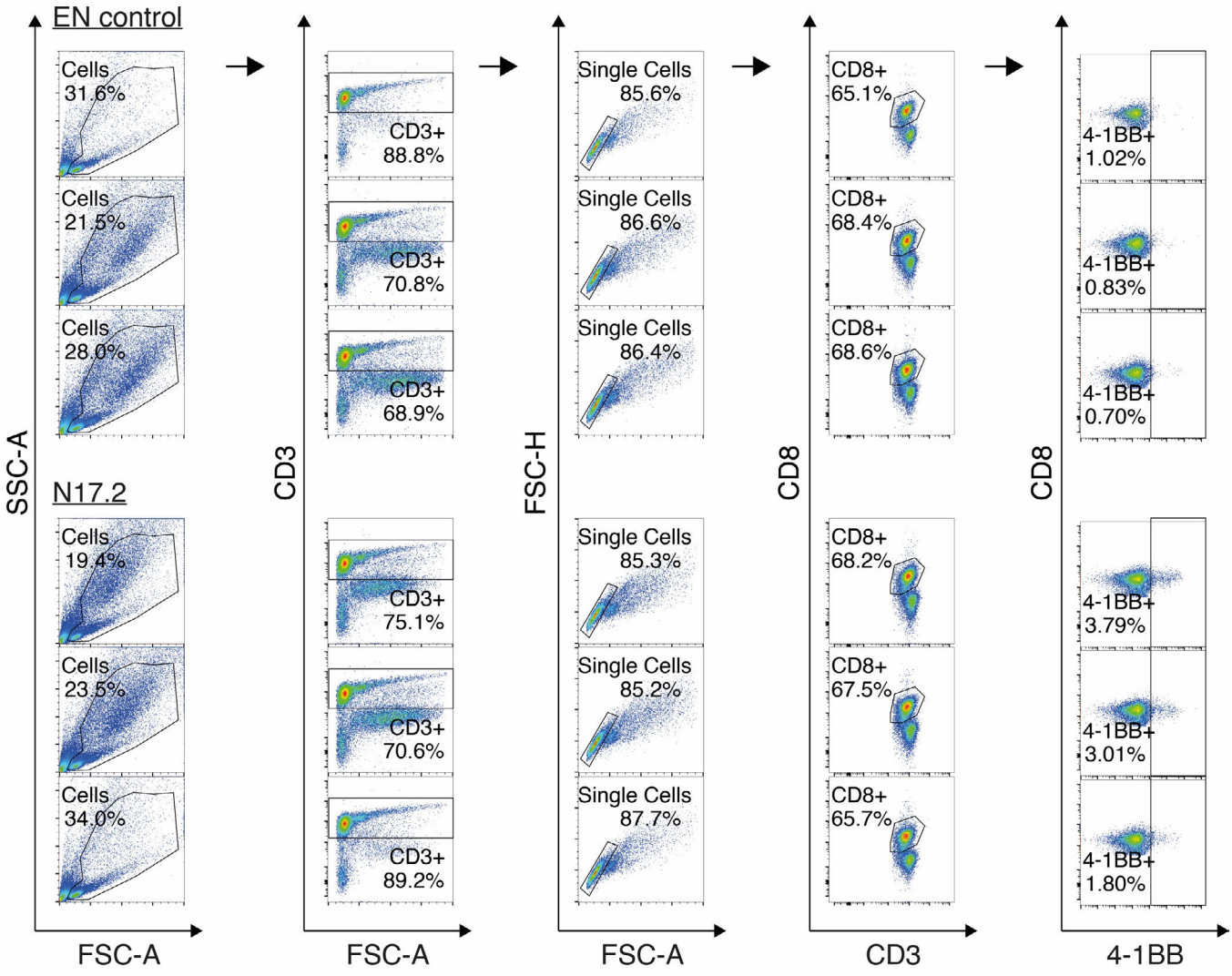

Supplementary figure 51: Flow-cytometry analysis of 4-1BB reactivity assay of N17. 2-electroporated T-cells co-incubated with 135T melanoma cell-line at 1:1 ratio. 'EN' = 'electroporated nothing'; i.e. a negative control of the same batch of healthy-donor T-cells which went through the same electroporation procedure but without mRNA. Biological triplicates were prepared for each condition.

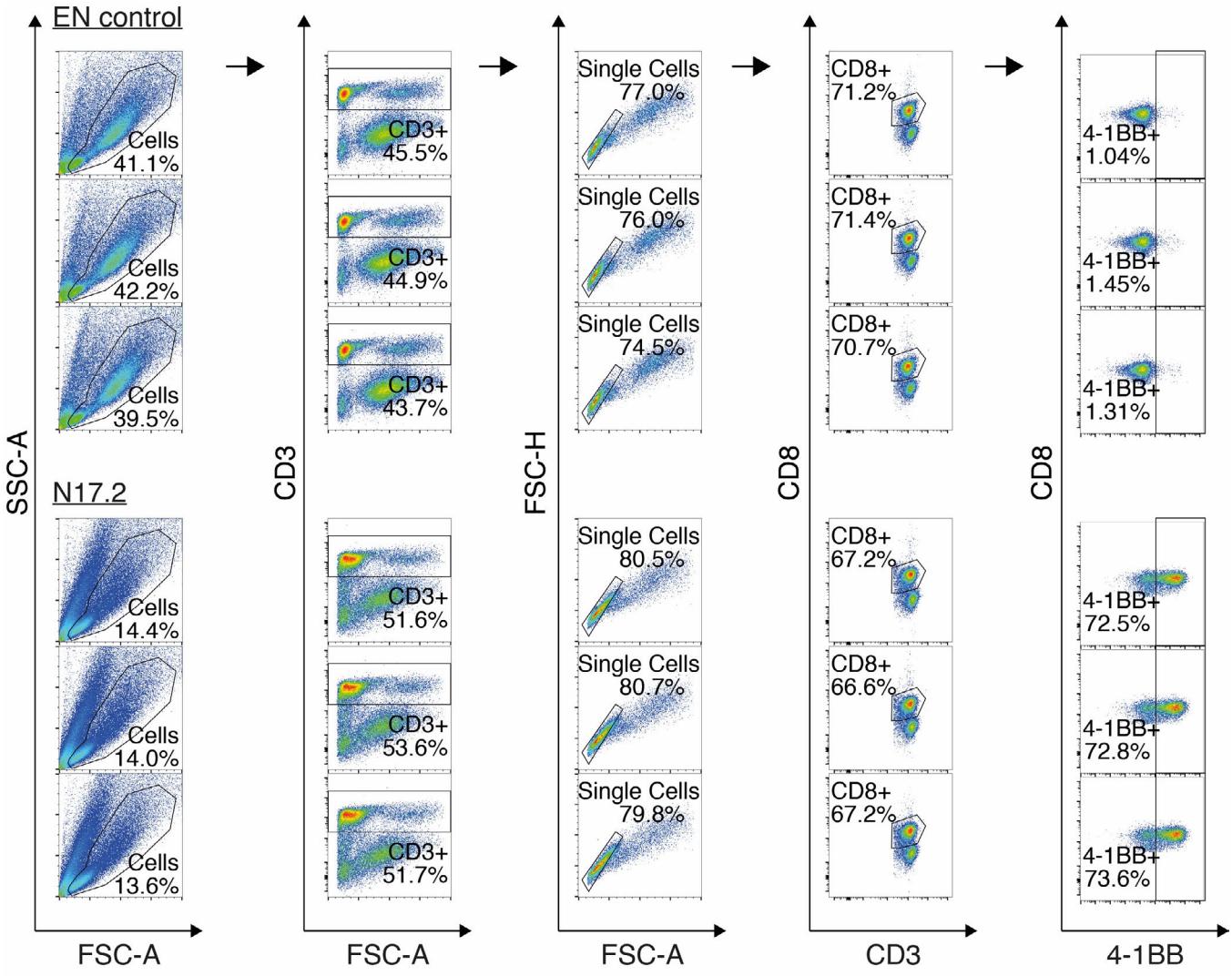

Supplementary figure 52: Flow-cytometry analysis of 4-1BB reactivity assay of N17. 2-electroporated T-cells co-incubated with SK-MEL-30 melanoma cell-line at 1:1 ratio. 'EN' = 'electroporated nothing'; i.e. a negative control of the same batch of healthy-donor T-cells which went through the same electroporation procedure but without mRNA. Biological triplicates were prepared for each condition.

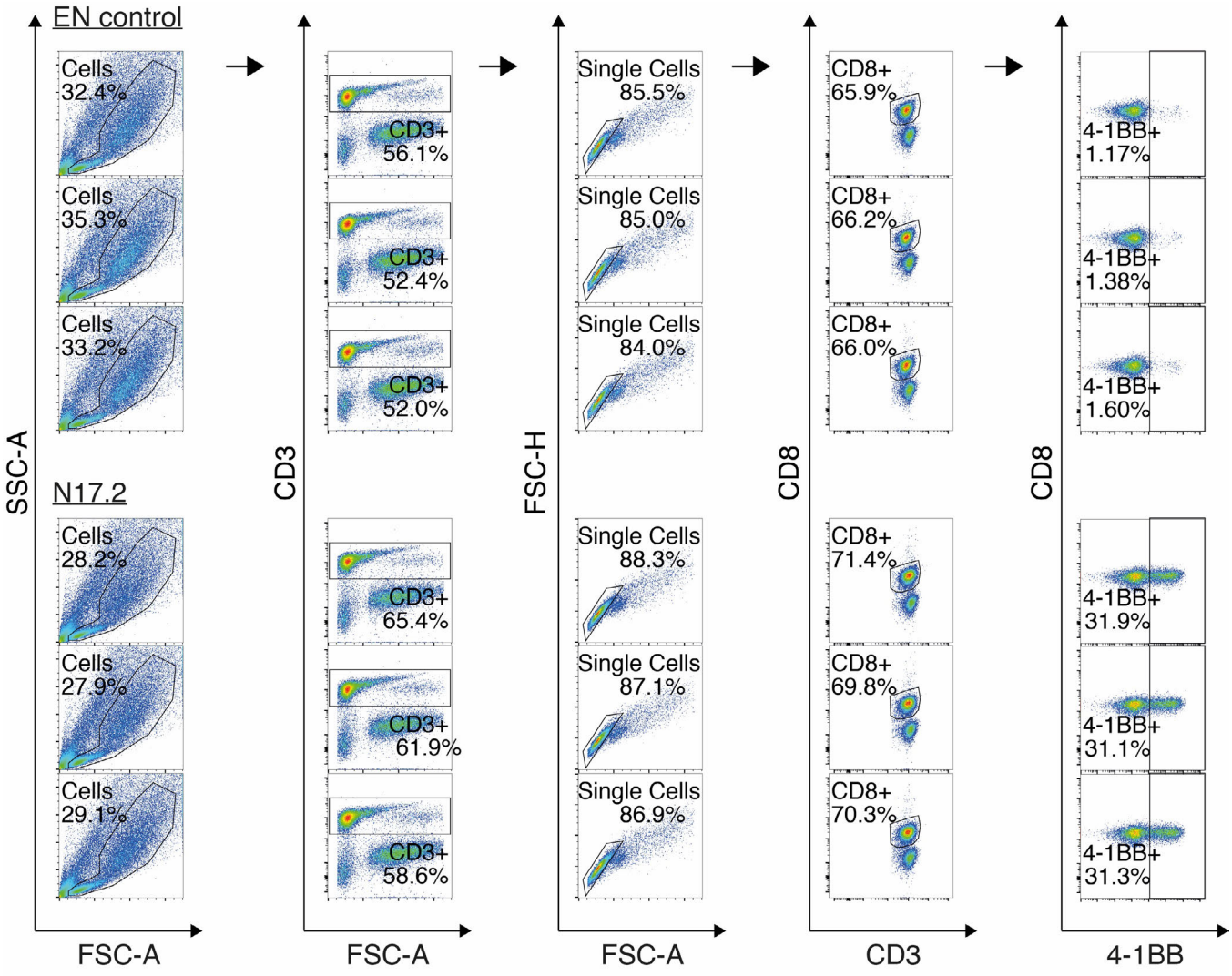

Supplementary figure 53: Flow-cytometry analysis of 4-1BB reactivity assay of N17. 2-electroporated T-cells co-incubated with MM121224 melanoma cell-line at 1:1 ratio. 'EN' = 'electroporated nothing'; i.e. a negative control of the same batch of healthy-donor T-cells which went through the same electroporation procedure but without mRNA. Biological triplicates were prepared for each condition.

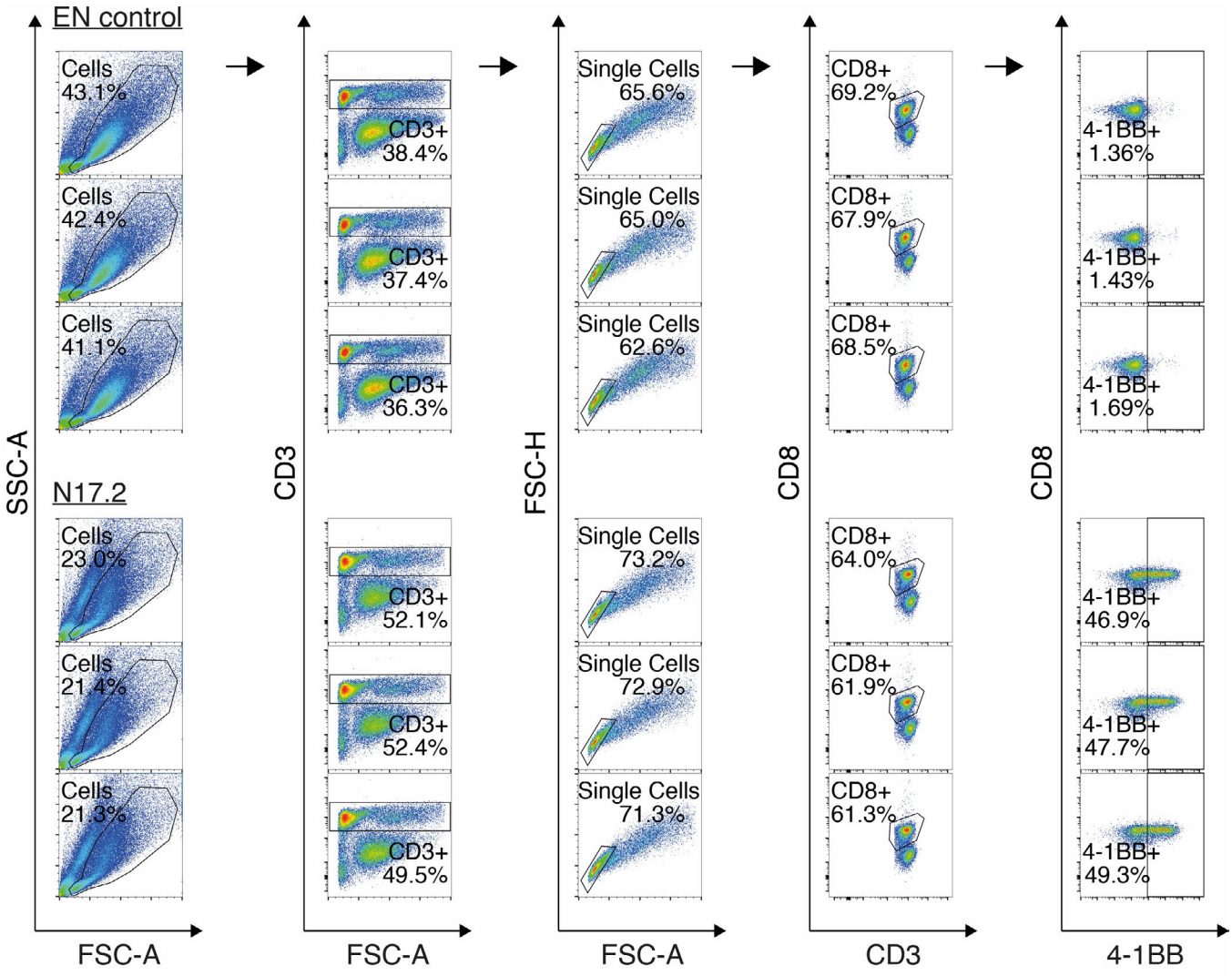

Supplementary figure 54: Flow-cytometry analysis of 4-1BB reactivity assay of N17. 2-electroporated T-cells co-incubated with MZ2-MEL melanoma cell-line at 1:1 ratio. 'EN' = 'electroporated nothing'; i.e. a negative control of the same batch of healthy-donor T-cells which went through the same electroporation procedure but without mRNA. Biological triplicates were prepared for each condition.

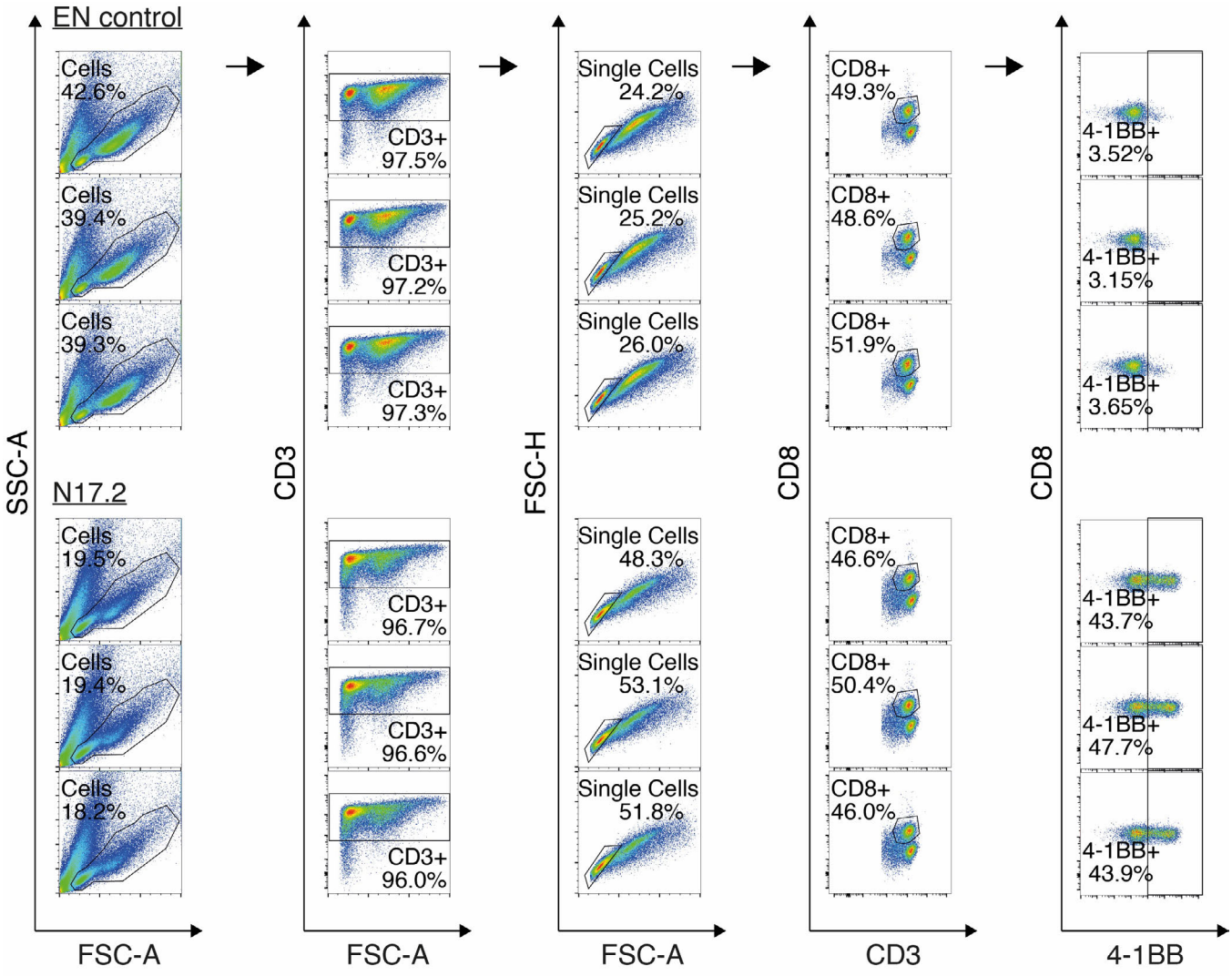

Supplementary figure 55: Flow-cytometry analysis of 4-1BB reactivity assay of N17. 2-electroporated T-cells co-incubated with HuT78 cutaneous T-cell lymphoma cell-line at 1:1 ratio. 'EN' = 'electroporated nothing'; i.e. a negative control of the same batch of healthy-donor T-cells which went through the same electroporation procedure but without mRNA. Biological triplicates were prepared for each condition.

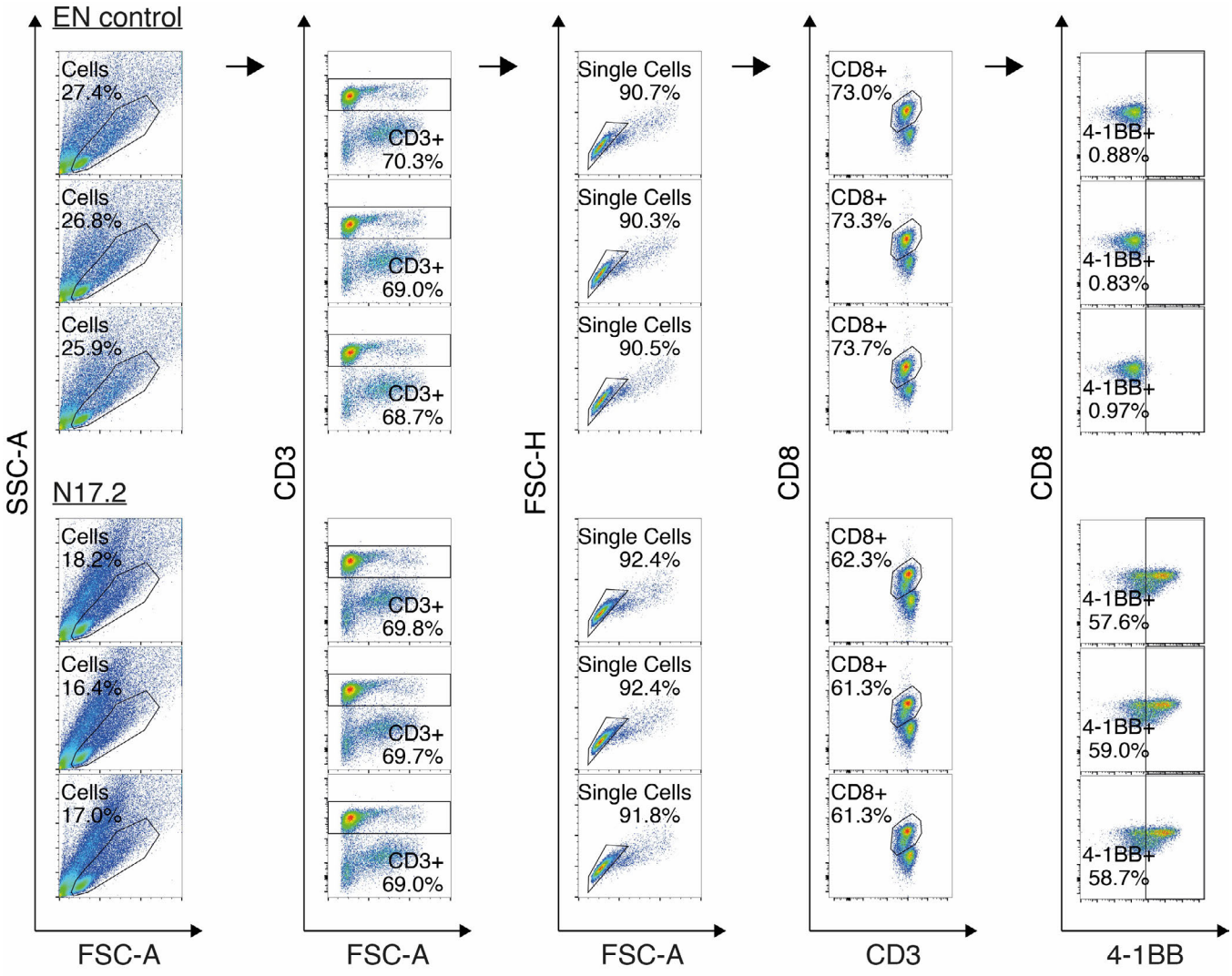

Supplementary figure 56: Flow-cytometry analysis of 4-1BB reactivity assay of N17. 2-electroporated T-cells co-incubated with Calu6 lung adenocarcinoma cell-line at 1:1 ratio. 'EN' = 'electroporated nothing'; i.e. a negative control of the same batch of healthy-donor T-cells which went through the same electroporation procedure but without mRNA. Biological triplicates were prepared for each condition.

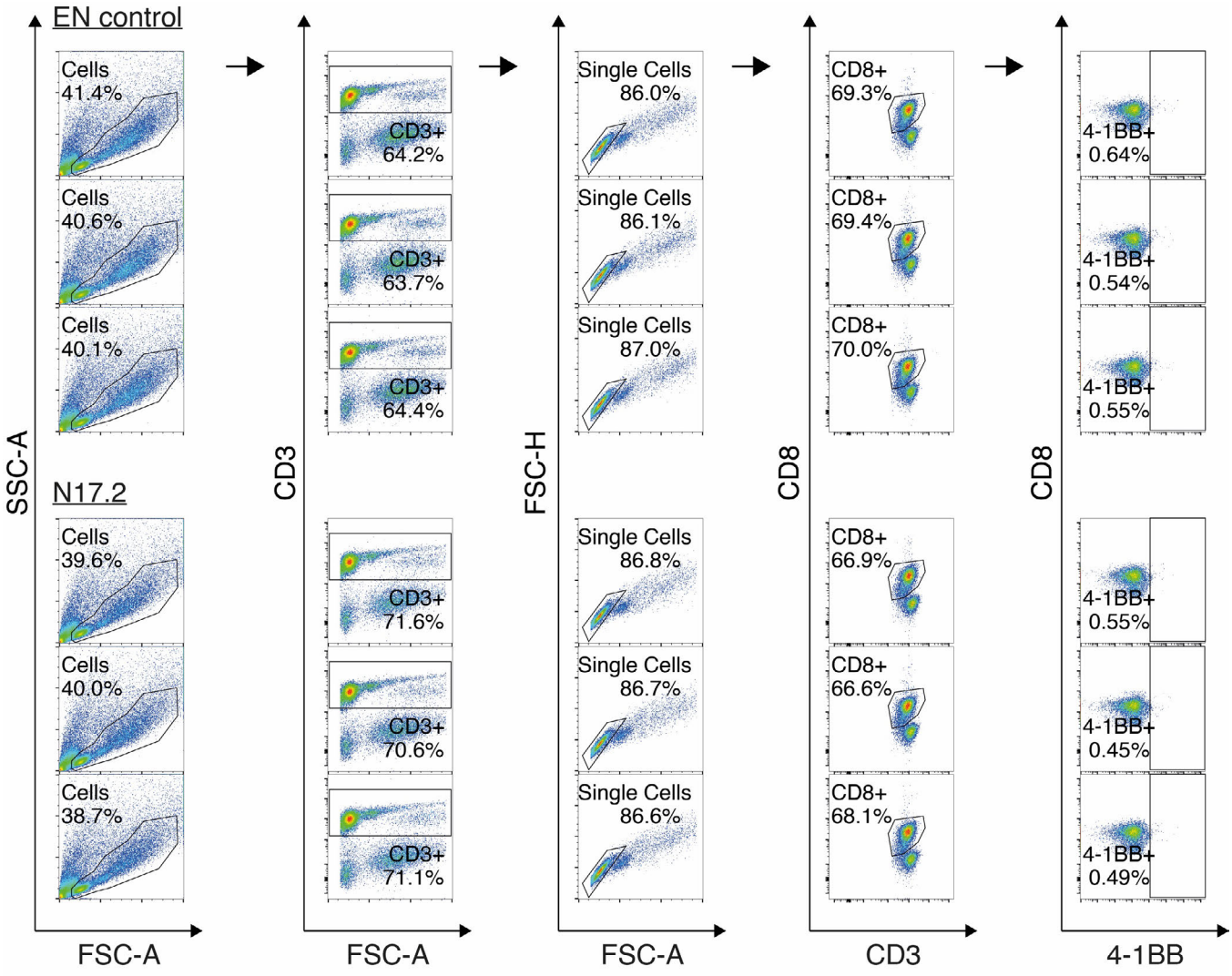

Supplementary figure 57: Flow-cytometry analysis of 4-1BB reactivity assay of N17. 2-electroporated T-cells co-incubated with 108T melanoma cell-line at 1:1 ratio. 'EN' = 'electroporated nothing'; i.e. a negative control of the same batch of healthy-donor T-cells which went through the same electroporation procedure but without mRNA. Biological triplicates were prepared for each condition.

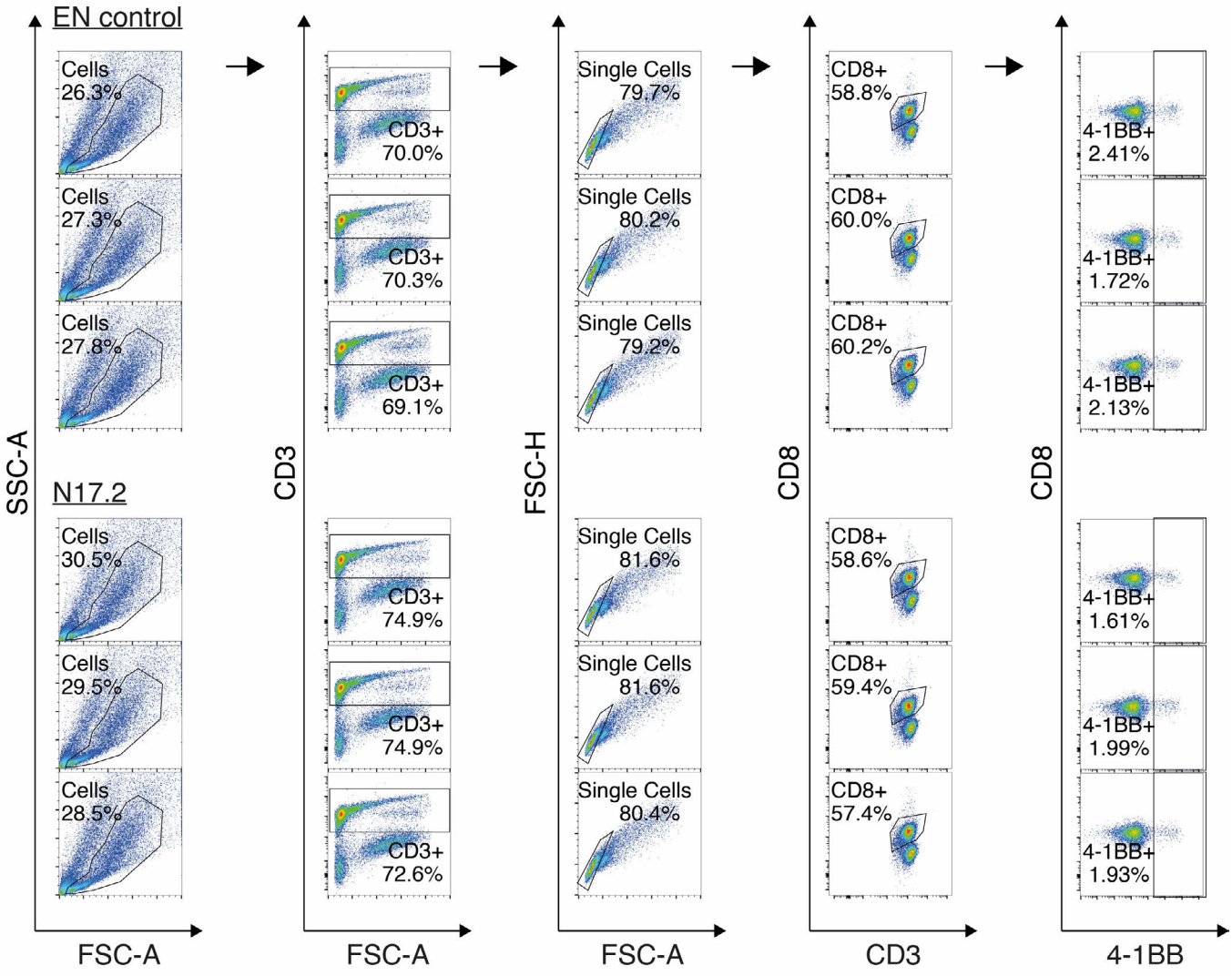

Supplementary figure 58: Flow-cytometry analysis of 4-1BB reactivity assay of N17. 2-electroporated T-cells co-incubated with MM150414 melanoma cell-line at 1:1 ratio. 'EN' = 'electroporated nothing'; i.e. a negative control of the same batch of healthy-donor T-cells which went through the same electroporation procedure but without mRNA. Biological triplicates were prepared for each condition.

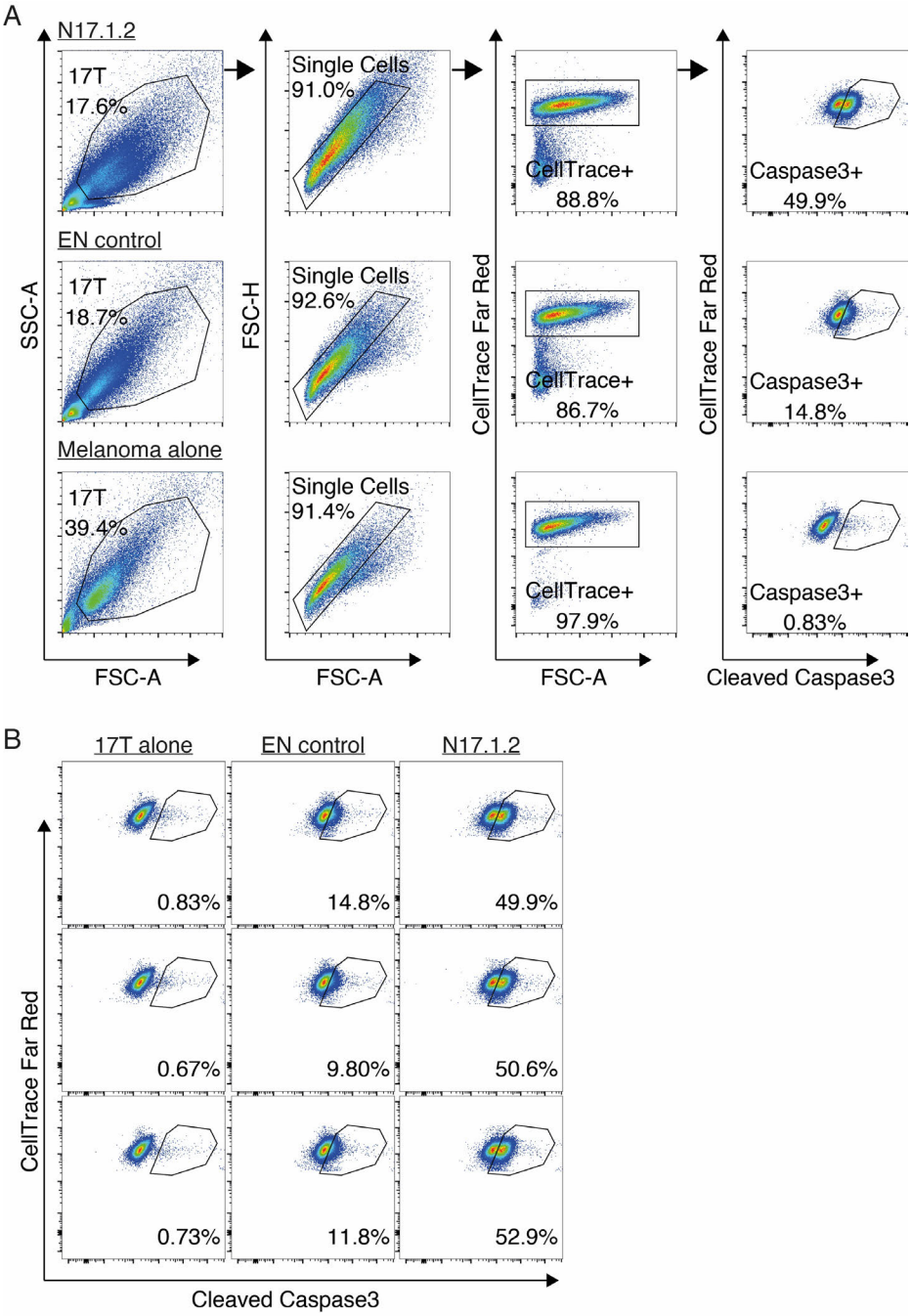

Supplementary figure 59: Flow-cytometry gating for cleaved Caspase3 cytotoxicity assay of N17.1.2-electroporated healthy-donor T-cells, co-incubated with melanoma cell-line 17T at 3:1 ratio for three hours. (A) Full gating strategy is demonstrated on representative replicates for each of the following conditions: *T-N17.1.2 : 17T*, *T-EN : 17T and 17T alone*. **(B)** Caspase3 gating for all replicates; Biological triplicates were prepared for each condition. 'EN' = 'electroporated nothing'; i.e. a negative control of the same batch of healthy-donor T-cells which went through the same electroporation procedure but without mRNA.

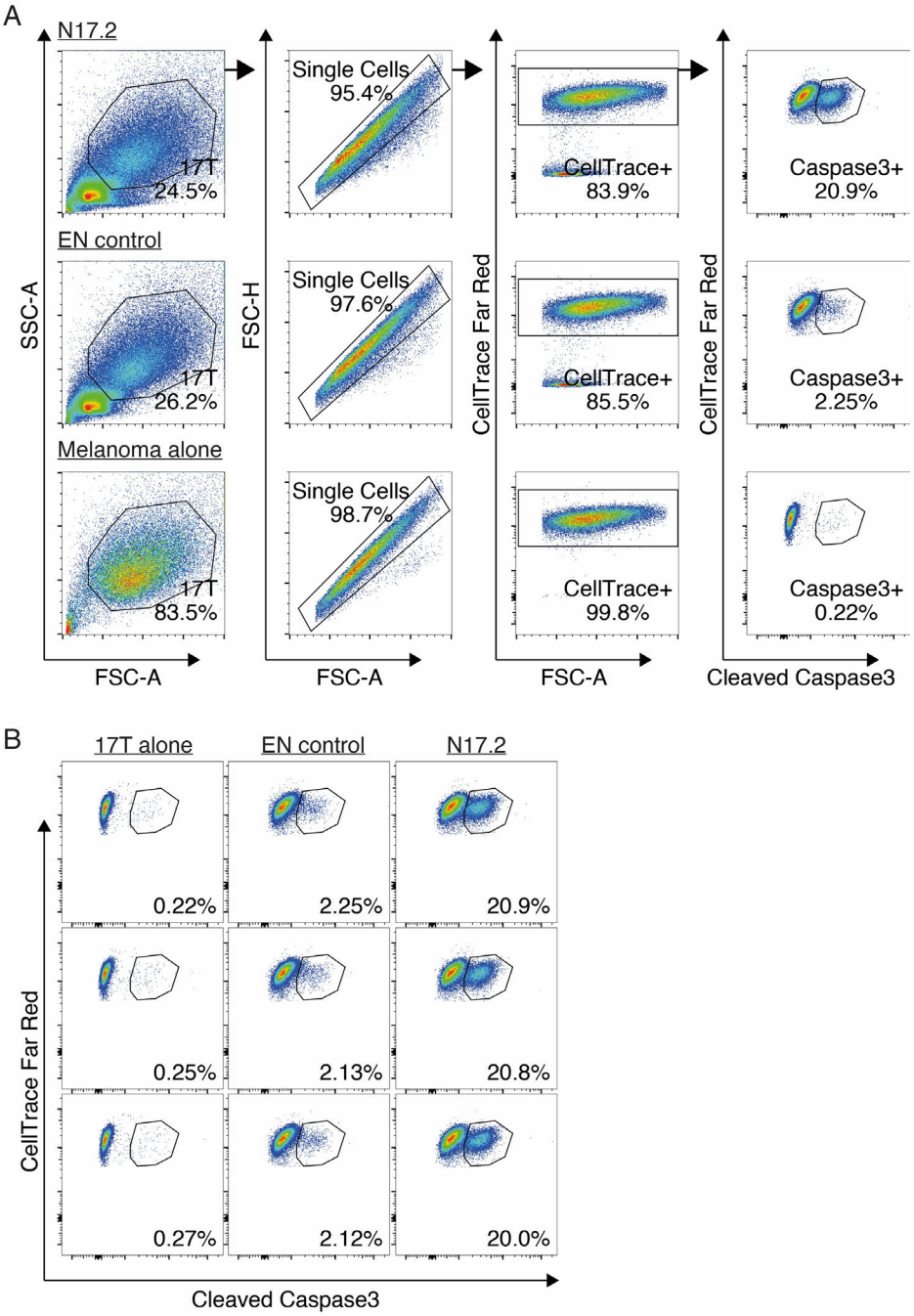

Supplementary figure 60: Flow-cytometry gating for cleaved Caspase3 cytotoxicity assay of N17.2-electroporated healthy-donor T-cells, co-incubated with melanoma cell-line 17T at 3:1 ratio for three hours. (A) Full gating strategy is demonstrated on representative replicates for each of the following conditions: *T-N17.2 : 17T*, *T-EN : 17T and 17T alone*. **(B)** Caspase3 gating for all replicates; Biological triplicates were prepared for each condition. 'EN' = 'electroporated nothing'; i.e. a negative control of the same batch of healthy-donor T-cells which went through the same electroporation procedure but without mRNA.

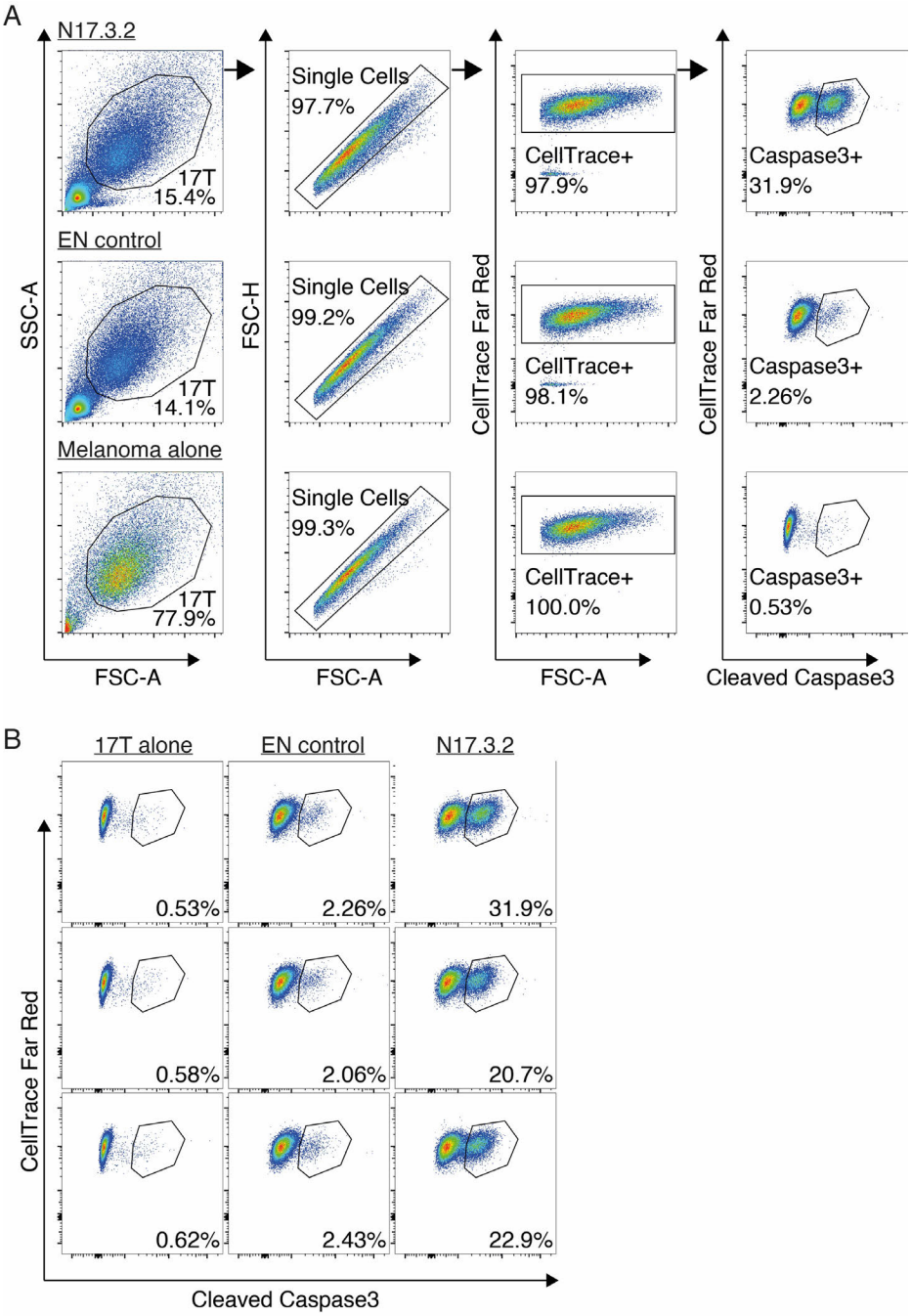

Supplementary figure 61: Flow-cytometry gating for cleaved Caspase3 cytotoxicity assay of N17.3.2-electroporated healthy-donor T-cells, co-incubated with melanoma cell-line 17T at 3:1 ratio for three hours. (A) Full gating strategy is demonstrated on representative replicates for each of the following conditions: *T-N17.3.2 : 17T*, *T-EN : 17T and 17T alone*. **(B)** Caspase3 gating for all replicates; Biological triplicates were prepared for each condition. 'EN' = 'electroporated nothing'; i.e. a negative control of the same batch of healthy-donor T-cells which went through the same electroporation procedure but without mRNA.

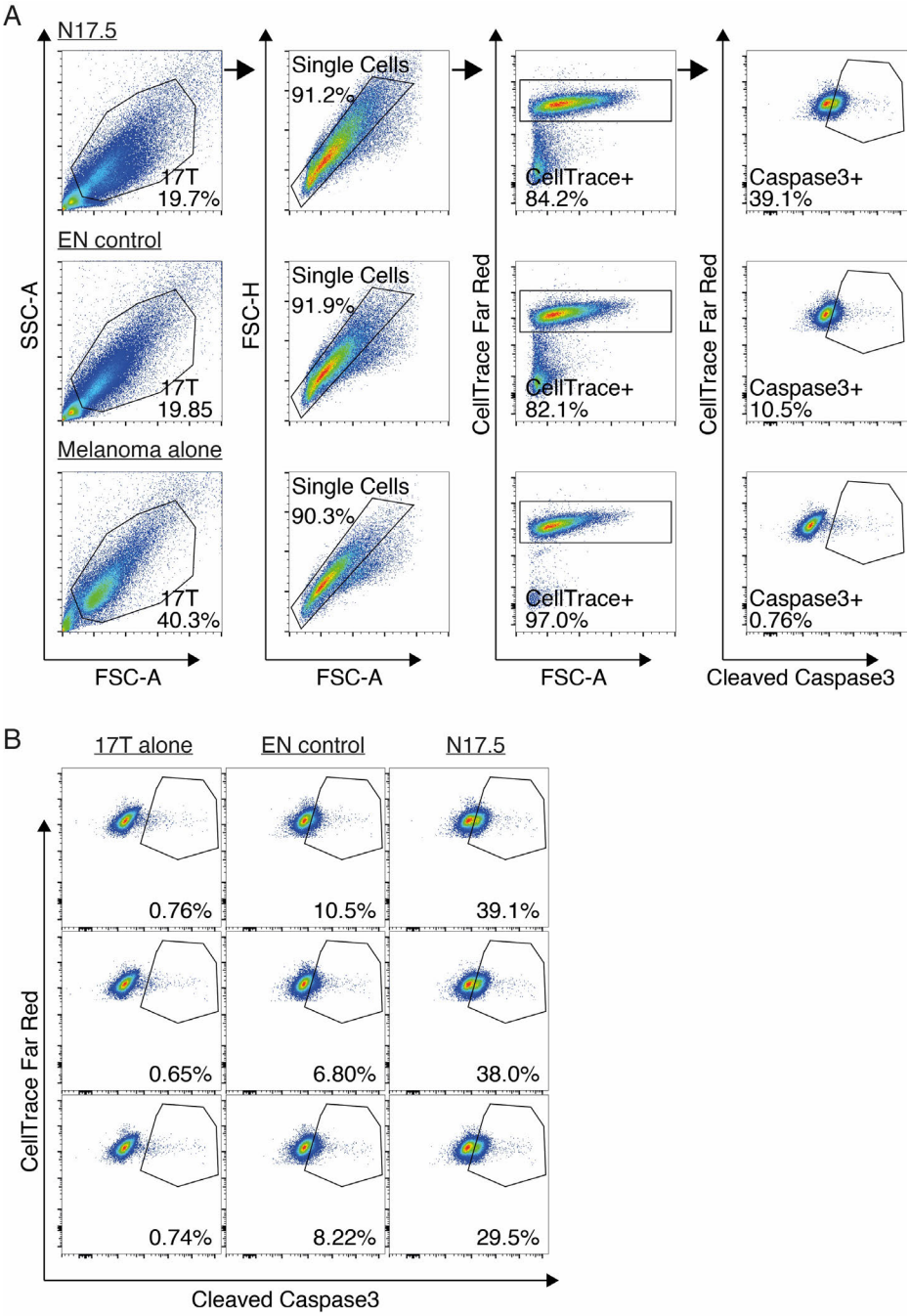

Supplementary figure 62: Flow-cytometry gating for cleaved Caspase3 cytotoxicity assay of N17.5-electroporated healthy-donor T-cells, co-incubated with melanoma cell-line 17T at 3:1 ratio for three hours. (A) Full gating strategy is demonstrated on representative replicates for each of the following conditions: *T-N17.5 : 17T*, *T-EN : 17T and 17T alone*. **(B)** Caspase3 gating for all replicates; Biological triplicates were prepared for each condition. 'EN' = 'electroporated nothing'; i.e. a negative control of the same batch of healthy-donor T-cells which went through the same electroporation procedure but without mRNA.

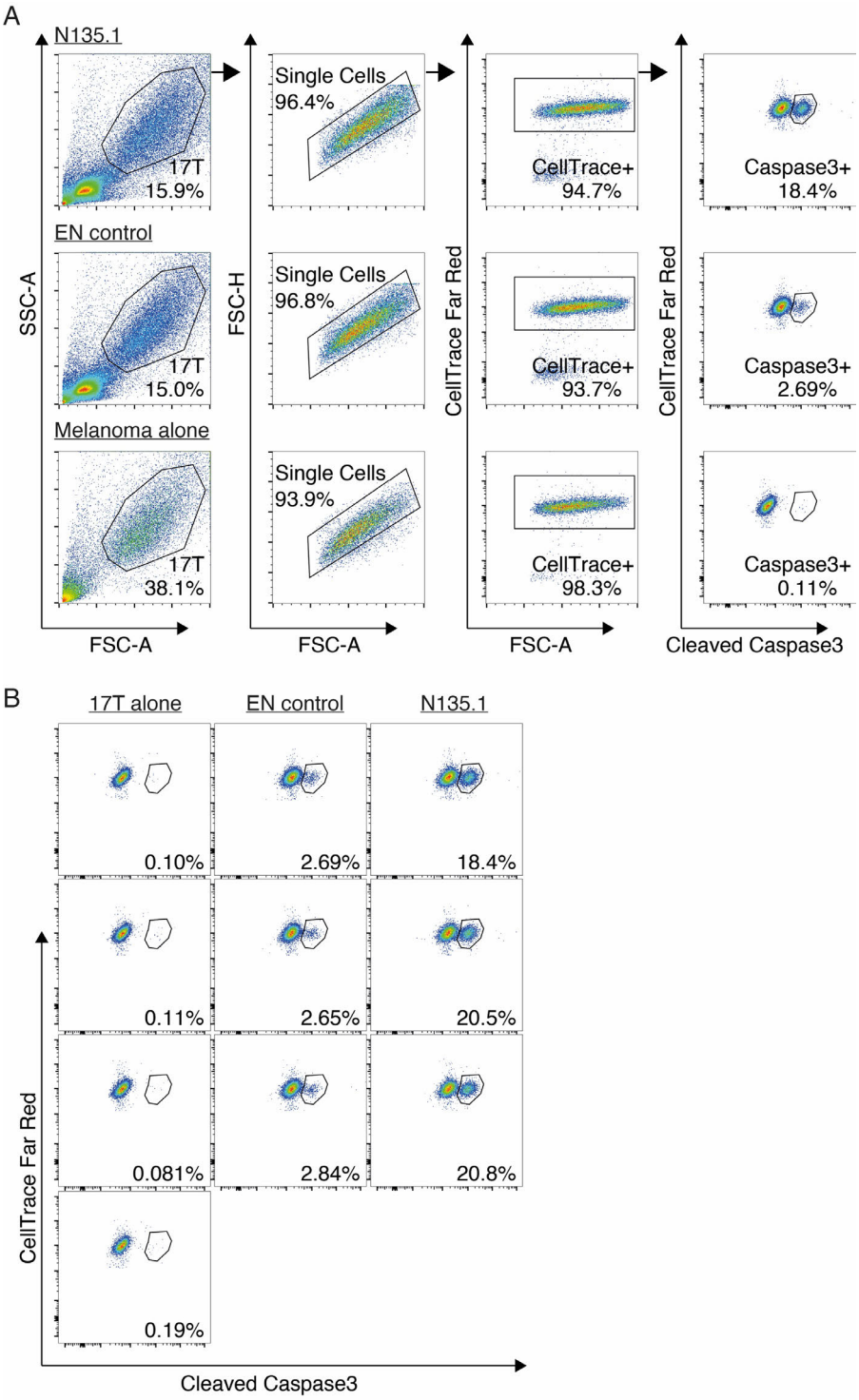

Supplementary figure 63: Flow-cytometry gating for cleaved Caspase3 cytotoxicity assay of N135.1-electroporated healthy-donor T-cells, co-incubated with melanoma cell-line 17T at 3:1 ratio for three hours. (A) Full gating strategy is demonstrated on representative replicates for each of the following conditions: *T-N135.1 : 17T*, *T-EN : 17T and 17T alone*. **(B)** Caspase3 gating for all replicates; Biological triplicates were prepared for each condition. 'EN' = 'electroporated nothing'; i.e. a negative control of the same batch of healthy-donor T-cells which went through the same electroporation procedure but without mRNA.

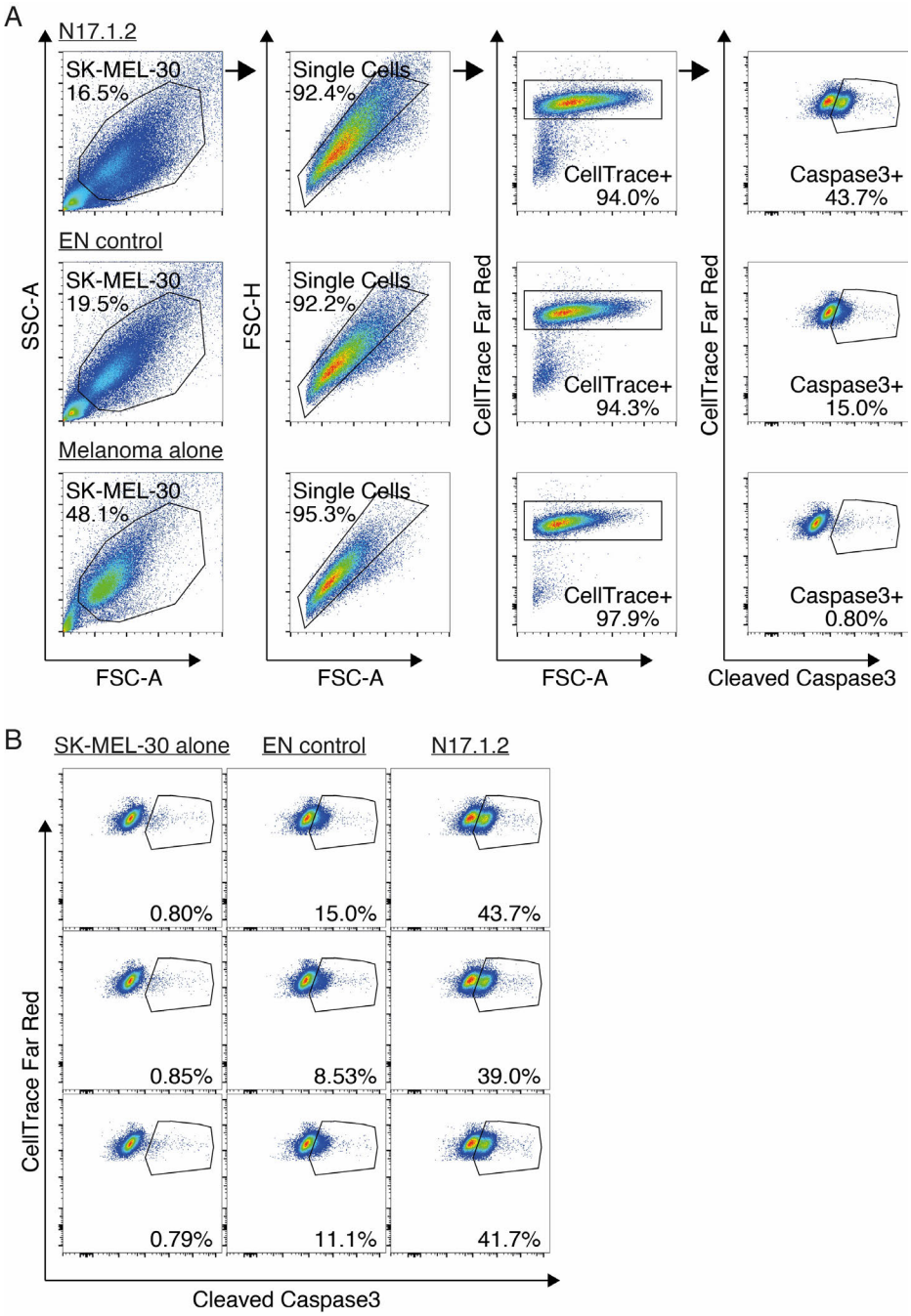

Supplementary figure 64: Flow-cytometry gating for cleaved Caspase3 cytotoxicity assay of N17.1.2-electroporated healthy-donor T-cells, co-incubated with melanoma cell-line SK-MEL-30 at 3:1 ratio for three hours. (A) Full gating strategy is demonstrated on representative replicates for each of the following conditions: *T-N17.1.2 : SK-MEL-30, T-EN : SK-MEL-30 and SK-MEL-30 alone.* **(B)** Caspase3 gating for all replicates; Biological triplicates were prepared for each condition. 'EN' = 'electroporated nothing'; i.e. a negative control of the same batch of healthy-donor T-cells which went through the same electroporation procedure but without mRNA.

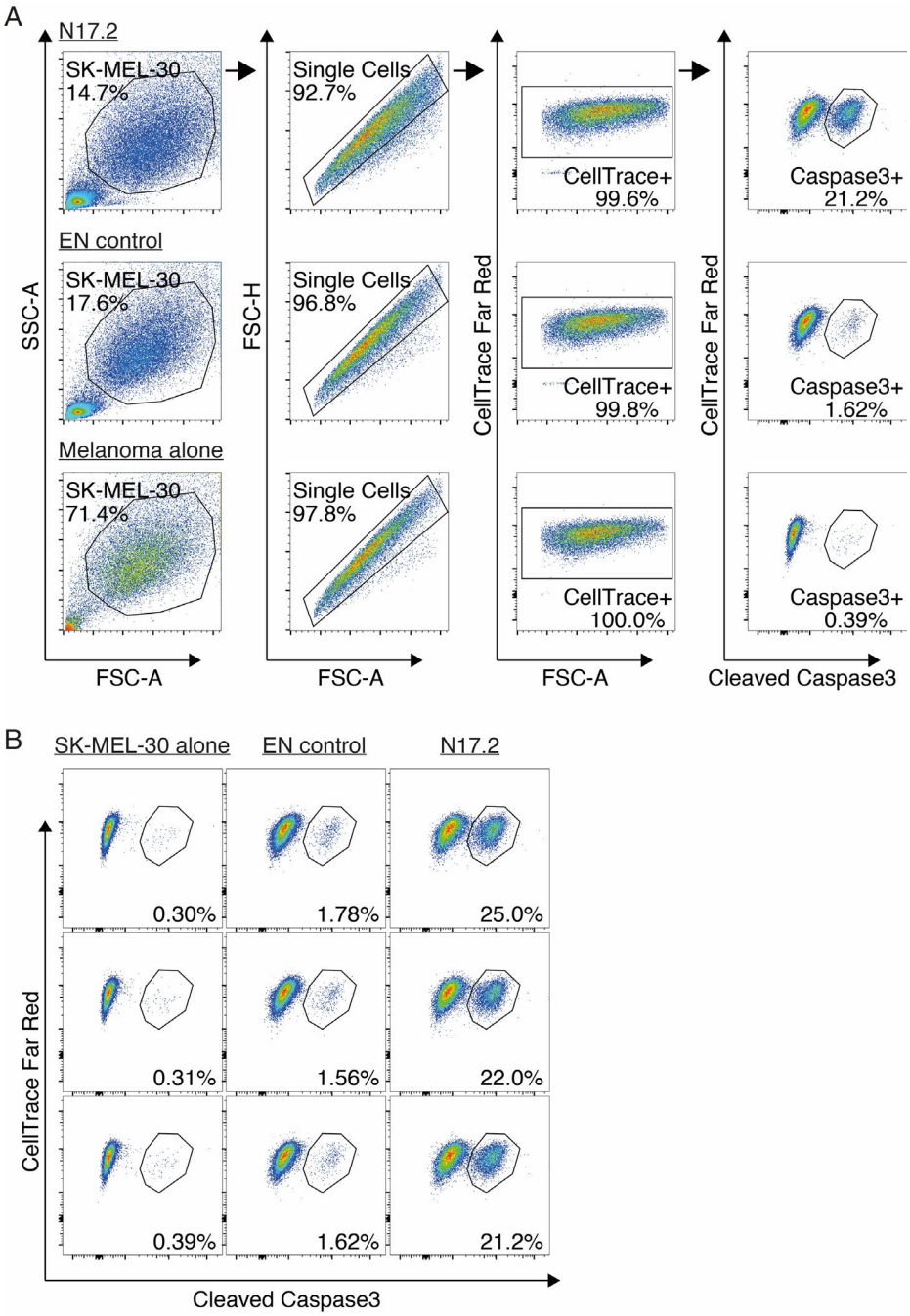

Supplementary figure 65: Flow-cytometry gating for cleaved Caspase3 cytotoxicity assay of N17.2-electroporated healthy-donor T-cells, co-incubated with melanoma cell-line SK-MEL-30 at 3:1 ratio for three hours. (A) Full gating strategy is demonstrated on representative replicates for each of the following conditions: *T-N17.2 : SK-MEL-30*, *T-EN : SK-MEL-30 and SK-MEL-30 alone*. **(B)** Caspase3 gating for all replicates; Biological triplicates were prepared for each condition. 'EN' = 'electroporated nothing'; i.e. a negative control of the same batch of healthy-donor T-cells which went through the same electroporation procedure but without mRNA.

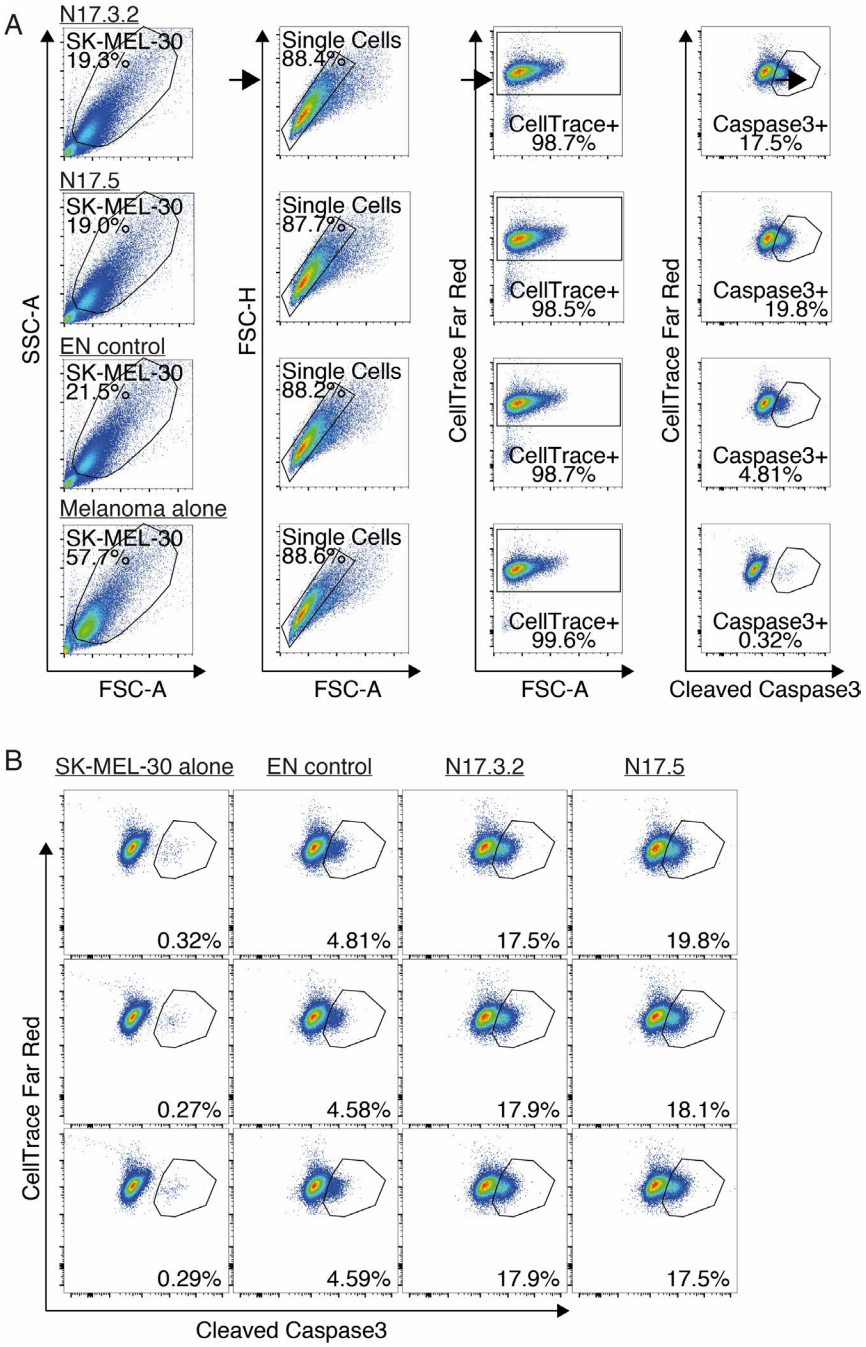

Supplementary figure 66: Flow-cytometry gating for cleaved Caspase3 cytotoxicity assay of N17.3.2- and N17.5-electroporated healthy-donor T-cells, co-incubated with melanoma cell-line SK-MEL-30 at 3:1 ratio for three hours. (A) Full gating strategy is demonstrated on representative replicates for each of the following conditions: *T-N17.3.2 : SK-MEL-30*, *T-N17.5 : SK-MEL-30, T-EN : SK-MEL-30 and SK-MEL-30 alone*. **(B)** Caspase3 gating for all replicates; Biological triplicates were prepared for each condition. 'EN' = 'electroporated nothing'; i.e. a negative control of the same batch of healthy-donor T-cells which went through the same electroporation procedure but without mRNA.

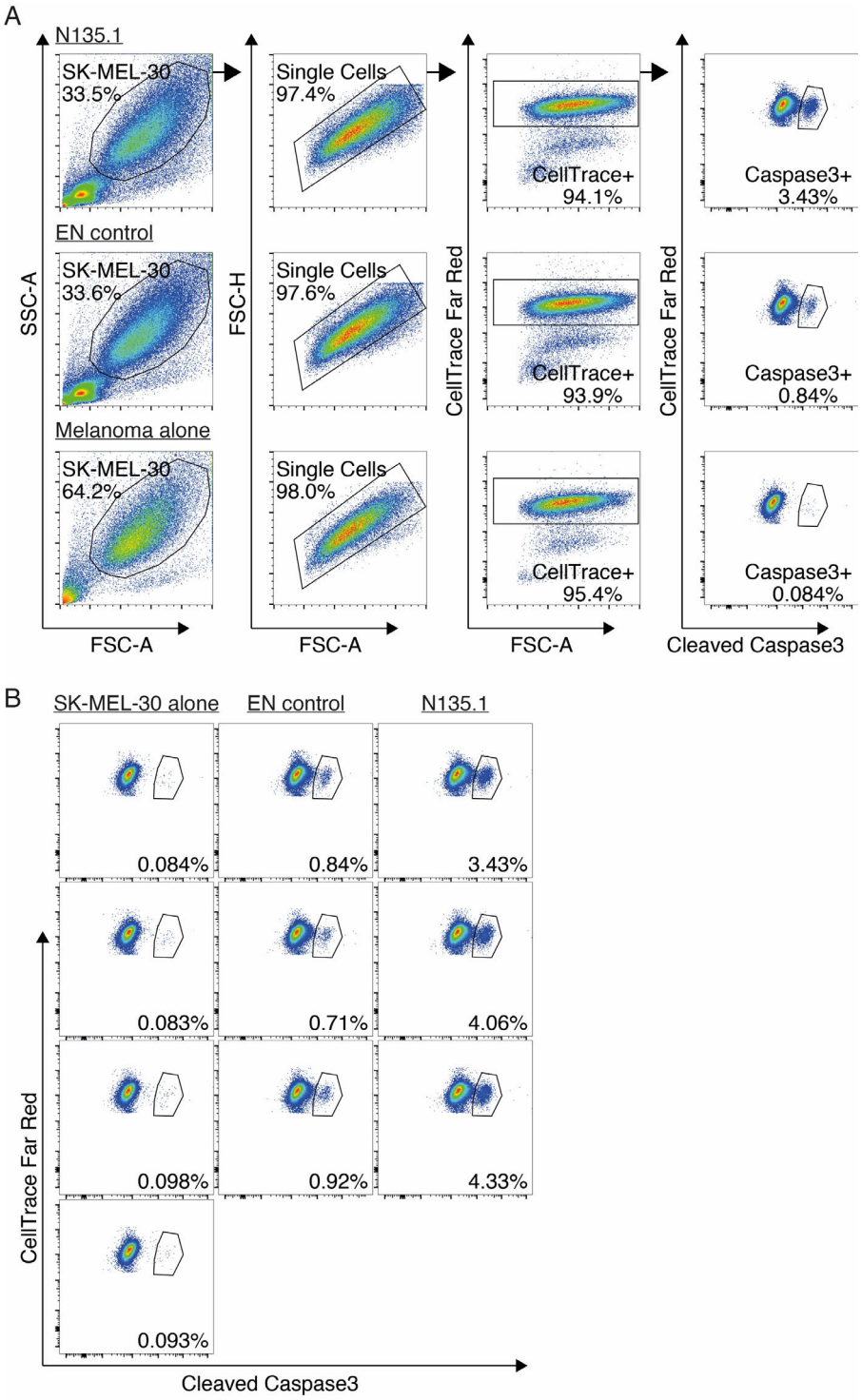

Supplementary figure 67: Flow-cytometry gating for cleaved Caspase3 cytotoxicity assay of N135.1-electroporated healthy-donor T-cells, co-incubated with melanoma cell-line SK-MEL-30 at 3:1 ratio for three hours. (A) Full gating strategy is demonstrated on representative replicates for each of the following conditions: *T-N135.1 : SK-MEL-30, T-EN : SK-MEL-30 and SK-MEL-30 alone*. **(B)** Caspase3 gating for all replicates; Biological triplicates were prepared for each condition. 'EN' = 'electroporated nothing'; i.e. a negative control of the same batch of healthy-donor T-cells which went through the same electroporation procedure but without mRNA.

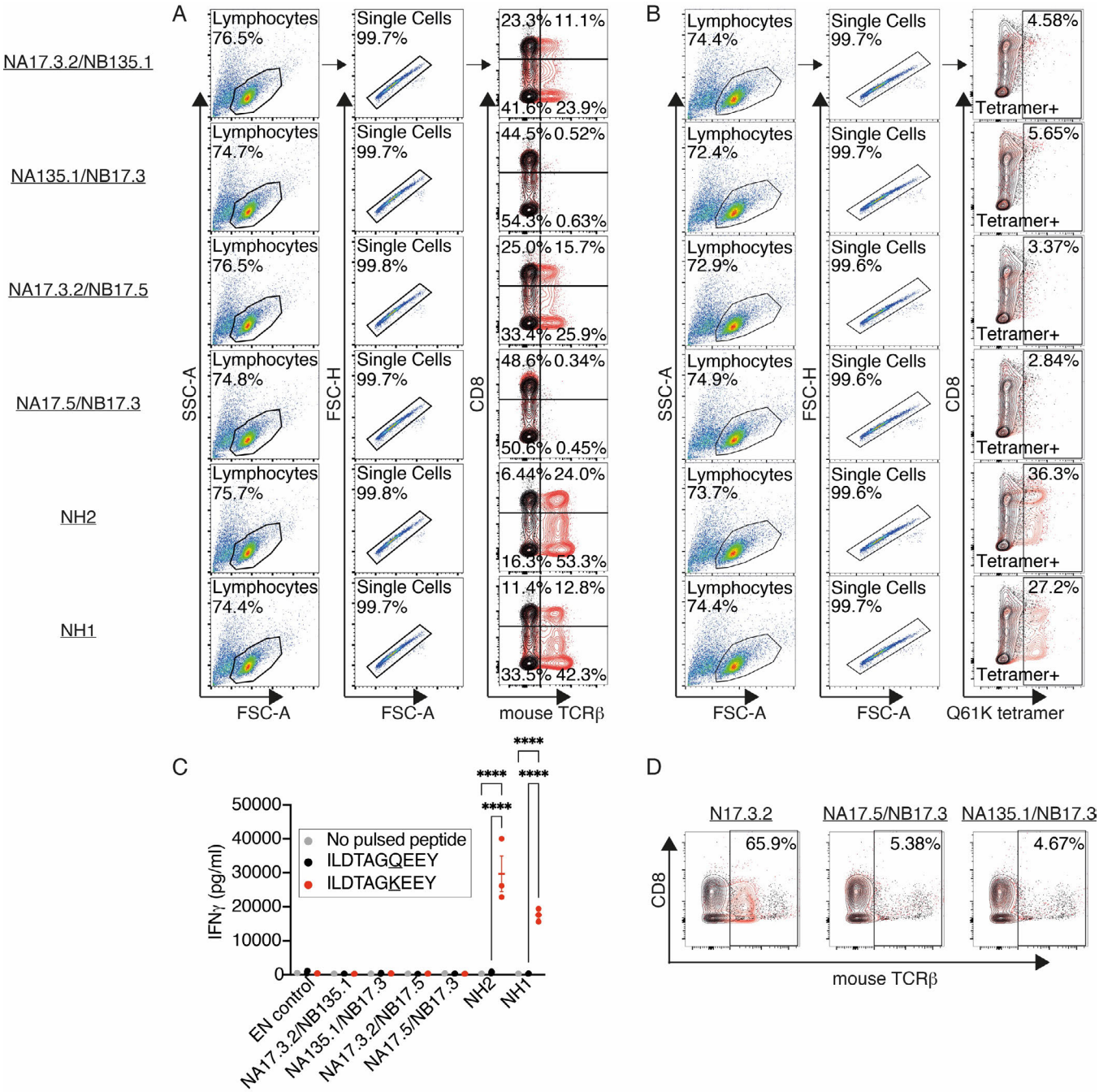

Supplementary figure 68: Testing TCR chain swaps within the neoantigen-specific convergence cluster. Healthy-donor peripheral T-cells were electroporated to express combinatorial α/β pairings within the neoantigen-specific convergence cluster. **(A)** CD8 and mouse constant TCRβ staining. (B) CD8 and HLA-A*01:01/*ILDTAGKEEY*-tetramer staining. **(C)** IFNg ELISA after overnight co-incubation of TCR-expressing cells with IHW01161 presenting-cells, pulsed with either the wild-type or mutant peptide, or with only DMSO. The experiment was conducted in biological triplicates, statistical analysis was conducted using 2-way ANOVA with Tukey's multiple comparisons correction. **(D)** CD8 and mouse constant TCRβ staining of a repeat experiment, using the same NB17.3 mRNA batch as in (A), confirming that the lack of surface expression of N17.5/NB17.3 and NA135.1/NB17.3 is not a technical artefact.

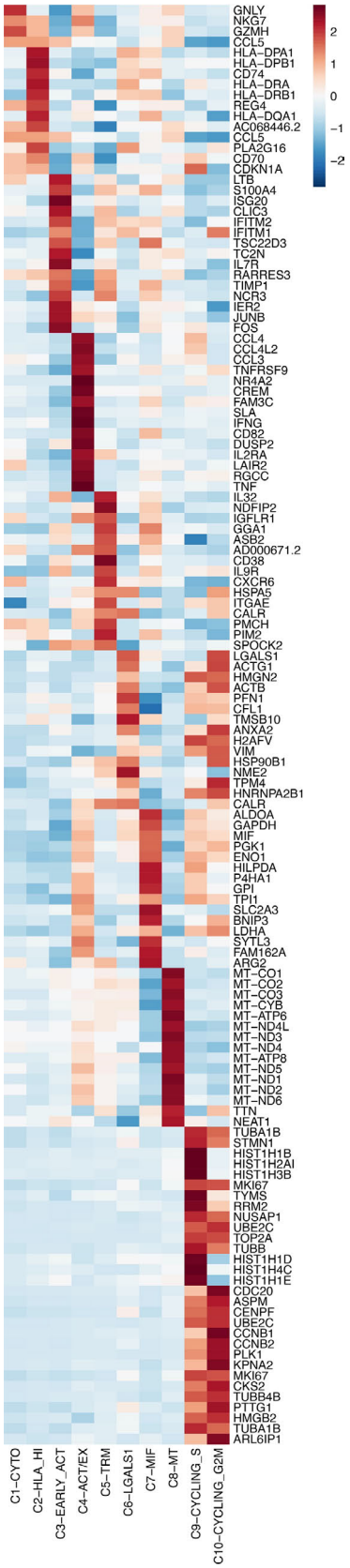

Supplementary figure 69

Heatmap of the top 15 significant (adjusted p-val < 0.01) differentially expressed genes by average fold change between bulk phenotype clusters.

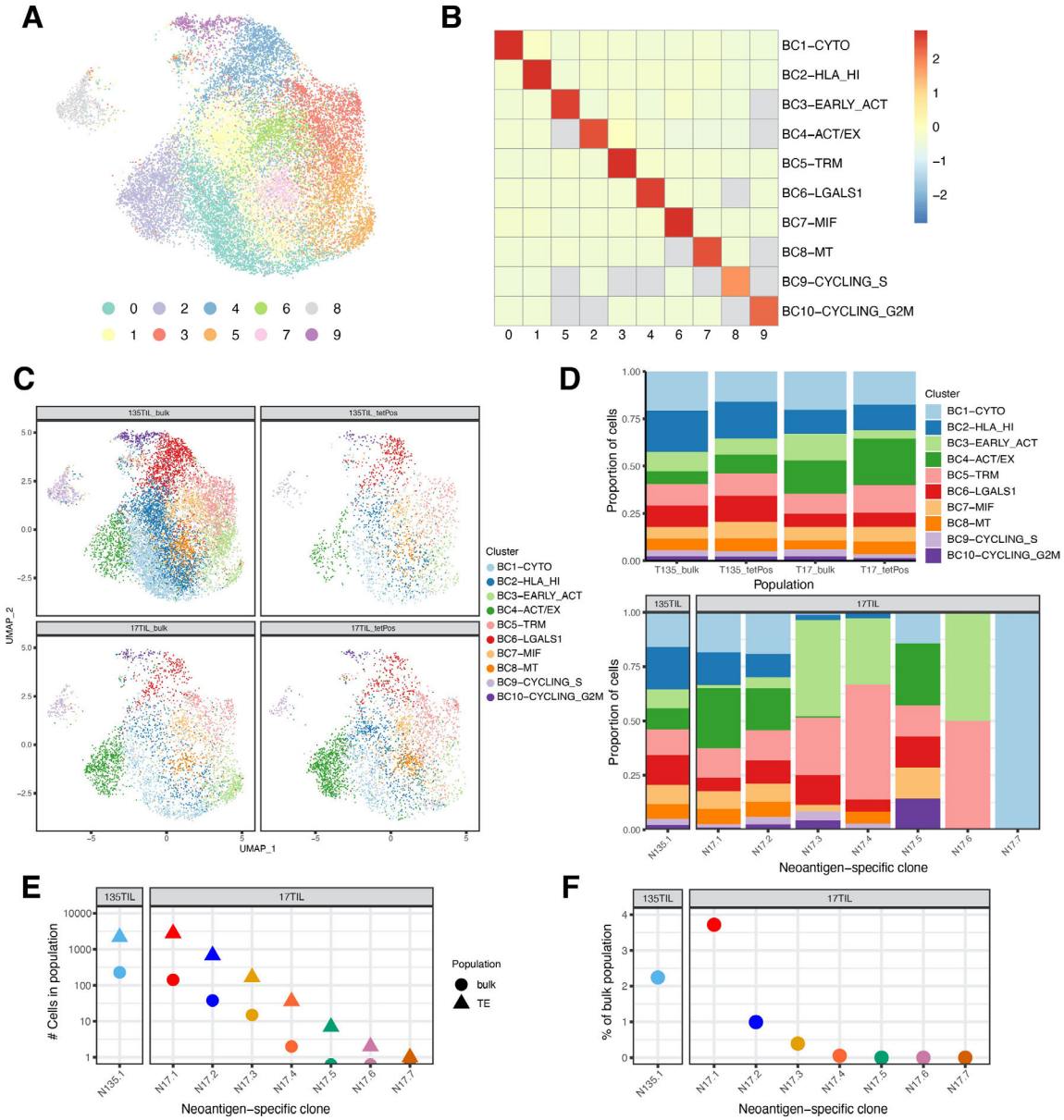

Supplementary figure 70.
(A) UMAP of cells from bulk and tetramer+ populations colored by phenotype cluster. **(B)** Phenotype cluster concordance between bulk-only clusters and bulk-tetramer+ clusters. Color values indicate normalized z-scores of cell numbers with each shared phenotype mapping. **(C)** UMAP of cells from each sorted population. **(D)** Distribution of cells across phenotype clusters within each sorted population (top) or tetramer-enriched clone (bottom). **(E)** Clone sizes of neoantigen-specific clones in the bulk and tetramer-enriched populations. **(F)** Percent of bulk populations contributed by each neoantigen-specific clone.

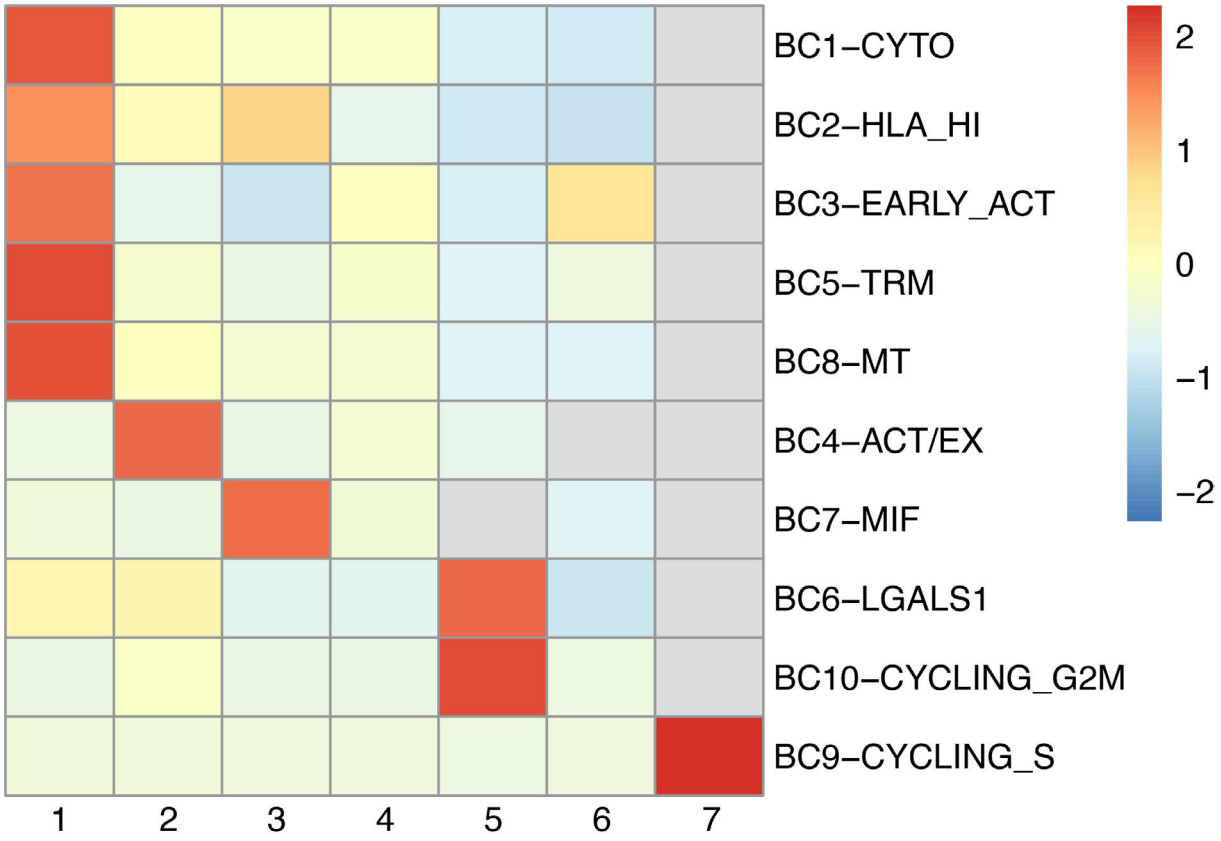

Supplementary figure 71
Phenotype cluster concordance between clusters from tetramer+ integrated samples (horizontal axis) and bulk-tetramer+ integrated clusters (vertical axis). Color values indicate normalized z-scores of cell numbers with each shared phenotype mapping.

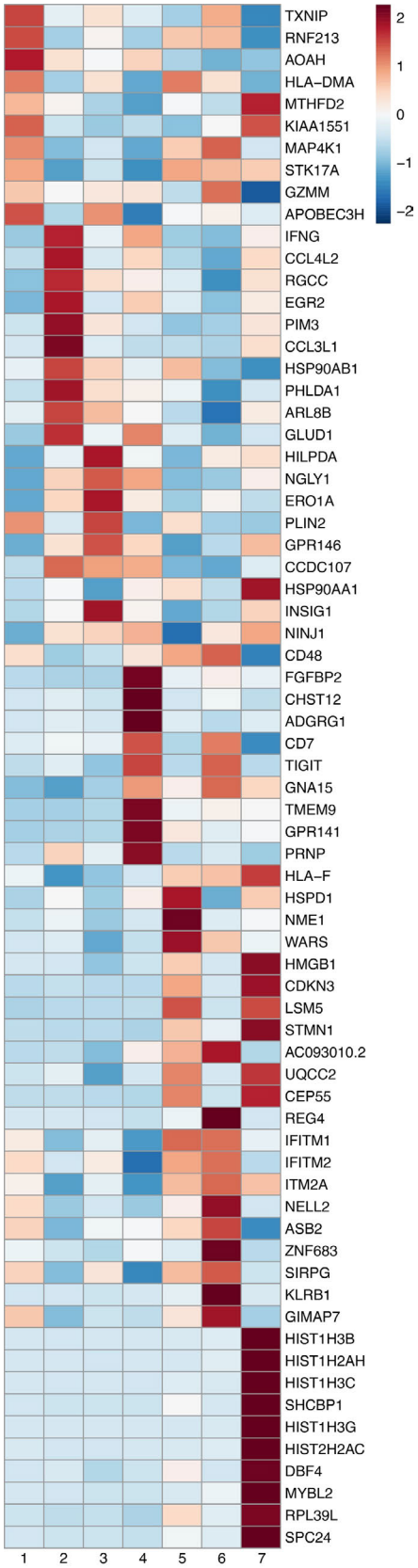

Supplementary figure 72

Heatmap of the top 15 significant (adjusted p-val < 0.01) differentially expressed genes by average fold change between tetramer+ phenotype clusters.

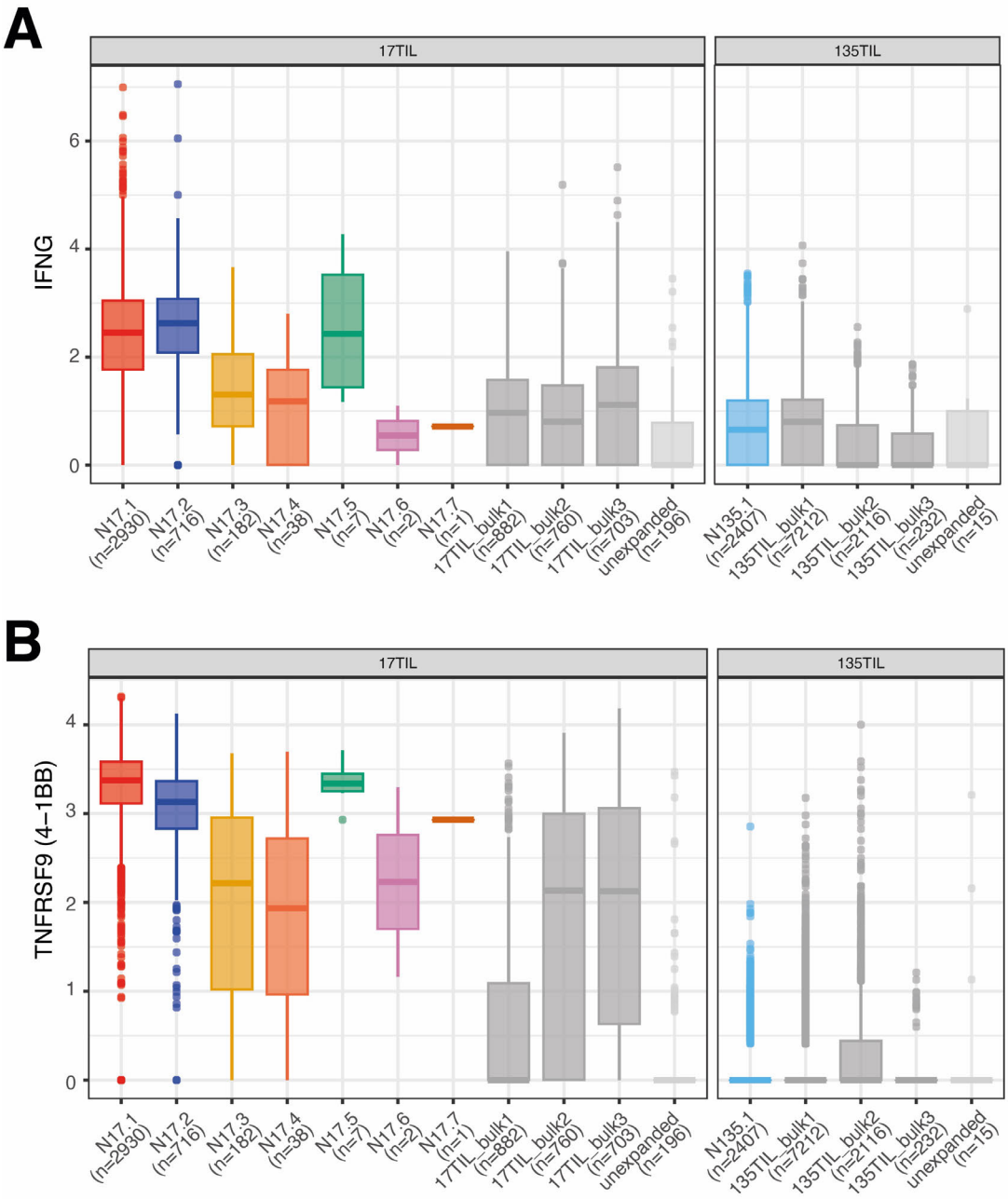

Supplementary figure 73
Expression levels of IFNG (A) and TNFRSF9 (B) among neoantigen-specific clones, other highly expanded bulk CD8+ clones, and all other unexpanded bulk clones. Number of cells in each clone or group is indicated.